THE ASTROPHYSICAL JOURNAL

An International Review of Spectroscopy and Astronomical Physics

FOUNDED IN 1895 BY GEORGE E. HALE AND JAMES E. KEELER

VOLUME 97

JANUARY–MAY 1943

THE UNIVERSITY OF CHICAGO PRESS
CHICAGO, ILLINOIS

THE CAMBRIDGE UNIVERSITY PRESS, LONDON

PUBLISHED JANUARY, MARCH, MAY, 1943

COMPOSED AND PRINTED BY THE UNIVERSITY OF CHICAGO PRESS
CHICAGO, ILLINOIS, U.S.A.

CONTENTS

NUMBER 1

NUMBER 2

NUMBER 3

THE ASTROPHYSICAL JOURNAL

AN INTERNATIONAL REVIEW OF SPECTROSCOPY AND ASTRONOMICAL PHYSICS

VOLUME 97 JANUARY 1943 NUMBER 1

THE STATISTICS OF THE GRAVITATIONAL FIELD ARISING FROM A RANDOM DISTRIBUTION OF STARS*

II. THE SPEED OF FLUCTUATIONS; DYNAMICAL FRICTION; SPATIAL CORRELATIONS

S. CHANDRASEKHAR AND J. VON NEUMANN

ABSTRACT

This paper is devoted principally to a statistical analysis of the speed of fluctuations in the force per unit mass, $\boldsymbol{F}$, acting on a star which is moving with a velocity $\boldsymbol{v}$ with respect to the centroid of the near-by stars. The solution to the problem depends on the evaluation of the first and the second moments of the rate of change of $\boldsymbol{F}$ for a given value of $\boldsymbol{F}$.

The statistical problem has been solved on the assumptions of a uniform Poisson distribution of the stars and a spherical distribution of the velocities with respect to the chosen local standard of rest. No other restrictions have been introduced; in particular, proper allowance has been made for a distribution over the different masses M.

It is found that

$$\bar{\dot{\boldsymbol{F}}}_{\boldsymbol{F},\boldsymbol{v}} = -\tfrac{2}{3}\pi G\overline{M}nB\left(\frac{|\boldsymbol{F}|}{Q_H}\right)\left(\boldsymbol{v} - 3\frac{\boldsymbol{v}\cdot\boldsymbol{F}}{|\boldsymbol{F}|^2}\boldsymbol{F}\right),$$

where G denotes the constant of gravitation, $\overline{M}$ the average mass of the stars, n the number of stars per unit volume, and B a certain function of $|\boldsymbol{F}|/Q_H$ (where Q_H is a certain "normal" field strength). It is indicated how in consequence of this lack of randomness in the rate of change of $\boldsymbol{F}$ for given $\boldsymbol{F}$ and $\boldsymbol{v}$ a star may experience *dynamical friction* (i.e., a systematic tendency to be decelerated in the direction of its motion by an amount proportional to $\boldsymbol{v}$).

The various second moments of $\dot{\boldsymbol{F}}$ have also been calculated and lead to an estimate of the mean life of the state $\boldsymbol{F}$.

The closely related problem of the correlations in $\boldsymbol{F}$ acting at two very close points in a system containing a random distribution of stars is also considered.

1. *Introduction.*—In an earlier paper[1] we analyzed certain statistical features of the fluctuating gravitational force acting at some fixed point in a system containing a random distribution of stars in motion. In this paper we propose to extend this discussion to the case of the fluctuations in the force acting on a star which is moving with a definite velocity $\boldsymbol{v}$ in an appropriately chosen local standard of rest. The discussion of this case requires an essential generalization of the analysis contained in I, since for our present

* Some of the results contained in this paper were included in and formed part of an essay written by S. Chandrasekhar and entitled "New Methods in Stellar Dynamics," for which an A. Cressy Morrison Prize was awarded by the New York Academy of Sciences.

[1] *Ap. J.*, **95**, 489, 1941. This paper will be referred to as I.

problem what is relevant is the distribution of the velocities of the other stars *relative* to the one under consideration, and we cannot assume that this has a random character,[2] for the distribution of the relative velocities V will show a marked asymmetry in that there will be a preponderance of negative velocities. More exactly, if the distribution of the velocities relative to the chosen standard of rest is characterized by randomness, then

$$\bar{V} = -v\,. \tag{1}$$

This asymmetry in the distribution of the relative velocities has important physical consequences. Thus, as we shall show (§ 11), it is as a direct result of this asymmetry that a star experiences *dynamical friction*, or, expressed differently, it suffers from a systematic tendency to be decelerated in the direction of its motion by an amount proportional to $|v|$.

A second problem we shall consider in this paper concerns the correlation in the forces acting at two very close points; this problem is closely related to the one formulated in the preceding paragraph.

2. *The general formula for* W (F, f).—Consider a star moving with a velocity v. The force F acting on the star per unit mass is given by

$$F = G\sum_i M_i \frac{r_i}{|r_i|^3}, \tag{2}$$

where M_i denotes the mass of a typical field star and r_i its instantaneous position vector relative to the star under consideration. Accordingly, the rate of change of F is given by

$$f = \frac{dF}{dt} = G\sum_i M_i \left(\frac{V_i}{|r_i|^3} - 3\frac{r_i\,[r_i \cdot V_i]}{|r_i|^5}\right), \tag{3}$$

where V_i denotes the velocity of a field star relative to the one under consideration.

It is clear that the speed of the fluctuations can be specified in terms of the distribution function

$$W(F, f), \tag{4}$$

which gives the simultaneous probability of a given force F acting and an associated rate of change of F of amount f. The general expression for this probability can be readily written down following Markoff's method outlined in I, § 2. We have (cf. I, eqs. [18] and [19])

$$W(F, f) = \frac{1}{64\pi^6}\int_{|\rho|=0}^{\infty}\int_{|\sigma|=0}^{\infty} e^{-i(\rho\cdot F+\sigma\cdot f)}\,A(\rho, \sigma)\,d\rho d\sigma\,, \tag{5}$$

where

$$A(\rho, \sigma) = \lim_{R\to\infty}\left[\frac{3}{4\pi R^3}\int_{0\le M<\infty}\int_{|r|<R}\int_{|V|<\infty} e^{i(\rho\cdot\phi+\sigma\cdot\psi)}\,\tau\,dr dV dM\right]^{4\pi R^3 n/3}. \tag{6}$$

In equations (5) and (6) ρ and σ are two auxiliary vectors, n denotes the average number of stars per unit volume,

$$\phi = GM\frac{r}{|r|^3}; \qquad \psi = GM\left(\frac{V}{|r|^3} - 3\frac{r\,[r\cdot V]}{|r|^5}\right), \tag{7}$$

and

$$\tau\,dV dM \equiv \tau(V; M)\,dV dM \tag{8}$$

[2] We use the word "random" in the sense defined in S. Chandrasekhar, *Principles of Stellar Dynamics*, p. 8, University of Chicago Press, 1942.

gives the probability that a star with a relative velocity in the range $(\boldsymbol{V}, \boldsymbol{V}+d\boldsymbol{V})$ and with a mass between M and $M+dM$ will be found. It should be further noted that in writing down equations (5) and (6) we have supposed that the fluctuations in the stellar distribution which occur are subject only to the restriction of a constant average density.

Since

$$\frac{3}{4\pi R^3}\int_{0<M<\infty}\int_{|\boldsymbol{r}|<R}\int_{|\boldsymbol{V}|<\infty}\tau\, d\boldsymbol{r}d\boldsymbol{V}dM = 1\,, \tag{9}$$

we can re-write equation (6) as

$$A(\boldsymbol{\rho},\boldsymbol{\sigma}) = \lim_{R\to\infty}\left[1-\frac{3}{4\pi R^3}\int_{0<M<\infty}\int_{|\boldsymbol{r}|<R}\int_{|\boldsymbol{V}|<\infty} \times\{1-e^{i(\boldsymbol{\rho}\cdot\boldsymbol{\phi}+\boldsymbol{\sigma}\cdot\boldsymbol{\psi})}\}\,\tau\, d\boldsymbol{r}d\boldsymbol{V}dM\right]^{4\pi R^3 n/3}. \tag{10}$$

We replace formula (10) by

$$A(\boldsymbol{\rho},\boldsymbol{\sigma}) = \lim_{R\to\infty}\left[1-\frac{3}{4\pi R^3}\int_0^{\infty}\int_{-\infty}^{+\infty}\int_{-\infty}^{+\infty}\{1-e^{i(\boldsymbol{\rho}\cdot\boldsymbol{\phi}+\boldsymbol{\sigma}\cdot\boldsymbol{\psi})}\}\,\tau\, d\boldsymbol{r}d\boldsymbol{V}dM\right]^{4\pi R^3 n/3}. \tag{11}$$

The integral which occurs in the foregoing equation is conditionally convergent. It should be noted that (among others) the integral $\int_{-\infty}^{+\infty}\ldots d\boldsymbol{r}$ is a triple integral, since $\boldsymbol{r}$ is a vector. The origin of the expression should make it plausible that one must integrate over the two polar angles ϑ and ω of $\boldsymbol{r}$ first and over $|\boldsymbol{r}|$ last. (Indeed, this $\int_{-\infty}^{+\infty}\ldots d\boldsymbol{r}$ or, rather, $\int_0^{\infty}\int_0^{\pi}\int_0^{2\pi}\ldots|\boldsymbol{r}|^2\sin\vartheta d\omega d\vartheta d|\boldsymbol{r}|$ originates from the $\int_{|\boldsymbol{r}|<R}\ldots d\boldsymbol{r}$ or, rather, $\int_0^{R}\int_0^{\pi}\int_0^{2\pi}\ldots|\boldsymbol{r}|^2\sin\vartheta d\omega d\vartheta d|\boldsymbol{r}|$, of equation (10) with $R\to\infty$.) A justification of this plausible procedure will be given elsewhere, by means of complex integration. This point is of importance, because an improper order of integrations may lead to incorrect results.

Now equation (11) can also be written as

$$A(\boldsymbol{\rho},\boldsymbol{\sigma}) = e^{-nC(\boldsymbol{\rho},\boldsymbol{\sigma})}\,, \tag{12}$$

where

$$C(\boldsymbol{\rho},\boldsymbol{\sigma}) = \int_0^{\infty}\int_{-\infty}^{+\infty}\int_{-\infty}^{+\infty}\{1-e^{i(\boldsymbol{\rho}\cdot\boldsymbol{\phi}+\boldsymbol{\sigma}\cdot\boldsymbol{\psi})}\}\,\tau\, d\boldsymbol{r}d\boldsymbol{V}dM\,. \tag{13}$$

In the foregoing expression for $C(\boldsymbol{\rho},\boldsymbol{\sigma})$ we shall introduce $\boldsymbol{\phi}$ as the variable of integration instead of $\boldsymbol{r}$. Since $\boldsymbol{\phi}$ and $\boldsymbol{r}$ have the same polar co-ordinates and since $|\boldsymbol{\phi}|$ and $|\boldsymbol{r}|$ determine each other, our earlier remarks concerning the $\boldsymbol{r}$-integration apply equally to the $\boldsymbol{\phi}$-integration. We have (cf. I, eqs. [22]–[24])

$$d\boldsymbol{r} = -\tfrac{1}{2}(GM)^{3/2}|\boldsymbol{\phi}|^{-9/2}d\boldsymbol{\phi}\,. \tag{14}$$

We can re-write equation (13) as

$$C(\boldsymbol{\rho}, \boldsymbol{\sigma}) = \tfrac{1}{2}G^{3/2}\int_0^{\infty}\int_{-\infty}^{+\infty} dM\, dV\, \tau M^{3/2}\left[\int_{-\infty}^{+\infty}\{1 - e^{i(\boldsymbol{\rho}\cdot\boldsymbol{\phi}+\boldsymbol{\sigma}\cdot\boldsymbol{\psi})}\}\,|\boldsymbol{\phi}|^{-9/2}d\boldsymbol{\phi}\right]. \tag{15}$$

In equation (15) $\boldsymbol{\sigma}\cdot\boldsymbol{\psi}$ will have to be expressed in terms of $\boldsymbol{\phi}$. Thus,

$$\boldsymbol{\sigma}\cdot\boldsymbol{\psi} = (GM)^{-1/2}\{\,|\boldsymbol{\phi}|^{3/2}(\boldsymbol{\sigma}\cdot\boldsymbol{V}) - 3\,|\boldsymbol{\phi}|^{-1/2}(\boldsymbol{\phi}\cdot\boldsymbol{V})\,(\boldsymbol{\phi}\cdot\boldsymbol{\sigma})\,\}\,. \tag{16}$$

If we now put

$$\boldsymbol{\sigma} = (GM)^{1/2}\boldsymbol{\sigma}_1\,, \tag{17}$$

$\boldsymbol{\sigma}\cdot\boldsymbol{\psi}$ can be expressed more conveniently as

$$\boldsymbol{\sigma}\cdot\boldsymbol{\psi} = |\boldsymbol{\phi}|^{3/2}(\boldsymbol{\sigma}_1\cdot\boldsymbol{V}) - 3\,|\boldsymbol{\phi}|^{-1/2}(\boldsymbol{\phi}\cdot\boldsymbol{V})\,(\boldsymbol{\phi}\cdot\boldsymbol{\sigma}_1)\,. \tag{18}$$

Returning to equation (15), we write it in the form

$$C(\boldsymbol{\rho}, \boldsymbol{\sigma}) = \tfrac{1}{2}G^{3/2}\int_0^{\infty}\int_{-\infty}^{+\infty} dM\, dV\, \tau M^{3/2} D(\boldsymbol{\rho}, \boldsymbol{\sigma})\,, \tag{19}$$

where

$$D(\boldsymbol{\rho}, \boldsymbol{\sigma}) = \int_{-\infty}^{+\infty}\{1 - e^{i(\boldsymbol{\rho}\cdot\boldsymbol{\phi}+\boldsymbol{\sigma}\cdot\boldsymbol{\psi})}\}\,|\boldsymbol{\phi}|^{-9/2}d\boldsymbol{\phi}\,. \tag{20}$$

An alternative form for $D(\boldsymbol{\rho}, \boldsymbol{\sigma})$ is

$$D(\boldsymbol{\rho}, \boldsymbol{\sigma}) = \int_{-\infty}^{+\infty}(1 - e^{i\boldsymbol{\rho}\cdot\boldsymbol{\phi}})\,|\boldsymbol{\phi}|^{-9/2}d\boldsymbol{\phi} + \int_{-\infty}^{+\infty} e^{i\boldsymbol{\rho}\cdot\boldsymbol{\phi}}(1 - e^{i\boldsymbol{\sigma}\cdot\boldsymbol{\psi}})\,|\boldsymbol{\phi}|^{-9/2}d\boldsymbol{\phi}\,. \tag{21}$$

The first of the two integrals which occur in the foregoing equation is equivalent to one we have already evaluated in I (eqs. [55]–[58]). We thus have

$$D(\boldsymbol{\rho}, \boldsymbol{\sigma}) = \tfrac{8}{15}(2\pi)^{3/2}\,|\boldsymbol{\rho}|^{3/2} + \int_{-\infty}^{+\infty} e^{i\boldsymbol{\rho}\cdot\boldsymbol{\phi}}(1 - e^{i\boldsymbol{\sigma}\cdot\boldsymbol{\psi}})\,|\boldsymbol{\phi}|^{-9/2}d\boldsymbol{\phi}\,. \tag{22}$$

Equations (5), (12), (18), (19), and (22) formally solve the problem of the determination of $W(\boldsymbol{F}, f)$. However, an explicit evaluation of $W(\boldsymbol{F}, f)$ would require a complete knowledge of the function $A(\boldsymbol{\rho}, \boldsymbol{\sigma})$. But if we are interested only in the moments of f for a given $\boldsymbol{F}$, we need only the behavior of $A(\boldsymbol{\rho}, \boldsymbol{\sigma})$ for $|\boldsymbol{\sigma}| \to 0$ or, according to equations (12) and (19), in the behavior of $D(\boldsymbol{\rho}, \boldsymbol{\sigma})$ for $|\boldsymbol{\sigma}| \to 0$. We can therefore expand

$$1 - e^{i\boldsymbol{\sigma}\cdot\boldsymbol{\psi}}\,, \tag{23}$$

which occurs under the integral sign in equation (22) in a power series in $\boldsymbol{\sigma}$. Retaining only the first two terms in this expansion, we obtain

$$D(\boldsymbol{\rho}, \boldsymbol{\sigma}) = \tfrac{8}{15}(2\pi)^{3/2}\,|\boldsymbol{\rho}|^{3/2} - D_1(\boldsymbol{\rho}, \boldsymbol{\sigma}) + D_2(\boldsymbol{\rho}, \boldsymbol{\sigma}) + O(|\boldsymbol{\sigma}|^3)\,, \tag{24}$$

where

$$D_1(\boldsymbol{\rho}, \boldsymbol{\sigma}) = i\int_{-\infty}^{+\infty} e^{i\boldsymbol{\rho}\cdot\boldsymbol{\phi}}(\boldsymbol{\sigma}\cdot\boldsymbol{\psi})\,|\boldsymbol{\phi}|^{-9/2}d\boldsymbol{\phi}\,, \tag{25}$$

and

$$D_2(\boldsymbol{\rho}, \boldsymbol{\sigma}) = \frac{1}{2}\int_{-\infty}^{+\infty} e^{i\boldsymbol{\rho}\cdot\boldsymbol{\Phi}} (\boldsymbol{\sigma}\cdot\boldsymbol{\psi})^2 |\boldsymbol{\phi}|^{-9/2} d\boldsymbol{\phi}. \tag{26}$$

3. *The evaluation of* $D_1(\boldsymbol{\rho}, \boldsymbol{\sigma})$.—Substituting for $\boldsymbol{\sigma}\cdot\boldsymbol{\psi}$ from equation (18) in equation (25), we have

$$D_1(\boldsymbol{\rho}, \boldsymbol{\sigma}) = i\int_{-\infty}^{+\infty} e^{i\boldsymbol{\rho}\cdot\boldsymbol{\phi}} \left\{ (\boldsymbol{\sigma}_1\cdot\boldsymbol{V}) - 3\,\frac{(\boldsymbol{\phi}\cdot\boldsymbol{V})\,(\boldsymbol{\phi}\cdot\boldsymbol{\sigma}_1)}{|\boldsymbol{\phi}|^2} \right\} |\boldsymbol{\phi}|^{-3} d\boldsymbol{\phi}. \tag{27}$$

To evaluate this integral we shall first choose a Cartesian system of co-ordinates with the z-axis in the direction of $\boldsymbol{\rho}$. Let the vectors $\boldsymbol{\sigma}_1$ and $\boldsymbol{V}$ in this system of co-ordinates be

$$\boldsymbol{\sigma}_1 = (s_1, s_2, s_3); \qquad \boldsymbol{V} = (V_1, V_2, V_3). \tag{28}$$

Further, let

$$\mathbf{1}_{\boldsymbol{\phi}} = (l, m, n) = (\sin\vartheta\cos\omega, \sin\vartheta\sin\omega, \cos\vartheta) \tag{29}$$

be a unit vector in the direction of $\boldsymbol{\phi}$. Equation (27) now becomes

$$\left.\begin{aligned} D_1(\boldsymbol{\rho}, \boldsymbol{\sigma}) &= i\int_0^{\infty}\int_0^{\pi}\int_0^{2\pi} d|\boldsymbol{\phi}|\, d\vartheta\, d\omega\, |\boldsymbol{\phi}|^{-1} \sin\vartheta\, e^{i|\boldsymbol{\rho}||\boldsymbol{\phi}|\cos\vartheta} \\ &\times [(s_1V_1+s_2V_2+s_3V_3) - 3(l^2 s_1V_1 + m^2 s_2V_2 + n^2 s_3V_3 + lm[s_2V_1+s_1V_2] \\ &\qquad + mn[s_3V_2+s_2V_3] + nl[s_1V_3+s_3V_1])]. \end{aligned}\right\} \tag{30}$$

The integral over ω is readily performed, and we obtain

$$\left.\begin{aligned} D_1(\boldsymbol{\rho}, \boldsymbol{\sigma}) &= 2\pi i\int_0^{\infty}\int_{-1}^{+1} e^{i|\boldsymbol{\rho}||\boldsymbol{\phi}|t} \{[s_3V_3 - \tfrac{1}{2}(s_1V_1+s_2V_2)] \\ &\qquad + [\tfrac{3}{2}(s_1V_1+s_2V_2) - 3s_3V_3]t^2\} |\boldsymbol{\phi}|^{-1} dt\, d|\boldsymbol{\phi}|, \end{aligned}\right\} \tag{31}$$

where we have written $t = \cos\vartheta$. Without altering its value we can clearly replace t by $-t$ in the foregoing expression. But this replacement changes

$$e^{i|\boldsymbol{\rho}||\boldsymbol{\phi}|t} \quad \text{into} \quad e^{-i|\boldsymbol{\rho}||\boldsymbol{\phi}|t} \tag{32}$$

under the integral sign; taking the arithmetic mean of the two resulting integrands, we obtain

$$\left.\begin{aligned} D_1(\boldsymbol{\rho}, \boldsymbol{\sigma}) &= 4\pi i\int_0^{\infty}\int_0^{1} \cos(|\boldsymbol{\rho}|\,|\boldsymbol{\phi}|t) \{[s_3V_3 - \tfrac{1}{2}(s_1V_1+s_2V_2)] \\ &\qquad + [\tfrac{3}{2}(s_1V_1+s_2V_2) - 3s_3V_3]t^2\} |\boldsymbol{\phi}|^{-1} dt\, d|\boldsymbol{\phi}|, \end{aligned}\right\} \tag{33}$$

or, writing $x = |\boldsymbol{\rho}|\,|\boldsymbol{\phi}|$, we have

$$\left.\begin{aligned} D_1(\boldsymbol{\rho}, \boldsymbol{\sigma}) &= 4\pi i\int_0^{\infty}\int_0^{1} \cos(xt) \{[s_3V_3 - \tfrac{1}{2}(s_1V_1+s_2V_2)] \\ &\qquad + [\tfrac{3}{2}(s_1V_1+s_2V_2) - 3s_3V_3]t^2\} x^{-1} dt\, dx. \end{aligned}\right\} \tag{34}$$

Both the x- and the t-integrations can now be carried out. According to the remarks made after equations (11) and (13), we must carry out the integration over t first and x

later. (We may note here that actually the reverse order of carrying out the integration over x first and t later leads to the value 0; this paradoxical result is, of course, caused by the conditional convergence of the multiple integral.) The t-integration gives (cf. I, eqs. [137])

$$\left.\begin{aligned} D_1(\boldsymbol{\rho}, \boldsymbol{\sigma}) &= 4\pi i \int_0^\infty \Big\{ (s_3 V_3 - \tfrac{1}{2}[\, s_1 V_1 + s_2 V_2 \,]) \frac{\sin x}{x} \\ &\quad + (\tfrac{3}{2}[\, s_1 V_1 + s_2 V_2 \,] - 3 s_3 V_3) \Big(\frac{\sin x}{x} - \frac{2}{x^3} [\sin x - x \cos x] \Big) \Big\} \frac{dx}{x} \\ &= 4\pi i (s_1 V_1 + s_2 V_2 - 2 s_3 V_3) \int_0^\infty (x^2 \sin x - 3 \sin x + 3x \cos x) \frac{dx}{x^4} . \end{aligned}\right\} \quad (35)$$

Now

$$\left.\begin{aligned} &\int_0^\infty (x^2 \sin x - 3 \sin x + 3x \cos x) \frac{dx}{x^4} \\ &\qquad = -\frac{1}{3} \int_0^\infty (x^2 \sin x - 3 \sin x + 3x \cos x) \frac{d}{dx} \left(\frac{1}{x^3} \right) dx \\ &\qquad = \frac{1}{3} \int_0^\infty (x \cos x - \sin x) \frac{dx}{x^2} \\ &\qquad = \frac{1}{3} \int_0^\infty \frac{d}{dx} \left(\frac{\sin x}{x} \right) dx = -\frac{1}{3} . \end{aligned}\right\} \quad (36)$$

Hence, combining equations (35) and (36), we have

$$D_1(\boldsymbol{\rho}, \boldsymbol{\sigma}) = -\tfrac{4}{3}\pi i (s_1 V_1 + s_2 V_2 - 2 s_3 V_3) , \quad (37)$$

where, it will be recalled, s_1, s_2, s_3 and V_1, V_2, V_3 are the components of $\boldsymbol{\sigma}_1$ and $\boldsymbol{V}$ in a system of co-ordinates in which the z-axis is in the direction of $\boldsymbol{\rho}$. If $\boldsymbol{\sigma} = (\sigma_1, \sigma_2, \sigma_3)$ in the same system, then, according to equation (17), we can re-write equation (37) as

$$D_1(\boldsymbol{\rho}, \boldsymbol{\sigma}) = -\tfrac{4}{3}\pi i (GM)^{-1/2} (\sigma_1 V_1 + \sigma_2 V_2 - 2 \sigma_3 V_3) . \quad (38)$$

4. *The evaluation of* $D_2(\boldsymbol{\rho}, \boldsymbol{\sigma})$.—According to equations (18) and (26),

$$D_2(\boldsymbol{\rho}, \boldsymbol{\sigma}) = \frac{1}{2} \int_{-\infty}^{+\infty} e^{i\boldsymbol{\rho}\cdot\boldsymbol{\phi}} [\, (\boldsymbol{\sigma}_1 \cdot \boldsymbol{V}) - 3 (\mathbf{1}_{\boldsymbol{\phi}} \cdot \boldsymbol{V}) (\mathbf{1}_{\boldsymbol{\phi}} \cdot \boldsymbol{\sigma}_1) \,]^2 |\boldsymbol{\phi}|^{-3/2} d\boldsymbol{\phi} , \quad (39)$$

where, as in equation (29), $\mathbf{1}_{\boldsymbol{\phi}}$ is a unit vector in the direction of $\boldsymbol{\phi}$. Using polar co-ordinates, we can express $D_2(\boldsymbol{\rho}, \boldsymbol{\sigma})$ as

$$\left.\begin{aligned} D_2(\boldsymbol{\rho}, \boldsymbol{\sigma}) = \frac{1}{2} \int_0^\infty \int_{-1}^{+1} \int_0^{2\pi} & e^{i|\boldsymbol{\rho}||\boldsymbol{\phi}| t} [\, (\boldsymbol{\sigma}_1 \cdot \boldsymbol{V}) - 3 (\mathbf{1}_{\boldsymbol{\phi}} \cdot \boldsymbol{V}) (\mathbf{1}_{\boldsymbol{\phi}} \cdot \boldsymbol{\sigma}_1) \,]^2 \\ & \times |\boldsymbol{\phi}|^{1/2} d\omega dt d |\boldsymbol{\phi}| , \end{aligned}\right\} \quad (40)$$

or, introducing a new variable z, defined as

$$z = |\boldsymbol{\rho}| \, |\boldsymbol{\phi}| , \quad (41)$$

we have

$$D_2(\boldsymbol{\rho}, \boldsymbol{\sigma}) = \tfrac{1}{2} |\boldsymbol{\rho}|^{-3/2} \int_0^{\infty} \int_{-1}^{+1} \int_0^{2\pi} e^{izt} [\, (\boldsymbol{\sigma}_1 \cdot \boldsymbol{V}) - 3\,(\mathbf{1}_{\boldsymbol{\phi}} \cdot \boldsymbol{V})\,(\mathbf{1}_{\boldsymbol{\phi}} \cdot \boldsymbol{\sigma}_1)\,]^2 z^{1/2} d\omega dt dz\,. \quad (42)$$

After performing the integration over ω, we obtain

$$D_2(\boldsymbol{\rho}, \boldsymbol{\sigma}) = \pi |\boldsymbol{\rho}|^{-3/2} \int_0^{\infty} \int_{-1}^{+1} e^{izt} \overline{[\, (\boldsymbol{\sigma}_1 \cdot \boldsymbol{V}) - 3\,(\mathbf{1}_{\boldsymbol{\phi}} \cdot \boldsymbol{V})\,(\mathbf{1}_{\boldsymbol{\phi}} \cdot \boldsymbol{\sigma}_1)\,]^2}\; z^{1/2} dt dz\,, \quad (43)$$

where we have used the bar over $[(\boldsymbol{\sigma}_1 \cdot \boldsymbol{V}) - 3(\mathbf{1}_{\boldsymbol{\phi}} \cdot \boldsymbol{V})(\mathbf{1}_{\boldsymbol{\phi}} \cdot \boldsymbol{\sigma}_1)]^2$ to indicate that the averaging over ω has been carried out.

In order now to evaluate the integral in equation (43) we first note that, since $\overline{[\boldsymbol{\sigma}_1 \cdot \boldsymbol{V} - 3(\mathbf{1}_{\boldsymbol{\phi}} \cdot \boldsymbol{V})(\mathbf{1}_{\boldsymbol{\phi}} \cdot \boldsymbol{\sigma}_1)]^2}$ is an even function in t (cf. eqs. [47] and [49] below), $D_2(\boldsymbol{\rho},\boldsymbol{\sigma})$ has the alternative form

$$D_2(\boldsymbol{\rho}, \boldsymbol{\sigma}) = \pi |\boldsymbol{\rho}|^{-3/2} \int_0^{\infty} \int_{-1}^{+1} \cos\,(zt)\; \overline{[\boldsymbol{\sigma}_1 \cdot \boldsymbol{V} - 3\,(\mathbf{1}_{\boldsymbol{\phi}} \cdot \boldsymbol{V})\,(\mathbf{1}_{\boldsymbol{\phi}} \cdot \boldsymbol{\sigma}_1)\,]^2}\; z^{1/2} dt dz\,. \quad (44)$$

The integration over z and t are now best performed by regarding them as complex variables and integrating along appropriately chosen contours. Thus, writing equation (44) as

$$D_2(\boldsymbol{\rho}, \boldsymbol{\sigma}) = \pi |\boldsymbol{\rho}|^{-3/2} \Re \int_{-1}^{+1} \int_0^{\infty} e^{izt} \overline{[\, (\boldsymbol{\sigma}_1 \cdot \boldsymbol{V}) - 3\,(\mathbf{1}_{\boldsymbol{\phi}} \cdot \boldsymbol{V})\,(\mathbf{1}_{\boldsymbol{\phi}} \cdot \boldsymbol{\sigma}_1)\,]^2}\; z^{1/2} dz dt \quad (45)$$

and choosing for z and t paths of integrations as in the appendix to our first paper, we obtain

$$\left.\begin{aligned} D_2(\boldsymbol{\rho}, \boldsymbol{\sigma}) = -\pi \Gamma\left(\tfrac{3}{2}\right) |\boldsymbol{\rho}|^{-3/2} \Re\, e^{-i\pi/4} \int_{-1}^{+1} & \overline{[\, (\boldsymbol{\sigma}_1 \cdot \boldsymbol{V}) - 3\,(\mathbf{1}_{\boldsymbol{\phi}} \cdot \boldsymbol{V})\,(\mathbf{1}_{\boldsymbol{\phi}} \cdot \boldsymbol{\sigma}_1)\,]^2} \\ & \times t^{-3/2} dt\,. \end{aligned}\right\} \quad (46)$$

In equation (46) the integration over t has to be carried out along a curve from -1 to $+1$ in the complex t-plane, which lies entirely in the domain $\Im t \geqslant 0$ and $|t| \leqslant 1$. In order to carry out this integration we must first expand $[(\boldsymbol{\sigma}_1 \cdot \boldsymbol{V}) - 3(\mathbf{1}_{\boldsymbol{\phi}} \cdot \boldsymbol{V})(\mathbf{1}_{\boldsymbol{\phi}} \cdot \boldsymbol{\sigma}_1)]^2$ and average over ω. We find that

$$\left.\begin{aligned} & \overline{[\, (\boldsymbol{\sigma}_1 \cdot \boldsymbol{V}) - 3\,(\mathbf{1}_{\boldsymbol{\phi}} \cdot \boldsymbol{V})\,(\mathbf{1}_{\boldsymbol{\phi}} \cdot \boldsymbol{\sigma}_1)\,]^2} \\ & = \overline{[\, (s_1 V_1 + s_2 V_2 + s_3 V_3) - 3 \{\!| l^2 s_1 V_1 + m^2 s_2 V_2 + n^2 s_3 V_3 + lm\,(s_1 V_2 + s_2 V_1) + mn\,(s_2 V_3 + s_3 V_2) + nl\,(s_3 V_1 + s_1 V_3) \}\!|\,]^2} \\ & = (s_1 V_1 + s_2 V_2 + s_3 V_3)^2 - 6\,(s_1 V_1 + s_2 V_2 + s_3 V_3)\,(\overline{l^2} s_1 V_1 + \overline{m^2} s_2 V_2 + \overline{n^2} s_3 V_3) \\ & + 9\,(\overline{l^4} s_1^2 V_1^2 + \overline{m^4} s_2^2 V_2^2 + \overline{n^4} s_3^2 V_3^2) + 9\overline{l^2 m^2}\,(s_2^2 V_1^2 + s_1^2 V_2^2 + 4 s_1 s_2 V_1 V_2) \\ & + 9\overline{m^2 n^2}\,(s_2^2 V_3^2 + s_3^2 V_2^2 + 4 s_2 s_3 V_2 V_3) + 9\overline{n^2 l^2}\,(s_3^2 V_1^2 + s_1^2 V_3^2 + 4 s_3 s_1 V_3 V_1)\,, \end{aligned}\right\} \quad (47)$$

where

$$l = \sin\vartheta\cos\omega\,; \qquad m = \sin\vartheta\sin\omega\,; \qquad n = \cos\vartheta\,(=t)\,. \tag{48}$$

Since

$$\left.\begin{aligned} \overline{l^2} = \overline{m^2} &= \tfrac{1}{2}(1-t^2)\,; & \overline{n^2} &= t^2\,,\\ \overline{n^2 l^2} = \overline{n^2 m^2} &= \tfrac{1}{2}t^2(1-t^2)\,; & \overline{l^2 m^2} &= \tfrac{1}{8}(1-t^2)^2\,,\\ \overline{l^4} = \overline{m^4} &= \tfrac{3}{8}(1-t^2)^2\,; & \overline{n^4} &= t^4\,, \end{aligned}\right\} \tag{49}$$

the integral we have to evaluate is

$$\left.\begin{aligned} I = \int_{-1}^{+1}\{\,&(s_1V_1+s_2V_2+s_3V_3)^2 t^{-3/2} - 6\,(s_1V_1+s_2V_2+s_3V_3)\\ &\times[\![\tfrac{1}{2}(s_1V_1+s_2V_2)\,(1-t^2)\,t^{-3/2} + s_3V_3t^{1/2}]\!] + \tfrac{27}{8}(s_1^2V_1^2+s_2^2V_2^2)\\ &\times(1-t^2)^2 t^{-3/2} + 9\,s_3^2V_3^2t^{5/2} + \tfrac{9}{8}(s_2^2V_1^2+s_1^2V_2^2+4\,s_2s_1V_1V_2)\\ &\times(1-t^2)^2 t^{-3/2} + \tfrac{9}{2}(s_2^2V_3^2+s_3^2V_2^2+s_3^2V_1^2+s_1^2V_3^2+4\,s_2s_3V_2V_3\\ &+4\,s_3s_1V_3V_1)\,(1-t^2)\,t^{1/2}\}\,dt\,. \end{aligned}\right\} \tag{50}$$

We readily verify that the various complex integrals which occur in the foregoing expression have the following values:

$$\left.\begin{aligned} \int_{-1}^{+1} t^{-3/2}dt &= -2\,(1+i)\,; & \int_{-1}^{+1}(1-t^2)\,t^{-3/2}dt &= -\tfrac{8}{3}(1+i)\,,\\ \int_{-1}^{+1} t^{1/2}dt &= +\tfrac{2}{3}(1+i)\,; & \int_{-1}^{+1}(1-t^2)^2 t^{-3/2}dt &= -\tfrac{64}{21}(1+i)\,,\\ \int_{-1}^{+1} t^{5/2}dt &= +\tfrac{2}{7}(1+i)\,; & \int_{-1}^{+1}(1-t^2)\,t^{1/2}dt &= +\tfrac{8}{21}(1+i)\,. \end{aligned}\right\} \tag{51}$$

Substituting these values in equation (50) and after some minor rearranging of the terms, we obtain

$$\left.\begin{aligned} I = -\tfrac{8}{7}(1+i)\,[\,&s_1^2(5V_1^2+4V_2^2-2V_3^2) + s_2^2(5V_2^2+4V_1^2-2V_3^2)\\ &+ s_3^2(4V_3^2-2V_1^2-2V_2^2) - 8\,s_2s_3V_2V_3 - 8\,s_3s_1V_3V_1 + 2\,s_1s_2V_1V_2]\,. \end{aligned}\right\} \tag{52}$$

Finally, combining equations (46) and (52) and remembering that

$$\mathcal{R}e^{-i\pi/4}(1+i) = \sqrt{2} \tag{53}$$

and returning to our original variable $\boldsymbol{\sigma} = (\sigma_1, \sigma_2, \sigma_3)$ according to equation (17), we find that

$$\left.\begin{aligned} D_2(\boldsymbol{\rho}, \boldsymbol{\sigma}) = \tfrac{3}{14}(2\pi)^{3/2}(GM)^{-1}\,|\boldsymbol{\rho}|^{-3/2}[\,&\sigma_1^2(5V_1^2+4V_2^2-2V_3^2) + \sigma_2^2(5V_2^2\\ &+4V_1^2-2V_3^2) + \sigma_3^2(4V_3^2-2V_1^2-2V_2^2) - 8\sigma_2\sigma_3V_2V_3 - 8\sigma_3\sigma_1V_3V_1\\ &+2\sigma_1\sigma_2V_1V_2]\,. \end{aligned}\right\} \tag{54}$$

5. *The expression for* $A(\rho, \sigma)$ *for* $|\sigma| \to 0$.—Combining equations (24), (38), and (54), we have

$$\left.\begin{aligned} D(\rho,\sigma) &= {}_{15}^{8}(2\pi)^{3/2}|\rho|^{3/2} + \tfrac{4}{3}\pi i(GM)^{-1/2}(\sigma_1 V_1 + \sigma_2 V_2 - 2\sigma_3 V_3) \\ &+ {}_{14}^{3}(2\pi)^{3/2}(GM)^{-1}|\rho|^{-3/2}[(5\sigma_1^2 + 4\sigma_2^2 - 2\sigma_3^2)V_1^2 + (4\sigma_1^2 + 5\sigma_2^2 - 2\sigma_3^2)V_2^2 \\ &+ (4\sigma_3^2 - 2\sigma_1^2 - 2\sigma_2^2)V_3^2 - 8\sigma_2\sigma_3 V_2 V_3 - 8\sigma_3\sigma_1 V_3 V_1 + 2\sigma_1\sigma_2 V_1 V_2] \\ &+ O(|\sigma|^3). \end{aligned}\right\} \quad (55)$$

Substituting this expression for $D(\rho, \sigma)$ in equation (19), we obtain

$$\left.\begin{aligned} C(\rho,\sigma) &= {}_{15}^{4}(2\pi)^{3/2}G^{3/2}\overline{M^{3/2}}|\rho|^{3/2} + \tfrac{2}{3}\pi i G(\sigma_1\overline{MV_1} + \sigma_2\overline{MV_2} - 2\sigma_3\overline{MV_3}) \\ &+ {}_{28}^{3}(2\pi)^{3/2}G^{1/2}|\rho|^{-3/2}[(5\sigma_1^2 + 4\sigma_2^2 - 2\sigma_3^2)\overline{M^{1/2}V_1^2} + (4\sigma_1^2 + 5\sigma_2^2 - 2\sigma_3^2) \\ &\times \overline{M^{1/2}V_2^2} + (4\sigma_3^2 - 2\sigma_1^2 - 2\sigma_2^2)\overline{M^{1/2}V_3^2} - 8\sigma_2\sigma_3\overline{M^{1/2}V_2V_3} - 8\sigma_3\sigma_1\overline{M^{1/2}V_3V_1} \\ &+ 2\sigma_1\sigma_2\overline{M^{1/2}V_1V_2}] + O(|\sigma|^3), \end{aligned}\right\} \quad (56)$$

where we have used bars to indicate that the corresponding quantities have been averaged with the weight function $\tau(V; M)$.

In all the foregoing equations $V = (V_1, V_2, V_3)$ represents, of course, the velocity of a typical field star relative to the one under consideration. If, now, u and v denote, respectively, the velocities of the field star and the star under consideration in the chosen standard of rest, then

$$V = u - v. \quad (57)$$

We shall now introduce the assumption that the distribution of the velocities u among the stars is spherical,[3] i.e., the distribution function $\Psi(u)$ has the form

$$\Psi(u) \equiv \Psi[j^2(M)\,|u|^2], \quad (58)$$

where Ψ is an arbitrary function of the argument specified and the parameter j (of the dimensions of [velocity]$^{-1}$) is allowed to be a function of the mass of the star. This assumption concerning the distribution of the "peculiar" velocities u implies that our probability function $\tau(V; M)$ must be expressible as

$$\tau(V; M) \equiv \Psi[j^2(M)\,|V + v|^2]\,\chi(M), \quad (59)$$

where $\chi(M)$ governs the distribution over the different masses. For a function τ of this form we clearly have

$$\left.\begin{aligned} &\overline{MV_\mu} = -\overline{M}v_\mu; \qquad \overline{M^{1/2}V_\mu^2} = \tfrac{1}{3}\overline{M^{1/2}|u|^2} + \overline{M^{1/2}}v_\mu^2, \qquad (\mu = 1, 2, 3) \\ &\overline{M^{1/2}V_\mu V_\nu} = \overline{M^{1/2}}v_\mu v_\nu \quad (\mu, \nu = 1, 2, 3,\ \mu \neq \nu). \end{aligned}\right\} \quad (60)$$

Substituting these values in equation (56) and after some minor reductions, we find that

$$\left.\begin{aligned} C(\rho,\sigma) &= {}_{15}^{4}(2\pi)^{3/2}G^{3/2}\overline{M^{3/2}}|\rho|^{3/2} - \tfrac{2}{3}\pi i G\overline{M}(\sigma_1 v_1 + \sigma_2 v_2 - 2\sigma_3 v_3) \\ &+ \tfrac{1}{4}(2\pi)^{3/2}G^{1/2}\overline{M^{1/2}|u|^2}|\rho|^{-3/2}(\sigma_1^2 + \sigma_2^2) + {}_{28}^{3}(2\pi)^{3/2}G^{1/2}\overline{M^{1/2}}|\rho|^{-3/2} \\ &\times [\sigma_1^2(5v_1^2 + 4v_2^2 - 2v_3^2) + \sigma_2^2(4v_1^2 + 5v_2^2 - 2v_3^2) + \sigma_3^2(4v_3^2 - 2v_1^2 - 2v_2^2) \\ &- 8\sigma_2\sigma_3 v_2 v_3 - 8\sigma_3\sigma_1 v_3 v_1 + 2\sigma_1\sigma_2 v_1 v_2] + O(|\sigma|^3), \end{aligned}\right\} \quad (61)$$

[3] It would be entirely feasible at this stage of our work to introduce a more general distribution of the velocities (e.g., an ellipsoidal distribution); but we shall not consider these refinements in this paper.

where we may recall that $(\sigma_1, \sigma_2, \sigma_3)$ and (v_1, v_2, v_3) are the components of $\boldsymbol{\sigma}$ and $\boldsymbol{v}$ in a system of co-ordinates in which the z-axis is in the direction of $\boldsymbol{\rho}$. We shall now specialize the co-ordinate system still further by arranging that the vector $\boldsymbol{v}$ lies in the xz-plane (see Fig. 1). With this choice of the co-ordinate system

$$v_1 = |\boldsymbol{v}| \sin\gamma\,; \qquad v_2 = 0\,; \qquad v_3 = |\boldsymbol{v}| \cos\gamma\,, \tag{62}$$

where

$$\gamma = \measuredangle(\boldsymbol{\rho}, \boldsymbol{v})\,. \tag{63}$$

The expression for $C(\boldsymbol{\rho}, \boldsymbol{\sigma})$ now simplifies to

$$\left.\begin{aligned} C(\boldsymbol{\rho}, \boldsymbol{\sigma}) &= {}^{4}_{15}(2\pi)^{3/2}G^{3/2}\overline{M^{3/2}}\,|\boldsymbol{\rho}|^{3/2} - \tfrac{2}{3}\pi i G\overline{M}\,|\boldsymbol{v}|\,(\sigma_1\sin\gamma - 2\sigma_3\cos\gamma) \\ &+ \tfrac{1}{4}(2\pi)^{3/2}G^{1/2}\overline{M^{1/2}|\boldsymbol{u}|^2}\,|\boldsymbol{\rho}|^{-3/2}(\sigma_1^2+\sigma_2^2) + \tfrac{3}{28}(2\pi)^{3/2}G^{1/2}\overline{M^{1/2}}\,|\boldsymbol{v}|^2\,|\boldsymbol{\rho}|^{-3/2} \\ &\times[\sigma_1^2(5\sin^2\gamma - 2\cos^2\gamma) + \sigma_2^2(4\sin^2\gamma - 2\cos^2\gamma) + \sigma_3^2(4\cos^2\gamma - 2\sin^2\gamma) \\ &\qquad - 8\sigma_1\sigma_3\sin\gamma\cos\gamma] + O(|\boldsymbol{\sigma}|^3)\,. \end{aligned}\right\} \tag{64}$$

Substituting this expression for $C(\boldsymbol{\rho}, \boldsymbol{\sigma})$ in equation (12), which defines $A(\boldsymbol{\rho}, \boldsymbol{\sigma})$, we obtain

$$A(\boldsymbol{\rho}, \boldsymbol{\sigma}) = e^{-a|\boldsymbol{\rho}|^{3/2} + igP(\boldsymbol{\sigma}) - b|\boldsymbol{\rho}|^{-3/2}[Q(\boldsymbol{\sigma}) + kR(\boldsymbol{\sigma})] + O(|\boldsymbol{\sigma}|^3)}\,, \tag{65}$$

where we have written

$$\left.\begin{aligned} a &= {}^{4}_{15}(2\pi)^{3/2}G^{3/2}\overline{M^{3/2}}n\,; & b &= \tfrac{1}{4}(2\pi)^{3/2}G^{1/2}\overline{M^{1/2}|\boldsymbol{u}|^2}n\,, \\ g &= \tfrac{2}{3}\pi G\overline{M}\,|\boldsymbol{v}|\,n\,; & k &= \tfrac{3}{7}\frac{\overline{M^{1/2}}\,|\boldsymbol{v}|^2}{\overline{M^{1/2}|\boldsymbol{u}|^2}}\,, \end{aligned}\right\} \tag{66}$$

[4]

and

$$\left.\begin{aligned} P(\boldsymbol{\sigma}) &= \sigma_1\sin\gamma - 2\sigma_3\cos\gamma\,; \qquad Q(\boldsymbol{\sigma}) = \sigma_1^2 + \sigma_2^2\,, \\ R(\boldsymbol{\sigma}) &= \sigma_1^2(5\sin^2\gamma - 2\cos^2\gamma) + \sigma_2^2(4\sin^2\gamma - 2\cos^2\gamma) \\ &\qquad + \sigma_3^2(4\cos^2\gamma - 2\sin^2\gamma) - 8\sigma_3\sigma_1\sin\gamma\cos\gamma\,. \end{aligned}\right\} \tag{67}$$

An alternative form for $A(\boldsymbol{\rho}, \boldsymbol{\sigma})$, which we shall find useful, may be noted here:

$$\left.\begin{aligned} A(\boldsymbol{\rho}, \boldsymbol{\sigma}) = e^{-a|\boldsymbol{\rho}|^{3/2}}[1 &+ igP(\boldsymbol{\sigma}) - \tfrac{1}{2}g^2[\![P(\boldsymbol{\sigma})]\!]^2 \\ &- b|\boldsymbol{\rho}|^{-3/2}[\![Q(\boldsymbol{\sigma}) + kR(\boldsymbol{\sigma})]\!] + O(|\boldsymbol{\sigma}|^3)]\,. \end{aligned}\right\} \tag{68}$$

Now, according to equation (5), $A(\boldsymbol{\rho}, \boldsymbol{\sigma})$ is the six-dimensional Fourier transform of the distribution function $W(\boldsymbol{F}, \boldsymbol{f})$. Consequently, for the purposes of this equation the vectors $\boldsymbol{\rho}$ and $\boldsymbol{\sigma}$ should be referred to a fixed system of co-ordinates. But the expressions for $P(\boldsymbol{\sigma})$, $Q(\boldsymbol{\sigma})$, and $R(\boldsymbol{\sigma})$ (eq. [67]) involve the components of $\boldsymbol{\sigma}$ referred to a variable

[4] It will be noted that our present definitions of a and b agree with those of our earlier paper (I, eq. [28]).

system of co-ordinates, depending on the direction of $\boldsymbol{\rho}$. We shall now give the linear transformation required to pass from this variable xyz-system to a fixed $\xi\eta\zeta$-system (see Fig. 1). This fixed $\xi\eta\zeta$-system is so chosen that the ζ-axis is in the direction of $\boldsymbol{F}$ and

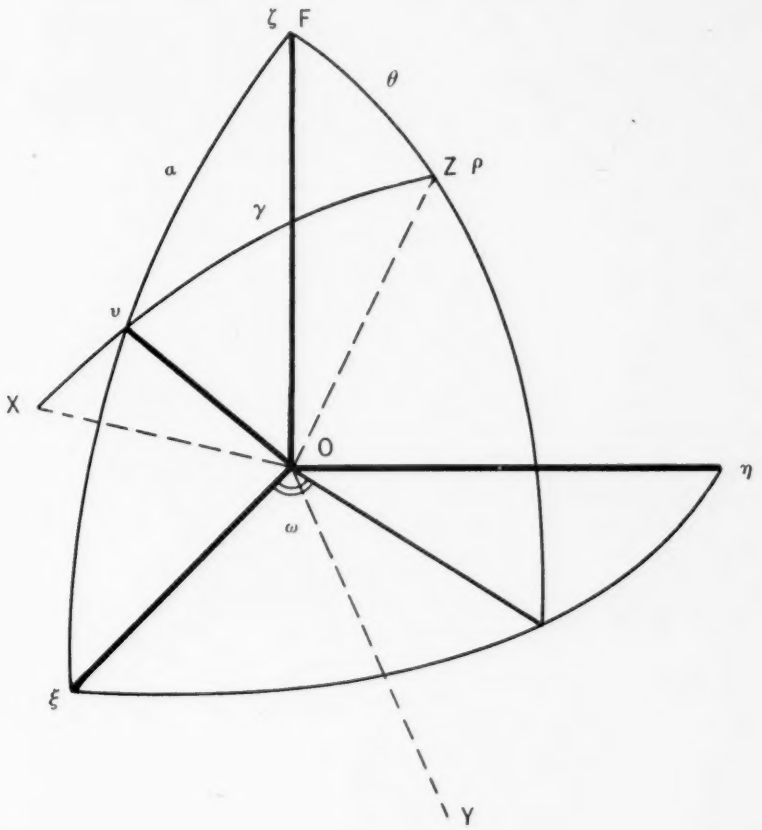

FIG. 1

the $\xi\zeta$-plane contains the vector $\boldsymbol{v}$. The accompanying table gives the direction cosines of the axes belonging to one system with respect to the axes belonging to the other.

	$O\xi$	$O\eta$	$O\zeta$
Ox	$\lambda_1 = \dfrac{\sin\alpha - l\cos\gamma}{\sin\gamma}$	$\mu_1 = -\dfrac{m\cos\gamma}{\sin\gamma}$	$\nu_1 = \dfrac{\cos\alpha - n\cos\gamma}{\sin\gamma}$
Oy	$\lambda_2 = \dfrac{m\cos\alpha}{\sin\gamma}$	$\mu_2 = \dfrac{n\sin\alpha - l\cos\alpha}{\sin\gamma}$	$\nu_2 = -\dfrac{m\sin\alpha}{\sin\gamma}$
Oz	$\lambda_3 = \sin\vartheta\cos\omega = l$	$\mu_3 = \sin\vartheta\sin\omega = m$	$\nu_3 = \cos\vartheta = n$

(69)

Here α is the angle between $\boldsymbol{F}$ and $\boldsymbol{v}$:

$$\alpha = \measuredangle(\boldsymbol{F}, \boldsymbol{v}), \tag{70}$$

and

$$\cos\gamma = \cos\measuredangle(\boldsymbol{\rho}, \boldsymbol{v}) = n\cos\alpha + l\sin\alpha\,. \tag{71}$$

Thus the required linear transformation is

$$\sigma_i = \lambda_i\sigma_\xi + \mu_i\sigma_\eta + \nu_i\sigma_\zeta\,, \qquad (i = 1, 2, 3) \tag{72}$$

where σ_ξ, σ_η, and σ_ζ are the components of $\boldsymbol{\sigma}$ referred to the fixed system of co-ordinates.

6. *The evaluation of the first moment of* f.—To determine the average value of f (for a given $\boldsymbol{F}$) in any specified direction, it would clearly be sufficient to evaluate the first moments of the components of f (namely, f_ξ, f_η, and f_ζ) along the three principal directions of the $\xi\eta\zeta$-system defined in § 5. We shall consider first the moment of f_ξ.

According to equation (5),

$$\int_{-\infty}^{+\infty} W(\boldsymbol{F}, f)\, f_\xi df = \frac{1}{64\pi^6}\int_{-\infty}^{+\infty}\int_{-\infty}^{+\infty}\int_{-\infty}^{+\infty} e^{-i(\boldsymbol{\rho}\cdot\boldsymbol{F}+\boldsymbol{\sigma}\cdot f)} A(\boldsymbol{\rho}, \boldsymbol{\sigma})\, f_\xi d\boldsymbol{\rho} d\boldsymbol{\sigma} df\,. \tag{73}$$

But

$$\frac{1}{8\pi^3}\int_{-\infty}^{+\infty} e^{-i\boldsymbol{\sigma}\cdot f} f_\xi df = i\delta'(\sigma_\xi)\,\delta(\sigma_\eta)\,\delta(\sigma_\zeta)\,, \tag{74}$$

where the δ's denote Dirac's δ-functions and δ' the first derivative of the δ-function. Remembering that

$$\int_{-\infty}^{+\infty} f(x)\,\delta'(x)\,dx = -f'(0)\,, \tag{75}$$

we can reduce equation (73) to

$$\int_{-\infty}^{+\infty} W(\boldsymbol{F}, f)\, f_\xi df = -\frac{i}{8\pi^3}\int_{-\infty}^{+\infty} e^{-i\boldsymbol{\rho}\cdot\boldsymbol{F}}\left[\frac{\partial}{\partial\sigma_\xi} A(\boldsymbol{\rho}, \boldsymbol{\sigma})\right]_{|\boldsymbol{\sigma}|=0} d\boldsymbol{\rho}\,. \tag{76}$$

But, according to equation (68),

$$\left[\frac{\partial}{\partial\sigma_\xi} A(\boldsymbol{\rho}, \boldsymbol{\sigma})\right]_{|\boldsymbol{\sigma}|=0} = ige^{-a|\boldsymbol{\rho}|^{3/2}}\frac{\partial P(\boldsymbol{\sigma})}{\partial\sigma_\xi}\,, \tag{77}$$

since P is linear in $\boldsymbol{\sigma}$. Thus,

$$\int_{-\infty}^{+\infty} W(\boldsymbol{F}, f)\, f_\xi df = \frac{g_i}{8\pi^3}\int_{-\infty}^{+\infty} e^{-a|\boldsymbol{\rho}|^{3/2}-i\boldsymbol{\rho}\cdot\boldsymbol{F}}\left(\frac{\partial P}{\partial\sigma_\xi}\right) d\boldsymbol{\rho}\,, \tag{78}$$

or, choosing polar co-ordinates (see Fig. 1),

$$\int_{-\infty}^{+\infty} W(\boldsymbol{F}, f)\, f_\xi df = \frac{g}{8\pi^3}\int_0^\infty\int_0^\pi\int_0^{2\pi} e^{-a|\boldsymbol{\rho}|^{3/2}-i|\boldsymbol{\rho}||\boldsymbol{F}|\cos\vartheta}\left(\frac{\partial P}{\partial\sigma_\xi}\right)|\boldsymbol{\rho}|^2\sin\vartheta\, d|\boldsymbol{\rho}|\, d\vartheta d\omega\,. \tag{79}$$

Performing the integration over ω, we obtain

$$\int_{-\infty}^{+\infty} W(\boldsymbol{F}, f)\, f_\xi df = \frac{g}{4\pi^2}\int_0^\infty\int_{-1}^{+1} e^{-a|\boldsymbol{\rho}|^{3/2}-i|\boldsymbol{\rho}||\boldsymbol{F}|t}\left(\overline{\frac{\partial P}{\partial\sigma_\xi}}\right)|\boldsymbol{\rho}|^2 d|\boldsymbol{\rho}|\, dt\,, \tag{80}$$

where we have used a bar over $\partial P/\partial\sigma_\xi$ to denote that the averaging over ω has been carried out; further, in equation (80) we have changed from the variable ϑ to $t = \cos\vartheta$. Putting (cf. I, eq. [134])

$$|\boldsymbol{\rho}|\,|\boldsymbol{F}| = x\,; \qquad |\boldsymbol{F}| = a^{2/3}\beta \tag{81}$$

in equation (80) and remembering that $\overline{\partial P/\partial\sigma_\xi}$ is even in t (cf. eq. [87] below), we obtain

$$\int_{-\infty}^{+\infty} W(\boldsymbol{F}, f)\, f_\xi\, df = \frac{g}{2\pi^2 a^2\beta^3}\int_0^\infty\!\!\int_0^1 e^{-(x/\beta)^3/3}\left(\overline{\frac{\partial P}{\partial\sigma_\xi}}\right) x^2\cos xt\,dx\,dt\,. \tag{82}$$

The first moment of f_ξ is now obtained by dividing the foregoing equation by $W(\boldsymbol{F})$ (I, eq. [117]). We thus have

$$\overline{f_\xi} = \frac{2g}{\pi\beta H(\beta)}\int_0^\infty\!\!\int_0^1 e^{-(x/\beta)^3/3}\left(\overline{\frac{\partial P}{\partial\sigma_\xi}}\right) x^2\cos xt\,dx\,dt\,. \tag{83}$$

We have similar expressions for $\overline{f_\eta}$ and $\overline{f_\zeta}$.

We shall now evaluate $\overline{\partial P/\partial\sigma_\xi}$, etc., According to equation (67),

$$P = \sigma_1\sin\gamma - 2\sigma_3\cos\gamma\,, \tag{84}$$

or, transforming to the $\xi\eta\zeta$-system according to equation (72), we have

$$P = (\lambda_1\sigma_\xi + \mu_1\sigma_\eta + \nu_1\sigma_\zeta)\sin\gamma - 2(\lambda_3\sigma_\xi + \mu_3\sigma_\eta + \nu_3\sigma_\zeta)\cos\gamma\,. \tag{85}$$

Using the table of direction cosines (69) and after some rearranging of the terms, we obtain

$$\left.\begin{aligned} P = \sigma_\xi(1-3l^2)\sin\alpha + \sigma_\zeta(1-3n^2)\cos\alpha - 3ln(\sigma_\xi\cos\alpha + \sigma_\zeta\sin\alpha) \\ - 3\sigma_\eta m(l\sin\alpha + n\cos\alpha)\,. \end{aligned}\right\} \tag{86}$$

From this equation we readily find that

$$\left.\begin{aligned} \left(\overline{\frac{\partial P}{\partial\sigma_\xi}}\right) &= (1-3\overline{l^2})\sin\alpha - 3\overline{ln}\cos\alpha = -\tfrac{1}{2}(1-3l^2)\sin\alpha\,, \\ \left(\overline{\frac{\partial P}{\partial\sigma_\eta}}\right) &= -3(\overline{ml}\sin\alpha + \overline{mn}\cos\alpha) = 0\,, \\ \left(\overline{\frac{\partial P}{\partial\sigma_\zeta}}\right) &= (1-3\overline{n^2})\cos\alpha - 3\overline{ln}\sin\alpha = +(1-3l^2)\cos\alpha\,. \end{aligned}\right\} \tag{87}$$

Thus, according to equations (83) and (87), we have

$$\overline{f_\xi} = -\frac{g}{\pi\beta H(\beta)}\mathcal{J}(\beta)\sin\alpha\,; \qquad \overline{f_\eta} = 0\,; \qquad \overline{f_\zeta} = \frac{2g}{\pi\beta H(\beta)}\mathcal{J}(\beta)\cos\alpha\,, \tag{88}$$

where we have written

$$\mathcal{J}(\beta) = \int_0^\infty\!\!\int_0^1 e^{-(x/\beta)^3/3}x^2(1-3l^2)\cos xt\,dx\,dt\,. \tag{89}$$

We shall now evaluate $\mathcal{J}(\beta)$. Performing the integration over t, we obtain

$$\mathcal{J}(\beta) = \int_0^\infty e^{-(x/\beta)^{3/2}} x^2 \left\{ \frac{\sin x}{x} - \frac{3}{x^3}(2x \cos x + x^2 \sin x - 2 \sin x) \right\} dx \quad (90)$$

or, after some rearranging of the terms,

$$\mathcal{J}(\beta) = 6\int_0^\infty e^{-(x/\beta)^{3/2}} (\sin x - x \cos x) \frac{dx}{x} - 2\int_0^\infty e^{-(x/\beta)^{3/2}} x \sin x \, dx . \quad (91)$$

The second of the two integrals which occur in equation (91) is seen to be related very simply to the Holtsmark function $H(\beta)$, defined in I, equation (116). Further, denoting by $K(\beta)$ the integral

$$K(\beta) = \frac{2}{\pi}\int_0^\infty e^{-(x/\beta)^{3/2}} (\sin x - x \cos x) \frac{dx}{x} , \quad (92)$$

we have

$$\mathcal{J}(\beta) = 3\pi K(\beta) - \pi\beta H(\beta) . \quad (93)$$

Now

$$\left.\begin{aligned} \frac{dK}{d\beta} &= \frac{3}{\pi\beta^{5/2}}\int_0^\infty e^{-(x/\beta)^{3/2}} (\sin x - x \cos x)\, x^{1/2} dx \\ &= -\frac{2}{\pi\beta}\int_0^\infty \frac{d}{dx}\left(e^{-(x/\beta)^{3/2}}\right) (\sin x - x \cos x)\, dx , \end{aligned}\right\} \quad (94)$$

or, after integrating by parts, we have

$$\frac{dK}{d\beta} = \frac{2}{\pi\beta}\int_0^\infty e^{-(x/\beta)^{3/2}} x \sin x \, dx = H(\beta) . \quad (95)$$

Hence

$$K(\beta) = \int_0^\beta H(\beta)\, d\beta . \quad (96)$$

Now, combining equations (88), (93), and (96), we have

$$\overline{f_\xi} = -gB(\beta) \sin \alpha ; \qquad \overline{f_\eta} = 0 ; \qquad \overline{f_\zeta} = 2gB(\beta) \cos \alpha , \quad (97)$$

where

$$B(\beta) = 3\,\frac{\int_0^\beta H(\beta)\, d\beta}{\beta H(\beta)} - 1 . \quad (98)$$

The asymptotic properties of $B(\beta)$ are easily derived from those of $H(\beta)$ (I, eqs. [118] and [119]). We find that

$$B(\beta) = {}_1^1{}_5\Gamma\left({}_3^1{}^0\right)\beta^2 + O(\beta^4) , \qquad (\beta \to 0) \quad (99)$$

and

$$B(\beta) \backsim \frac{8}{5}\sqrt{\frac{\pi}{2}}\,\beta^{3/2} . \qquad (\beta \to \infty) \quad (100)$$

Consider now an arbitrary direction (l, m, n). Then

$$\overline{f}_{l,m,n} = l\overline{f}_\xi + n\overline{f}_\zeta , \tag{101}$$

or, according to equation (97),

$$\overline{f}_{l,m,n} = -\tfrac{2}{3}\pi G\overline{M}nB(\beta)\,|\,v\,|\,(l\sin\alpha - 2n\cos\alpha), \tag{102}$$

where we have substituted for g from equation (66). Remembering that the direction cosines of v are $(\sin\alpha, 0, \cos\alpha)$, we have

$$\left.\begin{aligned} |\,v\,|\,(l\sin\alpha - 2n\cos\alpha) &= |\,v\,|\,(l\sin\alpha + n\cos\alpha) - 3n\,|\,v\,|\cos\alpha \\ &= v\cdot 1_{l,m,n} - 3\,\frac{(v\cdot F)}{|F|^2}\,F\cdot 1_{l,m,n}, \end{aligned}\right\} \tag{103}$$

where $1_{l,m,n}$ stands for a unit vector in the direction (l, m, n). Hence we can re-write equation (102) as

$$\bar{f}\cdot 1_{l,m,n} = -\tfrac{2}{3}\pi G\overline{M}nB(\beta)\left[v - 3\,\frac{(v\cdot F)}{|F|^2}\,F\right]\cdot 1_{l,m,n} \tag{104}$$

or, more simply, as

$$\bar{f} = -\tfrac{2}{3}\pi G\overline{M}nB\left(\frac{|F|}{Q_H}\right)\left(v - 3\,\frac{(v\cdot F)}{|F|^2}\,F\right). \tag{105}$$

We shall return to this equation in § 11.

7. *The evaluation of the second moment of f.*—There are in general six independent moments of the second order that we have to consider, namely,

$$\overline{f_\xi^2},\quad \overline{f_\eta^2},\quad \overline{f_\zeta^2},\quad \overline{f_\xi f_\eta},\quad \overline{f_\eta f_\zeta},\quad \text{and}\quad \overline{f_\zeta f_\xi}. \tag{106}$$

In terms of these six moments, the second moment of the resolved component of f along any arbitrary direction can be specified. For, if $f_{l,m,n}$ denotes the component of f in the direction (l, m, n), then

$$\left.\begin{aligned} \overline{f_{l,m,n}^2} &= \overline{(lf_\xi + mf_\eta + nf_\zeta)^2} \\ &= l^2\overline{f_\xi^2} + m^2\overline{f_\eta^2} + n^2\overline{f_\zeta^2} + 2lm\overline{f_\xi f_\eta} + 2mn\overline{f_\eta f_\zeta} + 2nl\overline{f_\zeta f_\xi}. \end{aligned}\right\} \tag{107}$$

In our particular problem we should expect on symmetry grounds (and this is verified to to be the case) that two of the six moments (eq. [106]), namely, $\overline{f_\xi f_\eta}$ and $\overline{f_\eta f_\zeta}$, vanish identically (cf. eq. [97], according to which $\overline{f}_\eta = 0$). Accordingly, equation (107) reduces in our case to

$$\overline{f_{l,m,n}^2} = l^2\overline{f_\xi^2} + m^2\overline{f_\eta^2} + n^2\overline{f_\zeta^2} + 2nl\overline{f_\zeta f_\xi}. \tag{107}'$$

We shall first consider the moments $\overline{f_\xi^2}$, $\overline{f_\eta^2}$, and $\overline{f_\zeta^2}$. We have (cf. I, eq. [123])

$$\int_{-\infty}^{+\infty} W(F, f)\, f_\tau^2\, df = -\frac{1}{8\pi^3}\int_{-\infty}^{+\infty} e^{-i\rho\cdot F}\left[\frac{\partial^2}{\partial\sigma_\tau^2}\,A(\rho, \sigma)\right]_{|\sigma|=0} d\rho, \tag{108}$$

where we have used τ to denote either ξ, η, or ζ. Now, according to equation (68),

$$\left.\begin{aligned}\left[\frac{\partial^2}{\partial\sigma_\tau^2}A(\boldsymbol{\rho},\boldsymbol{\sigma})\right]_{|\boldsymbol{\sigma}|=0} &= -e^{-a|\boldsymbol{\rho}|^{3/2}}\left\{\tfrac{1}{2}g^2\frac{\partial^2}{\partial\sigma_\tau^2}P^2(\boldsymbol{\sigma})\right.\\ &\left.+b|\boldsymbol{\rho}|^{-3/2}\left[\frac{\partial^2}{\partial\sigma_\tau^2}Q(\boldsymbol{\sigma})+k\frac{\partial^2}{\partial\sigma_\tau^2}R(\boldsymbol{\sigma})\right]\right\}.\end{aligned}\right\} \tag{109}$$

Hence,

$$\left.\begin{aligned}\int_{-\infty}^{+\infty}W(\boldsymbol{F},f)\,f_\tau^2df &= \frac{1}{8\pi^3}\int_{-\infty}^{+\infty}e^{-a|\boldsymbol{\rho}|^{3/2}-i\boldsymbol{\rho}\cdot\boldsymbol{F}}\\ &\times\left\{\tfrac{1}{2}g^2\frac{\partial^2P^2}{\partial\sigma_\tau^2}+b|\boldsymbol{\rho}|^{-3/2}\left[\frac{\partial^2Q}{\partial\sigma_\tau^2}+k\frac{\partial^2R}{\partial\sigma_\tau^2}\right]\right\}d\boldsymbol{\rho},\end{aligned}\right\} \tag{110}$$

or, choosing polar co-ordinates in the (ξ, η, ζ)-system,

$$\left.\begin{aligned}\int_{-\infty}^{+\infty}W(\boldsymbol{F},f)\,f_\tau^2df &= \frac{1}{8\pi^3}\int_0^\infty\int_{-1}^{+1}\int_0^{2\pi}e^{-a|\boldsymbol{\rho}|^{3/2}-i|\boldsymbol{\rho}||\boldsymbol{F}|t}\\ &\times\left\{\tfrac{1}{2}g^2\frac{\partial^2P}{\partial\sigma_\tau^2}+b|\boldsymbol{\rho}|^{-3/2}\left[\frac{\partial^2Q}{\partial\sigma_\tau^2}+k\frac{\partial^2R}{\partial\sigma_\tau^2}\right]\right\}|\boldsymbol{\rho}|^2d\omega dtd|\boldsymbol{\rho}|.\end{aligned}\right\} \tag{111}$$

Performing the integration over the azimuthal angle ω and introducing the variable

$$x = |\boldsymbol{\rho}|\,|\boldsymbol{F}|; \qquad |\boldsymbol{F}| = a^{2/3}\beta, \tag{112}$$

equation (111) becomes

$$\left.\begin{aligned}\int_{-\infty}^{+\infty}W(\boldsymbol{F},f)\,f_\tau^2df &= \frac{1}{2\pi^2a^2\beta^3}\int_0^\infty\int_0^1 e^{-(x/\beta)^{3/2}}\left\{\tfrac{1}{2}g^2\left(\overline{\frac{\partial^2P^2}{\partial\sigma_\tau^2}}\right)\right.\\ &\left.+ab\beta^{3/2}\left[\left(\overline{\frac{\partial^2Q}{\partial\sigma_\tau^2}}\right)+k\left(\overline{\frac{\partial^2R}{\partial\sigma_\tau^2}}\right)\right]x^{-3/2}\right\}x^2\cos xtdtdx,\end{aligned}\right\} \tag{113}$$

where the bars over $\partial^2P^2/\partial\sigma_\tau^2$, etc., indicate that the averaging over ω has been carried out. We shall presently show that $\overline{\partial^2P^2/\partial\sigma_\tau^2}$, etc., have the forms

$$\left.\begin{aligned}\left(\overline{\frac{\partial^2P^2}{\partial\sigma_\tau^2}}\right) &= \mathcal{P}_{0,\tau}+\mathcal{P}_{2,\tau}t^2+\mathcal{P}_{4,\tau}t^4,\\ \left(\overline{\frac{\partial^2Q}{\partial\sigma_\tau^2}}\right) &= \mathcal{Q}_{0,\tau}+\mathcal{Q}_{2,\tau}t^2,\\ \left(\overline{\frac{\partial^2R}{\partial\sigma_\tau^2}}\right) &= \mathcal{R}_{0,\tau}+\mathcal{R}_{2,\tau}t^2+\mathcal{R}_{4,\tau}t^4,\end{aligned}\right\} \quad(\tau=\xi,\eta,\zeta) \tag{114}$$

where $\mathcal{P}_{0,\tau}, \ldots, \mathcal{R}_{4,\tau}$ are constants with respect to the variables of integration in equation (113). Substituting these equivalents for $\overline{\partial^2P^2/\partial\sigma_\tau^2}$, etc., in equation (113) and di-

viding throughout by $W(\boldsymbol{F})$ according to I, equation (117), we obtain for the moment of f_τ^2 the expression

$$\left.\begin{aligned}\overline{f_\tau^2} = \frac{2ab\beta^{1/2}}{\pi H(\beta)} \int_0^\infty\!\!\int_0^1 e^{-(x/\beta)^{3/2}} (\mathfrak{L}_{0,\tau} + \mathfrak{L}_{2,\tau} t^2 + \mathfrak{L}_{4,\tau} t^4)\, x^{1/2} \cos(xt)\, dx dt \\ + \frac{g^2}{\pi\beta H(\beta)} \int_0^\infty\!\!\int_0^1 e^{-(x/\beta)^{3/2}} (\mathfrak{P}_{0,\tau} + \mathfrak{P}_{2,\tau} t^2 + \mathfrak{P}_{4,\tau} t^4)\, x^2 \cos(xt)\, dx dt ,\end{aligned}\right\} \quad (115)$$

where, for the sake of brevity, we have written

$$\mathfrak{L}_{0,\tau} = \mathfrak{Q}_{0,\tau} + k^2 \mathfrak{R}_{0,\tau}; \quad \mathfrak{L}_{2,\tau} = \mathfrak{Q}_{2,\tau} + k^2 \mathfrak{R}_{2,\tau}; \quad \mathfrak{L}_{4,\tau} = k^2 \mathfrak{R}_{4,\tau} \quad (\tau = \xi, \eta, \zeta). \quad (116)$$

In equation (115) the integration over t can now be effected. Using the elementary formulae

$$\left.\begin{aligned}\int_0^1 \cos xt\, dt &= \frac{\sin x}{x}, \\ \int_0^1 t^2 \cos xt\, dt &= \frac{\sin x}{x} - \frac{2}{x^3}(\sin x - x\cos x), \\ \int_0^1 t^4 \cos xt\, dt &= \frac{\sin x}{x} - \frac{4}{x^5}(-x^3\cos x + 6x\cos x + 3x^2 \sin x - 6\sin x),\end{aligned}\right\} \quad (117)$$

we readily obtain from equation (115)

$$\left.\begin{aligned}\overline{f_\tau^2} = ab\frac{\beta^{1/2}}{H(\beta)} \left\{ (\mathfrak{L}_{0,\tau} + \mathfrak{L}_{2,\tau} + \mathfrak{L}_{4,\tau}) G(\beta) - 2\mathfrak{L}_{2,\tau} I(\beta) - 4\mathfrak{L}_{4,\tau} J(\beta) \right\} \\ + \frac{g^2}{2\beta H(\beta)} \left\{ (\mathfrak{P}_{0,\tau} + \mathfrak{P}_{2,\tau} + \mathfrak{P}_{4,\tau})\, \beta H(\beta) - 2\mathfrak{P}_{2,\tau} K(\beta) - 4\mathfrak{P}_{4,\tau} L(\beta) \right\},\end{aligned}\right\} \quad (118)$$

where G, H, I, J, K, and L are functions of β defined by

$$\left.\begin{aligned}G(\beta) &= \frac{2}{\pi}\int_0^\infty e^{-(x/\beta)^{3/2}} x^{-1/2} \sin x\, dx, \\ H(\beta) &= \frac{2}{\pi\beta}\int_0^\infty e^{-(x/\beta)^{3/2}} x \sin x\, dx, \\ I(\beta) &= \frac{2}{\pi}\int_0^\infty e^{-(x/\beta)^{3/2}} x^{-5/2} (\sin x - x\cos x)\, dx, \\ J(\beta) &= \frac{2}{\pi}\int_0^\infty e^{-(x/\beta)^{3/2}} x^{-9/2} (-x^3\cos x + 6x\cos x + 3x^2\sin x - 6\sin x)\, dx, \\ K(\beta) &= \frac{2}{\pi}\int_0^\infty e^{-(x/\beta)^{3/2}} x^{-1} (\sin x - x\cos x)\, dx, \\ L(\beta) &= \frac{2}{\pi}\int_0^\infty e^{-(x/\beta)^{3/2}} x^{-3} (-x^3\cos x + 6x\cos x + 3x^2\sin x - 6\sin x)\, dx.\end{aligned}\right\} \quad (119)^5$$

[5] We may draw attention to the fact that we have not changed here our definition of $H(\beta)$; it represents the Holtsmark function as hitherto; similarly, our present definitions of $G(\beta)$ and $K(\beta)$ agree with those we have given earlier (I, eq. [159] and eq. [92] of this paper). However, the functions $I(\beta)$, $J(\beta)$, and $L(\beta)$ are introduced here for the first time.

It remains to obtain the expressions for $\mathcal{L}_{0,\tau}, \ldots, \mathcal{P}_{4,\tau}$ ($\tau = \xi, \eta, \zeta$). The calculations are straightforward but somewhat tedious. But we shall illustrate the method by outlining the derivation of $\mathfrak{R}_{0,\xi}$, $\mathfrak{R}_{2,\xi}$, and $\mathfrak{R}_{4,\xi}$:

According to equation (67)

$$\left.\begin{aligned}\frac{\partial^2 R}{\partial \sigma_\xi^2} = \frac{\partial^2}{\partial \sigma_\xi^2}\,(&\sigma_1^2[5\sin^2\gamma - 2\cos^2\gamma] + \sigma_2^2[4\sin^2\gamma - 2\cos^2\gamma] \\ &+ \sigma_3^2[4\cos^2\gamma - 2\sin^2\gamma] - 8\sigma_3\sigma_1\sin\gamma\cos\gamma)\,.\end{aligned}\right\} \quad (120)$$

To carry out the differentiation we must first apply to $(\sigma_1, \sigma_2, \sigma_3)$ the linear transformation (72). It is, however, not necessary to carry out this transformation explicitly. For, since clearly

$$\frac{\partial^2 \sigma_i^2}{\partial \sigma_\xi^2} = 2\lambda_i^2 \qquad (i = 1, 2, 3)\,; \qquad \frac{\partial^2 (\sigma_3\sigma_1)}{\partial \sigma_\xi^2} = 2\lambda_1\lambda_3\,, \quad (121)$$

we have

$$\left.\begin{aligned}\frac{\partial^2 R}{\partial \sigma_\xi^2} = 2\,[&\lambda_1^2(5\sin^2\gamma - 2\cos^2\gamma) + \lambda_2^2(4\sin^2\gamma - 2\cos^2\gamma) \\ &+ \lambda_3^2(4\cos^2\gamma - 2\sin^2\gamma) - 8\lambda_1\lambda_3\sin\gamma\cos\gamma]\end{aligned}\right\} \quad (122)$$

or, after some minor reductions,

$$\frac{\partial^2 R}{\partial \sigma_\xi^2} = 2\,[-2 + 6\lambda_3^2\cos^2\gamma + (7\lambda_1^2 + 6\lambda_2^2)\sin^2\gamma - 8\lambda_1\lambda_3\sin\gamma\cos\gamma]\,. \quad (123)$$

Substituting for λ_1, λ_2, and λ_3 from the table of direction cosines (69) and using for $\cos\gamma$ its equivalent (71), we obtain, after some rearranging of the terms,

$$\left.\begin{aligned}\frac{\partial^2 R}{\partial \sigma_\xi^2} = 2\,[&-2 + 21l^4\sin^2\alpha + 21l^2n^2\cos^2\alpha + 42l^3n\sin\alpha\cos\alpha + 7\sin^2\alpha \\ &+ 6m^2\cos^2\alpha - 22l^2\sin^2\alpha - 22ln\sin\alpha\cos\alpha]\,,\end{aligned}\right\} \quad (124)$$

where it will be recalled that α is the angle between $\boldsymbol{F}$ and $\boldsymbol{v}$. Averaging the quantity on the right-hand side of equation (142), we finally obtain

$$\left(\overline{\frac{\partial^2 R}{\partial \sigma_\xi^2}}\right) = (2 + \tfrac{7}{4}\sin^2\alpha) + (15 - \tfrac{49}{2}\sin^2\alpha)\,l^2 + (-21 + \tfrac{147}{4}\sin^2\alpha)\,l^4\,, \quad (125)$$

from which the values of $\mathfrak{R}_{0,\xi}$, $\mathfrak{R}_{2,\xi}$, and $\mathfrak{R}_{4,\xi}$ can at once be read. The evaluation of the other quantities proceeds similarly. Collecting all the results, we obtain the following table of values:

$$\left.\begin{aligned}\mathcal{P}_{0,\xi} &= \tfrac{11}{4}\sin^2\alpha\,; & \mathcal{P}_{2,\xi} &= +9 - \tfrac{33}{2}\sin^2\alpha\,; & \mathcal{P}_{4,\xi} &= -9 + \tfrac{63}{4}\sin^2\alpha\,,\\ \mathcal{P}_{0,\eta} &= \tfrac{9}{4}\sin^2\alpha\,; & \mathcal{P}_{2,\eta} &= +9 - \tfrac{37}{2}\sin^2\alpha\,; & \mathcal{P}_{4,\eta} &= -9 + \tfrac{45}{4}\sin^2\alpha\,,\\ \mathcal{P}_{0,\zeta} &= 2\cos^2\alpha\,; & \mathcal{P}_{2,\zeta} &= -12 + 21\sin^2\alpha\,; & \mathcal{P}_{4,\zeta} &= +18 - 27\sin^2\alpha\,;\end{aligned}\right\} \quad (126)$$

$$\left.\begin{aligned}\mathcal{Q}_{0,\xi} &= 1 & ;\ \mathcal{Q}_{2,\xi} &= +1 & ;\ \mathcal{Q}_{4,\xi} &= 0\,,\\ \mathcal{Q}_{0,\eta} &= 1 & ;\ \mathcal{Q}_{2,\eta} &= +1 & ;\ \mathcal{Q}_{4,\eta} &= 0\,,\\ \mathcal{Q}_{0,\zeta} &= 2 & ;\ \mathcal{Q}_{2,\zeta} &= -2 & ;\ \mathcal{Q}_{4,\zeta} &= 0\,;\end{aligned}\right\} \quad (127)$$

and

$$\left.\begin{aligned}
&\mathfrak{R}_{0,\xi} = 2 + \tfrac{7}{4}\sin^2\alpha\,; \quad \mathfrak{R}_{2,\xi} = +15 - \tfrac{49}{2}\sin^2\alpha\,; \quad \mathfrak{R}_{4,\xi} = -21 + \tfrac{147}{4}\sin^2\alpha\,,\\
&\mathfrak{R}_{0,\eta} = 2 - \tfrac{3}{4}\sin^2\alpha\,; \quad \mathfrak{R}_{2,\eta} = +15 - \tfrac{27}{2}\sin^2\alpha\,; \quad \mathfrak{R}_{4,\eta} = -21 + \tfrac{105}{4}\sin^2\alpha\,,\\
&\mathfrak{R}_{0,\zeta} = 10 - 8\sin^2\alpha\,; \quad \mathfrak{R}_{2,\zeta} = -44 + 59\sin^2\alpha\,; \quad \mathfrak{R}_{4,\zeta} = +42 - 63\sin^2\alpha\,.
\end{aligned}\right\} \tag{128}$$

We have still to evaluate the cross-moments $\overline{f_\xi f_\eta}$, $\overline{f_\eta f_\zeta}$, and $\overline{f_\zeta f_\xi}$. As we have already stated, the first two vanish identically, and we have only to consider $\overline{f_\zeta f_\xi}$. Analogous to equation (110) we now have

$$\left.\begin{aligned}
\int_{-\infty}^{+\infty} W(\boldsymbol{F},\boldsymbol{f})\, f_\xi f_\zeta d\boldsymbol{f} = \frac{1}{8\pi^3}\int_{-\infty}^{+\infty} e^{-a|\boldsymbol{\rho}|^{3/2} - i\boldsymbol{\rho}\cdot\boldsymbol{F}}\\
\times\left\{\tfrac{1}{2}g^2\frac{\partial^2 P^2}{\partial\sigma_\xi\partial\sigma_\zeta} + b\,|\boldsymbol{\rho}|^{-3/2}\left[\frac{\partial^2 Q}{\partial\sigma_\xi\partial\sigma_\zeta} + k\,\frac{\partial^2 R}{\partial\sigma_\xi\partial\sigma_\zeta}\right]\right\} d\boldsymbol{\rho}\,,
\end{aligned}\right\} \tag{129}$$

or, changing to polar co-ordinates and integrating over ω, we find (cf. eq. [113])

$$\left.\begin{aligned}
\int_{-\infty}^{+\infty} W(\boldsymbol{F},\boldsymbol{f})\, f_\xi f_\zeta d\boldsymbol{f} = \frac{1}{2\pi^2\alpha^2\beta^3}\int_0^\infty\!\!\int_0^1 e^{-(x/\beta)^{3/2}}\left\{\tfrac{1}{2}g^2\left(\overline{\frac{\partial^2 P}{\partial\sigma_\xi\partial\sigma_\zeta}}\right)\right.\\
\left. + a\,b\beta^{3/2}\left[\left(\overline{\frac{\partial^2 Q}{\partial\sigma_\xi\partial\sigma_\zeta}}\right) + k\left(\overline{\frac{\partial^2 R}{\partial\sigma_\zeta\partial\sigma_\zeta}}\right)\right] x^{-3/2}\right\} x^2\cos x t\, dt\, dx\,,
\end{aligned}\right\} \tag{130}$$

where we have made a further change of variables according to equation (112). In equation (130) the bars are again to be understood as indicating that the corresponding quantities have been averaged over ω. An elementary, but somewhat lengthy, calculation yields

$$\left.\begin{aligned}
\left(\overline{\frac{\partial^2 P^2}{\partial\sigma_\xi\partial\sigma_\zeta}}\right) &= (-1 + 15t^2 - 18t^4)\sin\alpha\cos\alpha\,,\\
\left(\overline{\frac{\partial^2 R}{\partial\sigma_\xi\partial\sigma_\zeta}}\right) &= (-3 + 37t^2 - 42t^4)\sin\alpha\cos\alpha\,.
\end{aligned}\right\} \tag{131}$$

Further,

$$\left(\overline{\frac{\partial^2 Q}{\partial\sigma_\xi\partial\sigma_\zeta}}\right) = 0\,. \tag{132}$$

Substituting these formulae in equations (130) and dividing throughout by $W(\boldsymbol{F})$ according to I, equation (117), we obtain

$$\left.\begin{aligned}
\overline{f_\xi f_\zeta} = \left\{\frac{2a\,bk\beta^{1/2}}{\pi H(\beta)}\int_0^\infty\!\!\int_0^1 e^{-(x/\beta)^{3/2}}(-3 + 37t^2 - 42t^4)\,x^{1/2}\cos x t\, dt\, dx\right.\\
\left. + \frac{g^2}{\pi\beta H(\beta)}\int_0^\infty\!\!\int_0^1 e^{-(x/\beta)^{3/2}}(-1 + 15t^2 - 18t^4)\,x^2\cos x t\, dt\, dx\right\}\sin\alpha\cos\alpha\,,
\end{aligned}\right\} \tag{133}$$

or, integrating over t and introducing the auxiliary functions $G, \ldots, L$, according to equation (119), we have

$$\left.\begin{aligned}\overline{f_\xi f_\zeta} = \Big\{ a\,b\,k\,\frac{\beta^{1/2}}{H(\beta)}\,[-8G(\beta) - 74I(\beta) + 168J(\beta)] \\ + \frac{g^2}{2\beta H(\beta)}\,[-4\beta H(\beta) - 30K(\beta) + 72L(\beta)]\Big\}\,\sin\alpha\cos\alpha\,.\end{aligned}\right\} \quad (134)$$

Equations (118) and (134), together with

$$\overline{f_\xi f_\eta} \equiv 0\,; \qquad \overline{f_\eta f_\zeta} \equiv 0\,, \quad (135)$$

represent, then, our expressions for the six independent second-order moments.

8. *The moment* $|f|^2$ *and its average* $\overline{|f|^2}$. *The mean life of the state* F.—In § 7 we evaluated all the independent second-order moments that exist and, as we have already stated, the second moment of the resolved component of f along any direction can be specified in terms of them. However, the most important quantity is the average value of $|f|^2$. This is clearly given by

$$\overline{|f|^2} = \sum_{\tau=\xi,\,\eta,\,\zeta} \overline{f_\tau^2} \quad (136)$$

or, according to equation (118), by

$$\left.\begin{aligned}\overline{|f|^2} = a\,b\,\frac{\beta^{1/2}}{H(\beta)}\,\Big\{\Big(\sum_{i=0,\,2,\,4}\ \sum_{\tau=\xi,\,\eta,\,\zeta} \mathcal{L}_{i,\,\tau}\Big)G(\beta) - 2\Big(\sum_{\tau=\xi,\,\eta,\,\zeta}\mathcal{L}_{2,\,\tau}\Big)I(\beta) \\ - 4\Big(\sum_{\tau=\xi,\,\eta,\,\zeta}\mathcal{L}_{4,\,\tau}\Big)J(\beta)\Big\} + \frac{g^2}{2\beta H(\beta)}\,\Big\{\Big(\sum_{i=0,\,2,\,4}\ \sum_{\tau=\xi,\,\eta,\,\zeta}\mathcal{P}_{i,\,\tau}\Big)\beta H(\beta) \\ - 2\Big(\sum_{\tau=\xi,\,\eta,\,\zeta}\mathcal{P}_{2,\,\tau}\Big)K(\beta) - 4\Big(\sum_{\tau=\xi,\,\eta,\,\zeta}\mathcal{P}_{4,\,\tau}\Big)L(\beta)\Big\}\,.\end{aligned}\right\} \quad (137)$$

On the other hand, from equations (126)–(128) we find that

$$\left.\begin{aligned}&\sum_\tau \mathcal{P}_{0,\,\tau} = 5\sin^2\alpha + 2\cos^2\alpha\,; \quad \sum_\tau \mathcal{P}_{2,\,\tau} = 6 - 9\sin^2\alpha\,; \quad \sum_\tau \mathcal{P}_{4,\,\tau} = 0\,, \\ &\sum_\tau \mathcal{Q}_{0,\,\tau} = 4\,; \quad \sum_\tau \mathcal{Q}_{2,\,\tau} = 0\,; \quad \sum_\tau \mathcal{Q}_{4,\,\tau} = 0\,, \\ &\sum_\tau \mathcal{R}_{0,\,\tau} = 14 - 7\sin^2\alpha\,; \quad \sum_\tau \mathcal{R}_{2,\,\tau} = -14 + 21\sin^2\alpha\,; \quad \sum_\tau \mathcal{R}_{4,\,\tau} = 0\,.\end{aligned}\right\} \quad (138)$$

Again, according to equations (138),

$$\sum_i \sum_\tau \mathcal{P}_{i,\,\tau} = 8 - 6\sin^2\alpha\,; \quad \sum_i \sum_\tau \mathcal{Q}_{i,\,\tau} = 4\,; \quad \sum_i \sum_\tau \mathcal{R}_{i,\,\tau} = 14\sin^2\alpha\,. \quad (139)$$

We thus have

$$\left.\begin{aligned}\overline{|f|^2}_{F,\,v} = 2\,a\,b\,\frac{\beta^{1/2}}{H(\beta)}\,\Big\{2G(\beta) + 7k\,[\sin^2\alpha\,G(\beta) - (3\sin^2\alpha - 2)\,I(\beta)]\Big\} \\ + \frac{g^2}{\beta H(\beta)}\,\Big\{(4 - 3\sin^2\alpha)\,\beta H(\beta) + 3\,(3\sin^2\alpha - 2)\,K(\beta)\Big\}\,.\end{aligned}\right\} \quad (140)$$

The foregoing expression gives the mean square value of the rate of change, f, to be expected in the intensity of the force, F, acting on a star when it is further known that the direction of F makes an angle α with the direction of motion. But the possible directions of F, for a given direction of motion, are distributed uniformly over the unit sphere. Hence, the mean square value of f for a given value of F and for all relative orientations of the two vectors F and v is obtained by simply averaging equation (140) over α. We thus obtain

$$\overline{|f|^2}_{|F|,\,|v|} = 4ab\left\{\frac{\beta^{1/2}G(\beta)}{H(\beta)}\left(1+\tfrac{2}{3}k\right)+\frac{g^2}{2ab}\right\}; \tag{141}$$

or, substituting for k and $g^2/2ab$ from equation (66), we find that

$$\overline{|f|^2}_{|F|,\,|v|} = 4ab\left\{\frac{\beta^{1/2}G(\beta)}{H(\beta)}\left(1+\frac{\overline{M^{1/2}}\,|v|^2}{\overline{M^{1/2}}\,|u|^2}\right)+\frac{5}{12\pi}\frac{\overline{M^2}\,|v|^2}{\overline{M^{3/2}}\,\overline{M^{1/2}}\,|u|^2}\right\}. \tag{142}$$

If $|v| \to 0$, we recover the formula of our earlier paper (cf. I, eq. [158]).

The formula (142) has an immediate application for estimating the mean life of the state of fluctuation in which a force F per unit mass acts on a star moving with a speed $|v|$. For, arguing as in I, § 9, we may define the mean life by the equation

$$T_{|F|,\,|v|} = \frac{|F|}{\sqrt{\overline{|f|^2}_{|F|,\,|v|}}}. \tag{143}$$

According to equations (112) and (142), we therefore have

$$\left.\begin{aligned} T_{|F|,\,|v|} = \left[\frac{a^{1/3}}{4b}\frac{\beta^{3/2}H(\beta)}{G(\beta)}\right]^{1/2}\left[1+\frac{\overline{M^{1/2}}\,|v|^2}{\overline{M^{1/2}}\,|u|^2}+\frac{5}{12\pi}\frac{\overline{M^2}\,|v|^2}{\overline{M^{3/2}}\,\overline{M^{1/2}}\,|u|^2}\right. \\ \left.\times\frac{H(\beta)}{\beta^{1/2}G(\beta)}\right]^{-1/2}. \end{aligned}\right\} \tag{144}$$

From this equation we derive the relation

$$T_{|F|,\,|v|} = T_{|F|,\,0}\left[1+\frac{\overline{M^{1/2}}\,|v|^2}{\overline{M^{1/2}}\,|u|^2}+\frac{5}{12\pi}\frac{\overline{M^2}\,|v|^2}{\overline{M^{3/2}}\,\overline{M^{1/2}}\,|u|^2}\frac{H(\beta)}{\beta^{1/2}G(\beta)}\right]^{-1/2}. \tag{145}$$

9. *The auxiliary functions* G, H, I, J, K, *and* L.—In §§ 6, 7, and 8 we have seen that our expressions for the various moments involve some or all of the functions $G(\beta)$, $H(\beta)$, $I(\beta)$, $J(\beta)$, $K(\beta)$, and $L(\beta)$. These functions are all defined by certain definite integrals (eq. [119]), the integrands of which contain β as a parameter. We shall now show how the functions $G(\beta)$, $I(\beta)$, $J(\beta)$, $K(\beta)$, and $L(\beta)$ can all be expressed in terms of the Holtsmark function, $H(\beta)$. We shall also establish certain relations which exist among them.

We have already seen that the functions $G(\beta)$ and $K(\beta)$ are related to $H(\beta)$, according to the formulae (eq. [96] and I, eq. [162]),

$$G(\beta) = \frac{3}{2}\int_0^\beta \beta^{-3/2}H(\beta)\,d\beta \tag{146}$$

and

$$K(\beta) = \int_0^\beta H(\beta)\,d\beta. \tag{147}$$

It remains to establish similar relations for I, J, and L.

Consider, first, $I(\beta)$. Writing the integral, defining it in the form

$$I(\beta) = -\frac{4}{3\pi}\int_0^\infty e^{-(x/\beta)^{3/2}}(\sin x - x\cos x)\frac{d}{dx}(x^{-3/2})\,dx\,, \tag{148}$$

and integrating by parts, we find

$$I(\beta) = \frac{4}{3\pi}\int_0^\infty e^{-(x/\beta)^{3/2}}x^{-1/2}\sin x\,dx - \frac{2}{\pi\beta^{3/2}}\int_0^\infty e^{-(x/\beta)^{3/2}}(\sin x - x\cos x)\frac{dx}{x}, \tag{149}$$

or, remembering our definition of $G(\beta)$ (eq. [119]), we have

$$I(\beta) = \tfrac{2}{3}G(\beta) - \frac{2}{\pi\beta^{3/2}}\int_0^\infty e^{-(x/\beta)^{3/2}}(\sin x - x\cos x)\,x^{-1}dx\,. \tag{150}$$

But

$$\frac{dI}{d\beta} = \frac{3}{\pi\beta^{5/2}}\int_0^\infty e^{-(x/\beta)^{3/2}}(\sin x - x\cos x)\,x^{-1}dx\,. \tag{151}$$

Hence,

$$I(\beta) = \tfrac{2}{3}G(\beta) - \tfrac{2}{3}\beta\frac{dI}{d\beta}; \tag{152}$$

in other words, $I(\beta)$ satisfies the differential equation

$$\beta\frac{dI}{d\beta} + \tfrac{3}{2}I = G(\beta)\,. \tag{153}$$

The solution of equation (153) appropriate for us is

$$I(\beta) = \beta^{-3/2}\int_0^\beta \beta^{1/2}G(\beta)\,d\beta\,. \tag{154}$$

This formula is useful for the purposes of numerically evaluating the function $I(\beta)$.

We shall now establish for $J(\beta)$ a relation similar to equation (154). We have

$$\left.\begin{aligned} J(\beta) &= -\frac{4}{7\pi}\int_0^\infty e^{-(x/\beta)^{3/2}}(-x^3\cos x + 6x\cos x + 3x^2\sin x - 6\sin x) \\ &\qquad\qquad \times\frac{d}{dx}(x^{-7/2})\,dx \\ &= \frac{4}{7\pi}\int_0^\infty e^{-(x/\beta)^{3/2}}x^{-1/2}\sin x\,dx \\ &\quad - \frac{6}{7\pi\beta^{3/2}}\int_0^\infty e^{-(x/\beta)^{3/2}}(-x^3\cos x + 6x\cos x + 3x^2\sin x - 6\sin x)\frac{dx}{x^3} \\ &= \tfrac{2}{7}G(\beta) - \tfrac{2}{7}\beta\frac{dJ}{d\beta}\,. \end{aligned}\right\} \tag{155}$$

Hence $J(\beta)$ satisfies the differential equation

$$\beta\frac{dJ}{d\beta} + \tfrac{7}{2}J = G(\beta)\,. \tag{156}$$

Consequently,

$$J(\beta) = \beta^{-7/2} \int_0^\beta \beta^{5/2} G(\beta)\, d\beta . \tag{157}$$

This is the required formula.

By following a procedure exactly similar to that adopted for treating $I(\beta)$ and $J(\beta)$ we can show that $L(\beta)$ satisfies the differential equation

$$\beta \frac{dL}{d\beta} + 2L = \beta H(\beta) \tag{158}$$

and that therefore

$$L(\beta) = \beta^{-2} \int_0^\beta \beta^2 H(\beta)\, d\beta . \tag{159}$$

Further, according to equations (150) and (155), we have the relations

$$I(\beta) = \tfrac{2}{3} G(\beta) - \beta^{-3/2} K(\beta) \tag{160}$$

and

$$J(\beta) = \tfrac{2}{7} G(\beta) - \tfrac{3}{7} \beta^{-3/2} L(\beta) . \tag{161}$$

Finally, we may note the following asymptotic forms for the various functions:

$$\left.\begin{array}{ll} \beta \to 0 & \beta \to \infty \\ G(\beta) \to \dfrac{4}{3\pi} \beta^{3/2} & G(\beta) \to \sqrt{\dfrac{2}{\pi}} \\ H(\beta) \to \dfrac{4}{3\pi} \beta^{2} & H(\beta) \to \dfrac{15}{8} \sqrt{\dfrac{2}{\pi}}\, \beta^{-5/2} \\ I(\beta) \to \dfrac{4}{9\pi} \beta^{3/2} & I(\beta) \to \dfrac{2}{3} \sqrt{\dfrac{2}{\pi}} \\ J(\beta) \to \dfrac{4}{15\pi} \beta^{3/2} & J(\beta) \to \dfrac{2}{7} \sqrt{\dfrac{2}{\pi}} \\ K(\beta) \to \dfrac{4}{9\pi} \beta^{3} & K(\beta) \to 1 \\ L(\beta) \to \dfrac{4}{15\pi} \beta^{3} & L(\beta) \to \dfrac{15}{4} \sqrt{\dfrac{2}{\pi}}\, \beta^{-3/2} \\ B(\beta) \to \tfrac{1}{15} \Gamma(\tfrac{1}{3}^{0})\, \beta^{2} & B(\beta) \to \dfrac{8}{5} \sqrt{\dfrac{\pi}{2}}\, \beta^{3/2} \end{array}\right\} \tag{162}$$

10. *The correlations in* $\boldsymbol{F}$ *acting at two very close points.*—The formal theory developed in the preceding sections has direct applications to a different problem, namely, that of the correlations in the force acting at two very close points, for the difference between the values of $\boldsymbol{F}$ acting at two points distant $\delta\boldsymbol{r}$ from each other is given by

$$\Delta \boldsymbol{F} = G \sum_i M_i \left\{ \frac{\delta \boldsymbol{r}}{|\boldsymbol{r}_i|^3} - 3 \frac{\boldsymbol{r}_i (\boldsymbol{r}_i \cdot \delta \boldsymbol{r}_i)}{|\boldsymbol{r}_i|^5} \right\}, \tag{163}$$[6]

where we have assumed that one of the points is at the origin of our system of coordinates. Comparing equations (3) and (163), we see that formally the problems of specifying the distributions $W(\boldsymbol{F}, \boldsymbol{f})$ and $W(\boldsymbol{F}, \Delta \boldsymbol{F})$ differ only to the extent that, while in the first case we have to allow for a distribution over the relative velocities $\boldsymbol{V}$, in our present problem $\delta\boldsymbol{r}$ is a fixed constant vector.

[6] We discuss later in this section the validity of this formula.

Thus, expressing $W(\boldsymbol{F}, \Delta\boldsymbol{F})$ in the form

$$W(\boldsymbol{F}, \Delta\boldsymbol{F}) = \frac{1}{64\pi^6}\int_{-\infty}^{+\infty}\int_{-\infty}^{+\infty} e^{-i(\boldsymbol{\rho}\cdot\boldsymbol{F}+\boldsymbol{\sigma}\cdot\Delta\boldsymbol{F})} A(\boldsymbol{\rho}, \boldsymbol{\sigma})\, d\boldsymbol{\rho} d\boldsymbol{\sigma}\,, \tag{164}$$

we have (cf. eq. [12])

$$A(\boldsymbol{\rho}, \boldsymbol{\sigma}) = e^{-nC(\boldsymbol{\rho}, \boldsymbol{\sigma})}\,, \tag{165}$$

where (cf. eq. [15])

$$C(\boldsymbol{\rho}, \boldsymbol{\sigma}) = \tfrac{1}{2}G^{3/2}\int_0^\infty dM\,\chi(M)\,M^{3/2}\int_{-\infty}^{+\infty}\{1 - e^{i(\boldsymbol{\rho}\cdot\boldsymbol{\Phi}+\boldsymbol{\sigma}\cdot\boldsymbol{\Psi})}\}\,|\,\boldsymbol{\Phi}\,|^{-9/2}d\boldsymbol{\Phi}\,. \tag{166}$$

In equation (166) $\boldsymbol{\Psi}$ now stands for (cf. eq. [16])

$$\boldsymbol{\Psi} = (GM)^{-1/2}\{\,|\,\boldsymbol{\Phi}\,|^{3/2}\delta\boldsymbol{r} - 3\,|\,\boldsymbol{\Phi}\,|^{-1/2}(\boldsymbol{\Phi}\cdot\delta\boldsymbol{r})\,\boldsymbol{\Phi}\}\,. \tag{167}$$

From this point on, the analysis proceeds exactly as in §§ 3, 4, and 5. It is thus seen that equation (64) is now replaced by (cf. eq. [56])

$$\left.\begin{aligned} C(\boldsymbol{\rho}, \boldsymbol{\sigma}) &= \tfrac{4}{15}(2\pi)^{3/2}G^{3/2}\overline{M^{3/2}}\,|\,\boldsymbol{\rho}\,|^{3/2} + \tfrac{2}{3}\pi i G\overline{M}\,|\,\delta\boldsymbol{r}\,|\,(\sigma_1\sin\gamma - 2\sigma_3\cos\gamma) \\ &+ \tfrac{3}{28}(2\pi)^{3/2}G^{1/2}\overline{M^{1/2}}\,|\,\delta\boldsymbol{r}\,|^2\,|\,\boldsymbol{\rho}\,|^{-3/2}[\sigma_1^2(5\sin^2\gamma - 2\cos^2\gamma) + \sigma_2^2(4\sin^2\gamma \\ &- 2\cos^2\gamma) + \sigma_3^2(4\cos^2\gamma - 2\sin^2\gamma) - 8\sigma_1\sigma_3\sin\gamma\cos\gamma] + O(|\,\boldsymbol{\sigma}\,|^3)\,, \end{aligned}\right\} \tag{168}$$

where

$$\gamma = \sphericalangle(\boldsymbol{\rho}, \delta\boldsymbol{r}) \tag{169}$$

and the co-ordinate system has been so chosen that the z-axis is in the direction of $\boldsymbol{\rho}$ and $\delta\boldsymbol{r}$ lies in the xz-plane (see Fig. 1). Hence,

$$A(\boldsymbol{\rho}, \boldsymbol{\sigma}) = e^{-a|\boldsymbol{\rho}|^{3/2} - ig'P(\boldsymbol{\sigma}) - b'|\boldsymbol{\rho}|^{-3/2}R(\boldsymbol{\sigma}) + O(|\boldsymbol{\sigma}|^2)}\,, \tag{170}$$

where a, $P(\boldsymbol{\sigma})$, and $R(\boldsymbol{\sigma})$ have the same meanings as in equations (66) and (67), while b' and g' now stand for

$$b' = \tfrac{3}{28}(2\pi)^{3/2}G^{1/2}\overline{M^{1/2}}\,|\,\delta\boldsymbol{r}\,|^2 n\,; \qquad g' = \tfrac{2}{3}\pi G\overline{M}\,|\,\delta\boldsymbol{r}\,|\,n\,. \tag{171}$$

The evaluation of the first and the second moments of $\Delta\boldsymbol{F}$ proceeds as in §§ 6, 7, and 8. Thus, analogous to equation (105), we now have

$$\overline{\Delta\boldsymbol{F}}_{\boldsymbol{F},\,\delta\boldsymbol{r}} = \tfrac{2}{3}\pi G\overline{M}\,nB\left(\frac{|\,\boldsymbol{F}\,|}{Q_H}\right)\left(\delta\boldsymbol{r} - 3\,\frac{(\boldsymbol{F}\cdot\delta\boldsymbol{r})}{|\,\boldsymbol{F}\,|^2}\,\boldsymbol{F}\right). \tag{172}$$

Similarly the moment of $|\,\Delta\boldsymbol{F}\,|^2$ is given by (cf. eq. [140])

$$\left.\begin{aligned} \overline{|\,\Delta\boldsymbol{F}\,|^2}_{\boldsymbol{F},\,\delta\boldsymbol{r}} &= 14\,a\,b'\,\frac{\beta^{1/2}}{H(\beta)}[\sin^2\alpha G(\beta) - (3\sin^2\alpha - 2)\,I(\beta)\,] \\ &+ \frac{g'^2}{\beta H(\beta)}[\,(4 - 3\sin^2\alpha)\,\beta H(\beta) + 3(3\sin^2\alpha - 2)\,K(\beta)\,]\,, \end{aligned}\right\} \tag{173}$$

or, substituting for a, b', and g' from equations (66) and (171), we have

$$\left.\begin{aligned}\overline{|\Delta F|^2}_{F,\,\delta r} = \frac{16\pi^3}{5} G^2 \overline{M^{3/2}}\,\overline{M^{1/2}} n^2 |\,\delta r\,|^2 \frac{\beta^{1/2}}{H(\beta)} [\sin^2 \alpha G(\beta) \\ - (3\sin^2\alpha - 2) I(\beta)\,] + \frac{4\pi^2}{9} G^2 \overline{M}^2 n^2 |\,\delta r\,|^2 \frac{1}{\beta H(\beta)} [\,(4 - 3\sin^2\alpha) \\ \times \beta H(\beta) + 3(3\sin^2\alpha - 2) K(\beta)\,].\end{aligned}\right\} \quad (174)$$

Averaging the foregoing expression over all α, we find

$$\overline{|\Delta F|^2}_{|F|,\,|\delta r|} = \frac{32\pi^3}{15} G^2 \overline{M^{3/2}}\,\overline{M^{1/2}} n^2 |\,\delta r\,|^2 \frac{\beta^{1/2} G(\beta)}{H(\beta)} + \frac{8\pi^2}{9} G^2 \overline{M}^2 n^2 |\,\delta r\,|^2 . \quad (175)$$

Now, according to equation (172) for a fixed $|\delta r|$, $\overline{\Delta F}$ tends to infinity as $|F| \to \infty$. This is contrary to what we should expect on physical grounds, namely, that $\overline{\Delta F}$ should tend to zero as $|F| \to \infty$, for, since the highest fields are approximately produced by the nearest neighbor,[7] it follows that, as $|F| \to \infty$, the particular star which effectively produces the field must be so close to one of the two points considered that no correlations in the *directions* of F acting at the two points can be expected. In other words, $\overline{\Delta F}$ should tend to vanish as $|F| \to \infty$. But this same argument shows why our present theory of spatial correlations fails as $|F| \to \infty$, for, given a $|\delta r|$, however small, we can always choose a $|F|$ so large that on the first-neighbor approximation, the "nearest neighbor" will be closer to one of the points than $|\delta r|$. Under these circumstances the contribution to ΔF arising from this nearest neighbor will no longer be represented to any degree of accuracy by a term of the series (163)— the Taylor expansion of $r/|r|^3$ on which this series is based will cease to be valid for at least that particular term corresponding to the nearest neighbor producing a $|F| \to \infty$. We therefore conclude that our present method gives only the asymptotic behavior of the true spatial correlations in the sense that, given a $|F|$, however large, we can choose a $|\delta r|$ sufficiently small for our formulae to be valid for $|F|$ less than the specified limit.

11. *Dynamical friction.*—We shall now return to equation (105) for a discussion of its implications for general dynamical theory. According to this equation,

$$\bar{F} = \left(\overline{\frac{dF}{dt}}\right)_{F,\,v} = -\tfrac{2}{3}\pi G \overline{M} n B \left(\frac{|F|}{Q_H}\right)\left(v - 3\,\frac{v\cdot F}{|F|^2} F\right), \quad (176)$$

where $B(\beta)$ is defined in equation (98). We shall first derive certain formal consequences of this equation.

Multiplying equation (176) scalarly with F, we obtain

$$F\cdot\left(\overline{\frac{dF}{dt}}\right)_{F,\,v} = \tfrac{1}{3}\pi G \overline{M} n B \left(\frac{|F|}{Q_H}\right)(v\cdot F) . \quad (177)$$

But

$$F\cdot\left(\overline{\frac{dF}{dt}}\right)_{F,\,v} = |F|\left(\overline{\frac{d|F|}{dt}}\right)_{F,\,v} . \quad (178)$$

Hence

$$\left(\overline{\frac{d|F|}{dt}}\right)_{F,\,v} = \tfrac{1}{3}\pi G \overline{M} n B \left(\frac{|F|}{Q_H}\right)\frac{v\cdot F}{|F|} . \quad (179)$$

[7] S. Chandrasekhar, *Ap. J.*, **94**, 511, 1941 (§§ 3 and 4).

On the other hand, if F_j denotes the component of $\boldsymbol{F}$ in an arbitrary direction at right angles to the direction of $\boldsymbol{v}$, then, according to equation (176),

$$\left(\overline{\frac{dF_j}{dt}}\right)_{\boldsymbol{F},\,\boldsymbol{v}} = 2\pi G\bar{M}nB\left(\frac{|\boldsymbol{F}|}{Q_H}\right)\frac{\boldsymbol{v}\cdot\boldsymbol{F}}{|\boldsymbol{F}|^2}F_j\,. \tag{180}$$

Combining equations (179) and (180), we have

$$\frac{1}{F_j}\left(\overline{\frac{dF_j}{dt}}\right)_{\boldsymbol{F},\,\boldsymbol{v}} = \frac{3}{2}\frac{1}{|\boldsymbol{F}|}\left(\overline{\frac{d|\boldsymbol{F}|}{dt}}\right)_{\boldsymbol{F},\,\boldsymbol{v}}. \tag{181}$$

Equation (181) is clearly equivalent to

$$\left[\overline{\frac{d}{dt}(\log|F_j| - \tfrac{3}{2}\log|\boldsymbol{F}|)}\right]_{\boldsymbol{F},\,\boldsymbol{v}} = 0\,. \tag{182}$$

In other words, we have proved that

$$\left[\overline{\frac{d}{dt}\left(\frac{F_j}{|\boldsymbol{F}|^{3/2}}\right)}\right]_{\boldsymbol{F},\,\boldsymbol{v}} = 0\,. \tag{183}$$

We shall now examine the physical consequences of equation (176) more closely. In words, the meaning of this equation is that the component of

$$-\tfrac{2}{3}\pi G\bar{M}nB\left(\frac{|\boldsymbol{F}|}{Q_H}\right)\left(\boldsymbol{v} - 3\,\frac{\boldsymbol{v}\cdot\boldsymbol{F}}{|\boldsymbol{F}|^2}\boldsymbol{F}\right) \tag{184}$$

along any particular direction gives the average value of the rate of change of the force per unit mass acting on a star that is to be expected in the specified direction when the star is moving with a velocity $\boldsymbol{v}$ in an appropriately chosen local standard of rest. Stated in this manner, the essential difference is at once seen in the stochastic variations of $\boldsymbol{F}$ with time in the two cases $|\boldsymbol{v}| = 0$ and $|\boldsymbol{v}| \neq 0$. In the former case $\bar{\boldsymbol{F}} \equiv 0$; but this is not generally true when $|\boldsymbol{v}| \neq 0$. Or, expressed somewhat differently, when $|\boldsymbol{v}| = 0$ the changes in $\boldsymbol{F}$ occur with equal probability in all directions, while this is not the case when $|\boldsymbol{v}| \neq 0$. The exact nature of this difference is brought out quite clearly when we consider

$$\left(\overline{\frac{d|\boldsymbol{F}|}{dt}}\right)_{\boldsymbol{F},\,\boldsymbol{v}} \tag{185}$$

according to equation (179). Remembering that $B(\beta) \gtrless 0$ for $\beta \gtrless 0$, we conclude from equation (179) that

$$\left(\overline{\frac{d|\boldsymbol{F}|}{dt}}\right)_{\boldsymbol{F},\,\boldsymbol{v}} > 0 \qquad \text{if} \qquad \boldsymbol{v}\cdot\boldsymbol{F} > 0 \tag{186}$$

and

$$\left(\overline{\frac{d|\boldsymbol{F}|}{dt}}\right)_{\boldsymbol{F},\,\boldsymbol{v}} < 0 \qquad \text{if} \qquad \boldsymbol{v}\cdot\boldsymbol{F} < 0\,. \tag{187}$$

In other words, if $\boldsymbol{F}$ has a positive component in the direction of $\boldsymbol{v}$, $|\boldsymbol{F}|$ increases on the average; while, if $\boldsymbol{F}$ has a negative component in the direction of $\boldsymbol{v}$, $|\boldsymbol{F}|$ decreases on the average. We shall now show that it is this essential asymmetry introduced by the direction of $\boldsymbol{v}$ that gives rise to the phenomenon of dynamical friction.

The characteristic aspects of the situation governed by equation (179) are best understood when we contrast it with the case $\bar{\boldsymbol{F}} \equiv 0$. Under these circumstances we can visualize the motion of the representative point in the velocity space somewhat as follows:[8] The representative point suffers small random displacements in a manner that can be adequately described by the theory of random flights.[9] More specifically, the star may be assumed to suffer a large number of discrete increases in velocity of amounts $\boldsymbol{F}T(\boldsymbol{F})$, where T is the "mean life" of the state $\boldsymbol{F}$; these increases are further assumed to take place in random directions. On these assumptions it readily follows that the mean square increase in the velocity, which we may expect the star to suffer in time t, is given by

$$\overline{|\Delta \boldsymbol{v}|^2} = \overline{|\boldsymbol{F}|^2 T}\, t\,. \tag{188}$$

An alternative way of describing the same situation is to assert that the function $P(\boldsymbol{v}, t; \boldsymbol{v}_0)$, which gives the probability that the star has a velocity $\boldsymbol{v}$ at time t, given that $\boldsymbol{v} = \boldsymbol{v}_0$ at $t = 0$, satisfies the diffusion equation

$$\frac{\partial P}{\partial t} = D\left(\frac{\partial^2 P}{\partial v_1^2} + \frac{\partial^2 P}{\partial v_2^2} + \frac{\partial^2 P}{\partial v_3^2}\right), \tag{189}$$

with the "coefficient of diffusion," D, having the value

$$D = \tfrac{1}{6}\overline{|\boldsymbol{F}|^2 T}\,. \tag{190}$$

The solution of equation (189) appropriate for our purposes is

$$P(\boldsymbol{v}, t; \boldsymbol{v}_0) = \frac{1}{(4\pi D t)^{3/2}}\, e^{-|\boldsymbol{v}-\boldsymbol{v}_0|^2/4Dt}\,. \tag{191}$$

The formula (188) is seen to follow immediately from the foregoing solution.

Returning to the discussion of the case governed by equations (176) and (179), we see at once that the idealization of the motion of the representative point in the velocity space as a true problem in random flights can no longer be valid. Moreover, according to equations (183), (186), and (187), during a given state of fluctuation the star is likely to suffer a greater amount of acceleration in the direction of $-\boldsymbol{v}$ when $(\boldsymbol{v}\cdot\boldsymbol{F})$ is negative than in the direction of $+\boldsymbol{v}$ when $(\boldsymbol{v}\cdot\boldsymbol{F})$ is positive. But the a priori probabilities for $(\boldsymbol{v}\cdot\boldsymbol{F})$ to be positive or negative are equal. Hence, when integrated over a large number of fluctuations, the star must suffer cumulatively a larger absolute amount of acceleration in the direction opposite to its direction of motion than in the direction of motion. In other words, there is a tendency for the star to be relatively decelerated in the direction of its motion; further, this tendency is proportional to $|\boldsymbol{v}|$. But these are exactly what are implied by the existence of dynamical friction.[10]

YERKES OBSERVATORY
WILLIAMS BAY, WISCONSIN
AND
INSTITUTE FOR ADVANCED STUDY
PRINCETON, NEW JERSEY

[8] Cf. *ibid.*, §§ 2 and 7. [9] See, e.g., Lord Rayleigh, *Phil. Mag.*, 6th ser., **37**, 321, 1919.

[10] See two forthcoming papers by one of us (S.C.) on "Dynamical friction" in an early issue of the *Ap. J.*

NUCLEAR EMISSION IN SPIRAL NEBULAE*

CARL K. SEYFERT†

ABSTRACT

Spectrograms of dispersion 37–200 A/mm have been obtained of six extragalactic nebulae with high-excitation nuclear emission lines superposed on a normal G-type spectrum. All the stronger emission lines from λ 3727 to λ 6731 found in planetaries like NGC 7027 appear in the spectra of the two brightest spirals observed, NGC 1068 and NGC 4151.

Apparent relative intensities of the emission lines in the six spirals were reduced to true relative intensities. Color temperatures of the continua of each spiral were determined for this purpose.

The observed relative intensities of the emission lines exhibit large variations from nebula to nebula. Profiles of the emission lines show that all the lines are broadened, presumably by Doppler motion, by amounts varying up to 8500 km/sec for the total width of the hydrogen lines in NGC 3516 and NGC 7469. The hydrogen lines in NGC 4151 have relatively narrow cores with wide wings, 7500 km/sec in total breadth. Similar wings are found for the Balmer lines in NGC 7469. The lines of the other ions show no evidence of wide wings. Some of the lines exhibit strong asymmetries, usually in the sense that the violet side of the line is stronger than the red.

In NGC 7469 the absorption K line of *Ca* II is shallow and 50 A wide, at least twice as wide as in normal spirals.

Absorption minima are found in six of the stronger emission lines in NGC 1068, in one line in NGC 4151, and one in NGC 7469. Evidence from measures of wave length and equivalent widths suggests that these absorption minima arise from the G-type spectra on which the emissions are superposed.

The maximum width of the Balmer emission lines seems to increase with the absolute magnitude of the nucleus and with the ratio of the light in the nucleus to the total light of the nebula. The emission lines in the brightest diffuse nebulae in other extragalactic objects do not appear to have wide emission lines similar to those found in the nuclei of emission spirals.

Many of the spectra of extragalactic nebulae obtained at the Mount Wilson and Lick observatories show one or more emission lines in addition to the usual absorption spectra. In particular, N. U. Mayall[1] finds that 50 per cent of his spectra of spirals show the [*O* II] doublet λ 3727 in emission either in the nuclear region or in the arms. However, only a very small proportion of extragalactic nebulae show spectra having many high-excitation emission lines localized in the nuclei. These emission features are similar to those found in planetary nebulae and are superposed on the characteristic solar-type absorption spectra. Twelve nebulae[2] are now known which probably belong to this unusual class of objects. Most of them are intermediate-type spirals with ill-defined amorphous arms, their most consistent characteristic being an exceedingly luminous stellar or semistellar nucleus which contains a relatively large percentage of the total light of the system. Plate I shows a photograph of NGC 4151, a typical example of this type of nebula.

Probably the earliest spectrographic observation of a member of this unusual class of objects was that of NGC 1068 by E. A. Fath,[3] in which he found five emission and two absorption lines. In 1917, V. M. Slipher[4] found hydrogen lines and the nebular lines N1 and N2 bright in the nucleus of NGC 5236. Shortly afterwards, Slipher[5] made the discovery that the emission lines in NGC 1068 were not monochromatic images of the slit but were small "discs." These findings were confirmed by Campbell and Moore,[6]

* *Contributions from the Mount Wilson Observatory, Carnegie Institution of Washington*, No. 671.

† Fellow of the National Research Council.

[1] *Lick Obs. Bull.*, **19**, 33, 1939.

[2] NGC 1068, 1275, 2782, 3077, 3227, 3516, 4051, 4151, 4258, 5548, 6814, and 7469.

[3] *Lick Obs. Bull.*, **5**, 71, 1908.

[4] *Pop. Astr.*, **25**, 36, 1917; *Proc. Amer. Phil. Soc.*, **56**, 403, 1917.

[5] *Lowell Obs. Bull.*, **3**, 59, 1917.

[6] *Lick Obs. Pub.*, **13**, 88, 1918.

who stated that the bright bands in NGC 1068 were "fully 30 Angstroms wide." Campbell and Moore[7] also found in NGC 4151 emission lines several angstroms wide. E. P. Hubble[8] refers to planetary-type emission in the nucleus of NGC 4051 (as well as NGC 1068 and NGC 4151) in a paper published in 1926. Detailed descriptions of the typical emission spirals NGC 1275 and NGC 4151 were published by M. L. Humason[9] and N. U. Mayall,[10] respectively. In addition, a private communication from Dr. Mayall indicates that NGC 3516 and NGC 7469 show broad bands of hydrogen in emission and hence belong in the group under consideration.

I. THE OBSERVATIONAL MATERIAL

The present investigation is an intensive study of six of the brightest extragalactic nebulae showing emission bands in their nuclei (Table 1). Of these six, special emphasis was placed on the three having the brightest nuclei, NGC 1068, 3516, and 4151, because

TABLE 1*

EMISSION SPIRALS OBSERVED

NGC	1950 R.A.	1950 Dec.	Type	m_{total}	$m_{nucl.}$	Spect.	Modulus	No. of Plates
1068	$2^h40.1$	$-0°14$	Sb	10.0	13.0	G3	26^m0	17
1275	3 15.6	+41 18	E:	13.0	15.5	G3	30.0	4
3516	11 3.4	+72 50	Sa	12.2	13.7	G2:	28.5	6
4051	12 0.6	+44 48	Sb	11.7	14.0	G2	26.0	4
4151	12 8.0	+39 41	Sb	11.2	12.0	G2	26.0	12
7469	23 0.7	+ 8 36	Sa	13.0	14.3:	G0:	29.8	2

* The total apparent photographic magnitudes are from the *Shapley-Ames Catalogue of External Galaxies* (*Harv. Ann.*, **88**, 43, 1932). The apparent magnitudes (photographic) of the nuclei were estimated from short-exposure plates, taken in series with selected areas. The distance moduli are new determinations derived from magnitudes of resolved stars in the arms (NGC 1068), radial velocity (NGC 1068, 3516, 7469), or from association with recognized clusters or groups (NGC 1275, 4051, 4151). The plates used for determinations of nuclear magnitudes and most of the data for computing the distance moduli were supplied by E. P. Hubble. The spectral types were determined by M. L. Humason.

it was possible to observe them with higher dispersion than could be used on the fainter objects.

The observations were obtained mainly at the Cassegrain focus of the 60-inch reflector using (1) the one-prism spectrograph and cameras of 3.5, 6, 9, 10, and 18 inches in focal length, and (2) the two-prism nebular spectrograph "VIA" with a 3-inch camera. In addition, a few plates were obtained with a grating spectrograph and Schmidt camera and with the "VIC" Cassegrain two-prism spectrograph and 10-inch camera at the 100-inch reflector. Table 2 lists the dispersions with the various combinations.

Spectral calibration strips for determining relative intensities at each wave length were placed beside the nebular spectrum on the same photographic plate during the course of the nebular exposure. These standardization exposures were never shorter than 5 minutes and were usually 30 minutes in length, or 13 per cent as long as the average nebular exposure. For a few plates the ratio of standard to nebular exposure was as low as 1 or 2 per cent. Examination showed that the photometric results obtained from these plates were not systematically different from plates with much larger ratios.

[7] *Lick Obs. Bull.*, **13**, 122, 1918.

[8] *Mt. W. Contr.*, No. 324; *Ap. J.*, **64**, 328, 1926.

[9] *Pub. A.S.P.*, **44**, 267, 1932.

[10] *Pub. A.S.P.*, **46**, 134, 1934.

Hence we believe that the relatively short standardization exposures do not introduce any serious errors.

The chief photographic plates used were Cramer Hi-Speed, Eastman 103-O, and Eastman 103-F. To increase their sensitivity, the two blue-sensitive emulsions (Hi-Speed and 103-O) were as a rule baked for three days at 50° C., and the red-sensitive 103-F plates were bathed in a 4 per cent ammonia solution for one minute.

II. IDENTIFICATION OF LINES

Table 3 lists the lines identified with certainty in any or all of the six nebulae under investigation. The intensities given are relative to $H\beta$ assumed equal to 100. The method of obtaining the intensities is described in a later paragraph.

TABLE 2

SPECTROGRAPH-CAMERA COMBINATIONS EMPLOYED

Spectrograph	Camera Focal Length	Dispersion at $H\gamma$	Telescope	
One-prism	3.5 inches	195 A/mm	60-inch	Cassegrain
One-prism	6	122	60	Cassegrain
One-prism	9	78	60	Cassegrain
One-prism	10	71	60	Cassegrain
One-prism	18	36	60	Cassegrain
Two-prism "VIA"	3	200	60	Cassegrain
Grating	1.3	400	60	Cassegrain
Two-prism "VIC"	10	66	100	Cassegrain

All the lines identified, with the exception of those of hydrogen and helium, arise from forbidden transitions. The identification of the lines in Table 3 is complete with the single exception of λ 5670.5, which was measured on two plates of NGC 4151. For purposes of comparison, the relative intensities determined by A. B. Wyse[11] for the emission lines in the planetary nebula NGC 7027 are given in Table 3.

The chief features of the spectra which appear in absorption are the cyanogen band (effective wave length, λ 3873); H and K lines of *Ca* II (λ 3934 and λ 3969); the G band, composed chiefly of *CH* (measured position, λ 4303); and the D lines of *Na* (λ 5890 and λ 5896). Since the absorption lines are usually ill-defined and sometimes absent altogether, the spectral types in Table 1 may be subject to fairly large uncertainties.

III. RELATIVE INTENSITIES OF THE EMISSION LINES

The conventional method of obtaining the true relative intensity of a wide emission line is to measure the intensity (corrected for the background) at each wave length in the line relative to the intensity at the corresponding wave length in a comparison star of known color temperature. These values are multiplied by the relative intensity of a black body[12] of temperature equal to that of the comparison star and summed over all wave lengths in the line. The ratio of such summations for two different emission lines, corrected for differential extinction, gives the ratio of relative intensities of the lines freed of instrumental and atmospheric absorption, i.e., the true relative intensities.

The method described above has been used for determining true relative intensities for the six objects under investigation. However, the continuum of each spiral was used

[11] *Ap. J.*, **95**, 356, 1942.

[12] The black-body intensities may be calculated from Table VII in Jahnke and Emde, *Tables of Functions*, p. 46 (Leipzig, 1933).

instead of stars for comparison standards. Not only does this make it possible to use all the plates on which this continuum appears, but it eliminates uncertainties due to differential extinction, exposure time, changes during exposure of plate-sensitivity and sky conditions.

TABLE 3

INTENSITIES OF EMISSION LINES IN SIX EXTRAGALACTIC NEBULAE

Atom	λ	NGC 1068	NGC 1275	NGC 3516	NGC 4051	NGC 4151			NGC 7469		NGC 7027*
						Core	Wing	Core+Wing	Core	Core+Wing	
[O II]	3726.2	80:	140:	.....	.....	100:	.....	25:	48:	15:	8
[O II]	3729.7										4
[Ne III]	3869	65:†	35:	.....	P	65:	.....	15:	.....	.....	40
H ζ	3889.1	5:	.....	.....	.....	.....	.....	.....	.....	.....	7
[Ne III]	3968	25:†	20:	.....	.....	25:	.....	5:	.....	.....	15
H ε	3970.1										8
[S II]	4068.5	20	50	.....	.....	25	.....	5	.....	.....	5
[S II]	4076.5										2
H δ	4101.8	20	10:	25	.....	20	20	20	.....	35:	12
H γ	4340.5	40	50	40‡	40	35	30	35	.....	60:‡	20
[O III]	4363.2	35	40	.....	20	75	.....	18	.....	.....	10
C IV[Fe III]	4658.6	.....	.....	.....	.....	5	.....	1	.....	.....	0.9
He II	4685.8	40	.....	.....	25	25	.....	5	.....	.....	40
[A IV]	4711.4	.....	.....	.....	.....	10	.....	2	.....	.....	3
[A IV]	4740.3	.....	.....	.....	.....	10	.....	2	.....	.....	7
H β	4861.3	100§	100	100	100	100	100	100	100	100	100
[O III]	4959.5	400§	80	15	55	375	.....	90	125	35	430
[O III]	5007.6	1200§	270	40	190	1150	.....	275	300	80	1190
[Fe VII]	5158.3	5	.....	.....	.....	P‖	.....	P	.....	.....	2
[N I]	5199.2	25	.....	.....	.....	15	.....	5	.....	.....	3
[Fe VII]	5276.1	5:	.....	.....	.....	P:	.....	P:	.....	.....	1.5±
	5670.5	.....	.....	.....	.....	P	.....	P	.....	.....	.....
[Fe VII]	5720.9	10	.....	.....	.....	20	.....	5	.....	.....	4
[N II]	5755.0	10	.....	.....	.....	.....	.....	.....	.....	.....	20
He I	5875.6	15:	.....	.....	.....	30	.....	5	.....	.....	35
[Fe VII] [Ca V]	6085.7	30	.....	.....	.....	35	.....	10	.....	.....	5
[O I]	6300.2	85	100	.....	30	150	.....	35	.....	.....	40
[S III]	6310.2										15
[O I]	6363.9	30	40	.....	20	50	.....	10	.....	.....	20
[N II]	6548.4				25:	100		25	.....	.....	90
H α	6562.8	1000¶	700	600	600	400	375	400	.....	.....	420
[N II]	6583.9				50:	200		50	.....	.....	190
[S II]	6717.3	140	210	.....	40:	180	.....	40	.....	.....	8
[S II]	6731.5										15

* The intensities in the planetary nebula NGC 7027 (included for comparison) are from the paper by A. B. Wyse, *Ap. J.*, **95**, 356, 1942.

† The measures of λ 3869 and λ 3968 in NGC 1068 are probably affected by the strong absorptions in the underlying G-type spectrum. The true values are probably somewhat greater (see pp. 37, 38).

‡ The G band in the underlying continuum affects the measures of $H\gamma$ in NGC 3516 and NGC 7469 (wing). The true values are probably somewhat larger.

§ The effect of the narrow central minima in λλ 4861, 4959, and 5007 on the measures is negligibly small.

‖ P indicates the presence of a line which is too weak to measure.

¶ The sum of the [N II] intensities (λ 6548 and λ 6583) approximately equals that of $H\alpha$ in NGC 1068.

The method necessitates ascertaining the color temperature of the continuum of each nebula. For this purpose a special series of red-sensitive plates (103-F) was taken with the small-scale VIA spectrograph and 3-inch camera. Suitable bright comparison stars

of well-determined color gradient[13] were taken at the beginning and end of the nebular exposures. The stellar exposures were lengthened to 10 or 15 minutes by interposing several thicknesses of copper mesh about 8 inches in front of the slit. The nebular exposures ranged from 40 to 110 minutes. A slit approximately 6 inches wide was used, and both nebular and stellar spectra were widened by trailing along the slit. Differential extinction corrections were computed from Table 767 of the *Smithsonian Physical Tables* (8th ed.) by F. E. Fowle. The gradient of the nebular continuum relative to the standard stars was found to be closely linear from λ 4000 to λ 6700, and the black-body temperature corresponding to this gradient was determined.[14]

Mean color temperatures were found in this way for the continua of NGC 1068, 3516, and 4151. The temperatures of NGC 1275, 4051, and 7469 were deduced by means of photometric comparisons with spectrograms of NGC 1068, 3516, and 4151 obtained on plates of the same type with similar development but taken one or more months apart. The adopted values of the temperatures of the continua are in Table 4.

TABLE 4

COLOR TEMPERATURES OF CONTINUA OF 6 EMISSION SPIRALS

NGC	T	NGC	T
1068	5250°	4051	5250:
1275	5250:	4151	4750
3516	5250	7469	8000:

The investigations of Stebbins and Whitford[15] indicate that the continua of nebulae deviate from black-body radiation, particularly in the ultraviolet and infrared. I am very grateful to Dr. Stebbins, who, at my request, kindly measured photoelectrically the spectral radiation of NGC 1068 at the following mean wave lengths: λλ 3510, 4220, 4880, 5700, 7190, and 10300. He finds that the intensity distribution from λ 3510 to λ 10300 is nearly identical with that of the nonemission spiral NGC 4826 (same nebular type and spectrum as NGC 1068). From λ 4220 to λ 7190 the intensity distribution corresponds closely to that of a black body of temperature 4800°. From λ 3510 to λ 4220, Stebbins' measures indicate a temperature of 5600°. Considering the relatively low accuracy of my measures and the fact that the emission lines affect the photoelectric measures somewhat,[16] the agreement with the mean value (5250°) used in this paper for NGC 1068 is considered satisfactory. Furthermore, even though the nebular spectral radiation deviates from that corresponding to the color temperatures adopted, the effect of such deviations or errors on the relative intensities is comparatively small. For example, an error of 500° in the color temperature of the continuum of NGC 1068 introduces an error at λ 6720 of 14 per cent and at λ 3727 of only 9 per cent relative to the intensity of $H\beta$. The uncertainty is, of course, correspondingly less for lines less widely separated.

The final true relative intensities are given in Table 3. The estimated uncertainty is of the order of 10 per cent, though it may exceed this value for NGC 7469 for which the measures are from a single plate. In view of the ultraviolet excess mentioned above, the intensities given for lines less than λ 4000 may be somewhat too small and have been marked with a colon.

[13] Chosen from the Greenwich list (*M.N.*, **100**, 189, 1939). The comparison stars were 13 Eri for NGC 1068, 21 LMi; and χ Her for NGC 3516 and NGC 4151, and ρ_1 and ρ_2 Lyr for NGC 3516.

[14] The Greenwich relative gradients must be reduced to absolute gradients by adding a correction for the Greenwich zero point. The value adopted is 1.10 in accordance with *M.N.*, **100**, 189, 1939.

[15] *Pub. Amer. Astr., Soc.*, **10**, 239, 1942.

[16] A rough calculation indicated that the effect of the emission lines in NGC 1068 would probably not be large but would tend to make the observed photoelectric color temperature too small.

NGC 1068.—Thirteen per cent of the total light of the nucleus in the photographic region is in the emission lines. The intensities of the lines are similar to those in the planetary nebula NGC 7027 except that the [*O* II], [*S* II], [*N* I], and [*Fe* VII] lines are considerably stronger in NGC 1068. The line λ 6086 [*Fe* VII] is unusually strong, although [*Ca* V] probably contributes to its strength. The corresponding [*Ca* V] line at λ 5308 is, however, absent or very weak. On the other hand, λ 5276 of [*Fe* VII] is possibly weakened by the superposed absorption λλ 5262–76 of *Ca*, *Fe*, and other metals. This blend would also probably obscure λ 5270 of [*Fe* III] if it were present. Further evidence regarding absorptions superposed on emissions will be discussed later (p. 37). The absence of λ 5270 of [*Fe* III] and of the lines λλ 5802 and 5812 of *C* IV makes it impossible to determine with certainty whether [*Fe* III] or *C* IV is responsible for the line λ 4658.6.

NGC 1275.—The intensities resemble those in NGC 1068 except that the [*O* II] and [*S* II] lines are stronger and N1 and N2 [*O* III] considerably weaker while λ 4686 *He* II is absent altogether.

NGC 3516.—The emission spectrum consists practically of nothing but hydrogen. The only other lines visible are extremely weak N1 and N2; λ 3727 [*O* II] is absent. Only 5 per cent of the total photographic light of the nucleus is in the emission lines. The K line of (*Ca* II) is visible in absorption, and the G band (λ 4303) is present at the edge of *Hγ* (λ 4340).

NGC 4051.—N1 and N2 are relatively weak. The plates are not sufficiently strong in the violet to establish the existence of λ 3727 [*O* II].

NGC 4151.—The intensities of the cores of the lines are very similar to those in NGC 1068 except that the [*O* I] lines are considerably stronger in NGC 4151. The Balmer decrement of the core of the lines is the same as that of the wings. The hydrogen wings contribute 8 per cent of the total photographic light of the nucleus, the rest of the emissions 14 per cent.

NGC 7469.—N1 and N2 are weaker than in NGC 1068 and NGC 4151. The Balmer decrement seems to be normal for the cores of the lines, but that for the wings appears to be extremely slow. The G band and the K line of *Ca* II are visible, despite the relatively high color temperature (8000°).

IV. PROFILES OF THE EMISSION LINES

All spectrograms of suitable dispersion were analyzed with the microphotometer for the purpose of measuring profiles of the emission lines. No attempt was made to allow for the instrumental profile, since only those spectrograms were used for which the instrumental widening was a negligible fraction of the width of the emission lines. The profiles of the hydrogen lines are similar when expressed in kilometers per second rather than angstroms. In Figure 1 are microphotometer tracings of *Hβ*, N2 and N1 showing the main types of emission lines observed. Figures 2–4 are the mean profiles obtained from the measures. Most of the lines in NGC 1068 were sufficiently symmetrical to warrant combining the two halves of the line. Table 5 lists, for the lines measured in each object, the total widths in kilometers per second derived from the mean measured profile.

NGC 1068.—The line widths range from 2400 km/sec for λ 4686 (*He* II) to 3600 km/sec for the hydrogen lines and the [*S* II] doublet λ 6717, λ 6731. The profiles of the lines of NGC 1068 fall into two main groups; lines with rounded maxima which are relatively wide in the range from 0.25 to 0.50 of the central intensity (λλ 3727 [*O* II],[17] 4363 [*O* III], 6086 [*Fe* VII],[17] 6300 and 6364 [*O* I], and 6717, 6731 [*S* II][18] and lines with sharp maxima

[17] The profile of λ 3727 is uncertain, owing to the presence of the strong absorption features at λ 3720 and λ 3736. The profile of λ 6086 is uncertain, owing to the possibility that λ 6073 (unknown origin) and λ 6102 [*K* IV] may be present.

[18] The lines λ 4069 and λ 4076 probably belong in the group, but because of blending, the profile is too uncertain to be included.

which are relatively narrow in the range from 0.25 to 0.50 of the central intensities (λλ 3869, 3968 [*Ne* III], 4686 *He* II, and 4959 and 5007 [*O* III]). The profile of the hydrogen lines seems to belong between the two groups.

The question whether the absorption lines are also widened in NGC 1068 is not readily answered, because the prominent absorption lines visible (*CN;* K (*Ca* II); G and D) are either intrinsically very wide or composite. Measures from microphotometer tracings,

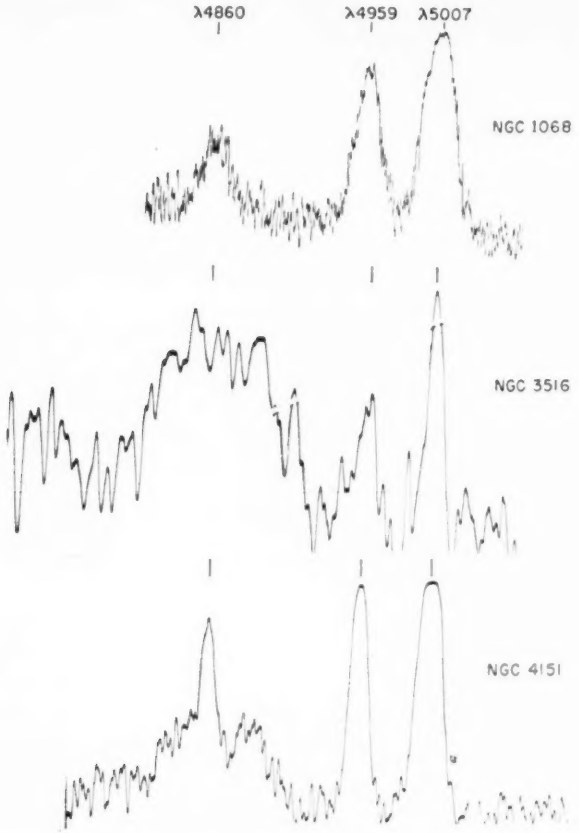

FIG. 1.—Microphotometer tracings of the emission lines λλ 4860 ($H\beta$), 4959 and 5007 [*O* III] in the nebulae NGC 1068, 3516, and 4151.

however, show that the K line in NGC 1068 is not significantly wider than the corresponding line in M 32 and has about the same width as in a star of type dG5.

NGC 1275.—Owing to the faintness of this object, only the line N1 has a well-determined profile. Not only is it the broadest N1 line measured, among the six nebulae investigated, but it shows the largest amount of asymmetry. The blue part of the line is 60 per cent wider than the red part at $I = 0.25\, I_{max}$ (Fig. 4). Comparisons of the widths of the other emission lines from smaller-scale spectra indicate that the lines in NGC 1275 are probably somewhat wider than the corresponding lines in NGC 1068. In particular, the [*Ne* III] lines are unusually wide in NGC 1275.

NGC 3516.—Only the hydrogen and N1 and N2 lines are present in emission. N1 and N2 are weak and much narrower (1400 km/sec wide) than the corresponding lines

in NGC 1068 and NGC 1275. The hydrogen lines, however, are great shallow bands 8500 km/sec wide, the widest found among the objects studied. The lines are all fairly symmetrical (Fig. 4).

NGC 4051.—The N1 and N2 lines are relatively narrow (1200 km/sec), and the hydrogen lines are peaked and wide (3600 km/sec). The N1, N2, and hydrogen lines appear

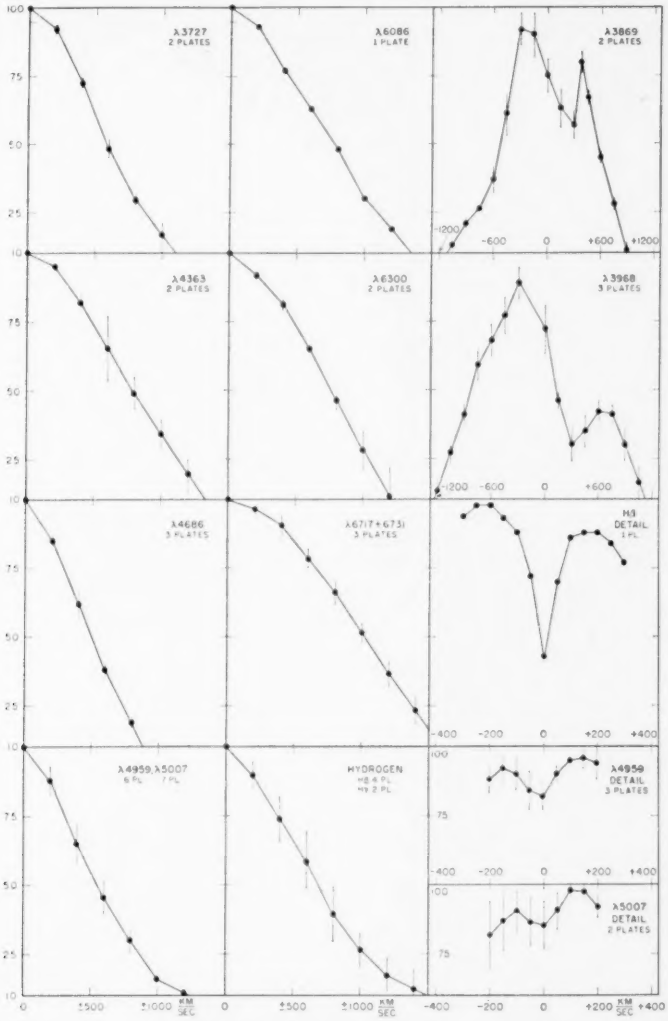

FIG. 2.—Profiles of emission lines in NGC 1068. Ordinates are intensities, abscissae distances from the center of each line in km/sec. The vertical lines indicate the average deviation of the individual observations from the plotted means. For symmetrical lines the two halves of each profile have been combined.

symmetrical within the accuracy of the measures. Small-scale spectrograms indicate that the remaining lines are probably similar in width to those in NGC 1068.

NGC 4151.—The hydrogen lines are markedly different from the other lines in that each hydrogen line has very broad wings (7500 km/sec wide) extending outward from

the relatively narrow core. The discontinuity between the core and the wing is so sharp that the Balmer lines appear to be composite, with sharp cores centrally superposed on broad emission bands. All the forbidden lines, as well as λ 4686 and the cores of the hydrogen lines, are similar in shape and relatively narrow (<1800 km/sec).

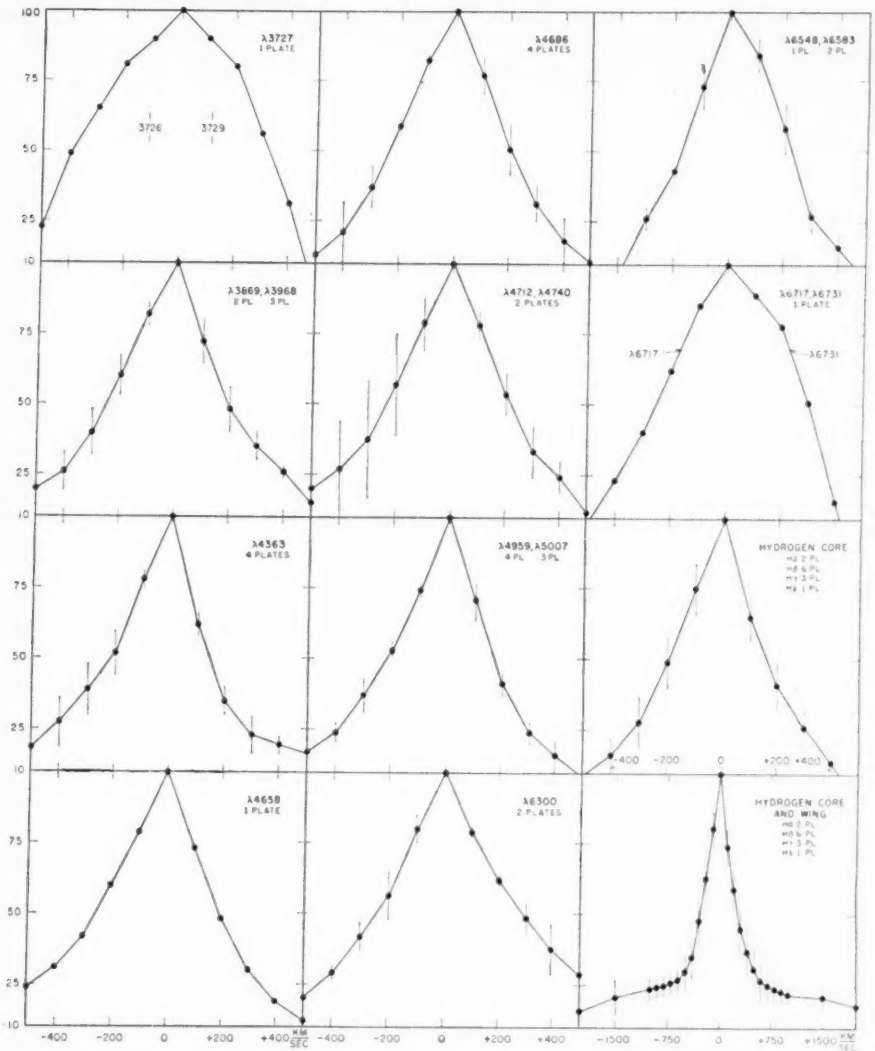

FIG. 3.—Profiles of emission lines in NGC 4151. Ordinates are intensities, abscissae distances from the center of each line in km/sec. The vertical lines indicate the average deviation of the individual observations from the plotted means. The scale of the abscissae for the profile of hydrogen core and wing (*lower right corner*) is widely different from that of the other profiles.

Most of the lines in NGC 4151 are asymmetrical in the sense that the blue part of the line is, on the average, 16 per cent wider than the red part at the point where the intensity drops to 0.25 of the central intensity. The profile of λ 6300, the only outstanding exception, is undoubtedly distorted by the presence of λ 6310 on the red side of λ 6300.

PLATE I

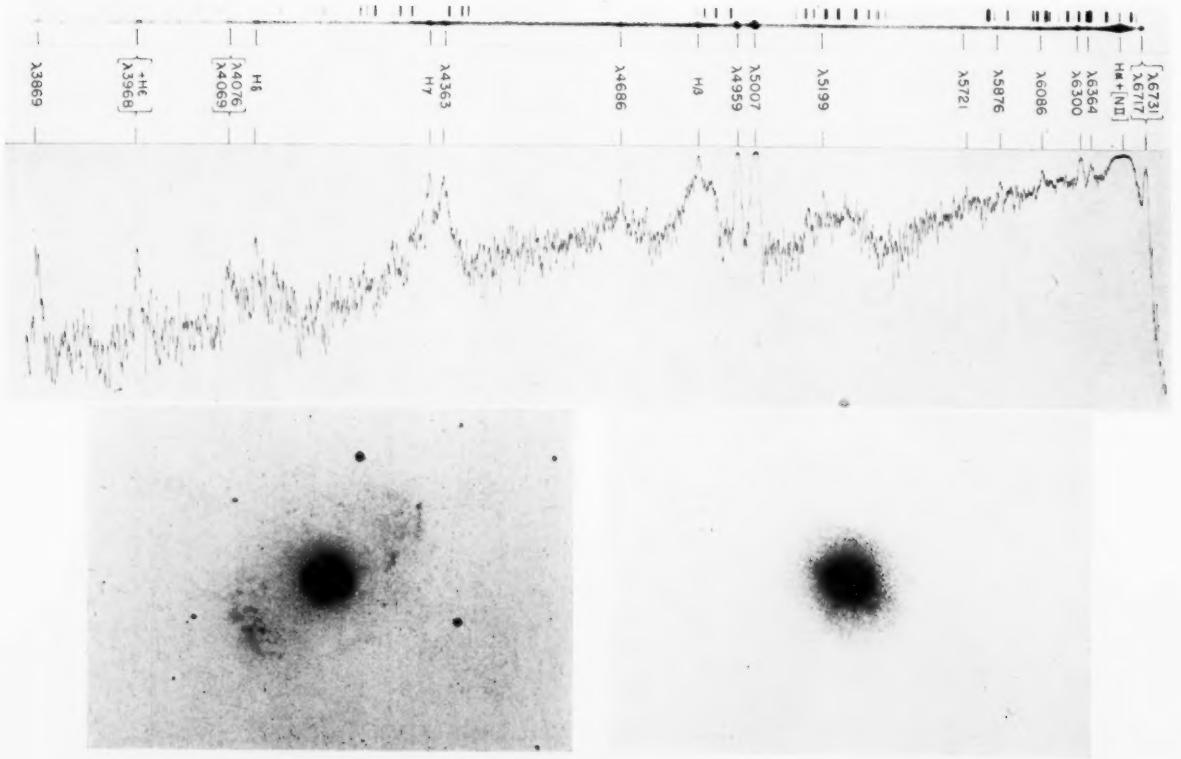

NGC 4151

Spectrum, microphotometer tracing, and direct photographs. The spectrum is an enlargement from a 325^{m} exposure taken with the one-prism Cassegrain spectrograph and 10-inch camera at the 60-inch reflector. The photographs (enlargements from a plate taken with the 100-inch reflector) show the weak, amorphous arms on the left and the semistellar nucleus on the right.

NGC 7469.—The spectrum is similar to that of NGC 4151 in that the N1 and N2 lines are relatively narrow (<1400 km/sec), and the hydrogen lines have cores and very wide wings. However, both cores and wings seem wider than those in NGC 4151 and the wings more intense. Absorption K (*Ca* II) is extremely shallow and at least 50 A wide, twice as wide as in the other nebulae. The large apparent asymmetry for $H\beta$ in NGC 7469 may not be real, since the profile is determined from only one blue-sensitive plate. The rapidly changing background over the great width of the $H\beta$ line (8500 km/sec) makes the profile somewhat uncertain.

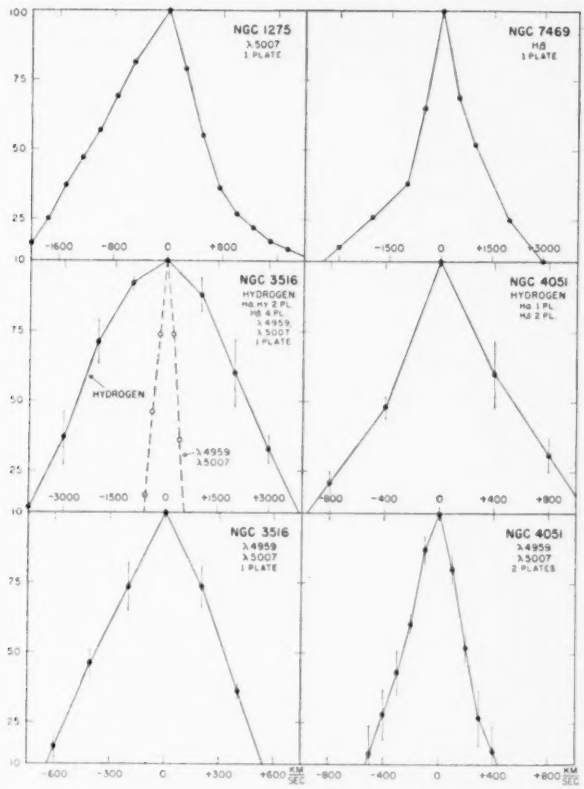

FIG. 4.—Profiles of emission lines in NGC 1275, 3516, 7469, and 4051. Ordinates are intensities, abscissae distances from line center in km/sec. The vertical lines indicate the average deviation of the individual observations from the plotted means.

V. MINIMA IN EMISSION LINES

An unusual feature of six of the strongest lines in NGC 1068 and one line each in NGC 4151 and NGC 7469 is the presence of minima in the emission lines (see Fig. 2). A tentative explanation of these apparent reversals is that the broad emission lines are superposed on a G-type spectrum which contains strong absorption lines at or near the position of the emission lines. Table 6 lists the emission lines in which the minima appear, the observed wave lengths of the minima, the suggested identifications, and the equivalent widths of the minima as measured in the nebular spectrum. Measures of the equivalent widths of the corresponding lines in the sun are included in the table for comparison. The measured wave lengths and equivalent widths agree with the corresponding solar

TABLE 5

TOTAL WIDTHS OF EMISSION LINES (IN KM/SEC)

λ	NGC 1068	NGC 1275	NGC 3516	NGC 4051	NGC 4151	NGC 7469
3727	2600	.....	.....	.....	1050	.....
3869, 3968	2500:	>4000	.....	.....	1700	.....
4363	2800	.....	.....	.....	1800	.....
4659	.....	.....	.....	.....	1250	.....
4686	2400	.....	.....	.....	1300	.....
4711, 4740	.....	.....	.....	.....	1150	.....
4959, 5007	3000	4500	1400	1200	1300	<1400
6086	3000*	.....	.....	.....	.....	.....
6300	2700	.....	.....	.....	1800†	.....
6548, 6563	.....	.....	.....	.....	950	.....
6717, 6731	3600‡	.....	.....	.....	1000: 900:	.....
H lines	3600	⩾4500	8500	3600	7500	8500
H (core of line)	.....	.....	.....	.....	1100	2500:

* The true width of the line λ 6086 in NGC 1068 may be considerably smaller than that indicated, owing to the possible presence of λ 6073 (unknown origin) and λ 6102 [*K* IV].

† In NGC 4151, since λ 6310 influences the profile, the true width of λ 6300 is probably considerably smaller than that indicated.

‡ The fact that the two lines are blended in NGC 1068 contributes only a negligible amount to the width of the line.

TABLE 6

SUGGESTED IDENTIFICATIONS OF ABSORPTION MINIMA IN EMISSION LINES

NGC	Emission Line	Observed λ of Abs. Min.*	Suggested Identification of Abs. Min.	E. W. Nebula	E. W.† Sun
	λ	λ	λ		
1068	3869	3873±	3872 (*CN*)	3.6 A	4.0: A
1068	3968	3972±	3968.5 (*Ca* II) 3970.1 (*Hε*)	2.0	1.0
7469	4340.5	4300±	4303 (*CH G* band)	2.0	3.5
1068	4340.5	4340±	4340.5 (*Hγ*)	1.0	2.3
1068	4861.3	4862.0	4861.3 (*Hβ*)	2.0	2.9
4151	4861.3	4873	4870.8 (*Cr, Ni*) 4871.3 (*Fe*) 4872.1 (*Fe*)	1.8	0.6
1068	4959.5	4958.1	4957.3 (*Fe*) 4957.6 (*Fe*)	0.6	0.8
1068	5007.6	5007.3	5005.7 (*Fe*) 5006.1 (*Fe*) 5007.2 (*Ti*) 5007.3 (*Fe*)	1.3	0.6

* The wave length of each absorption minimum is measured on the tracings relative to the emission line.

† Determined from the *Photometric Atlas of the Solar Spectrum* by Minnaert, Mulders, and Houtgast (Amsterdam, 1940).

values within the accuracy of the measures except for the *H* (*Ca* II) and *Hε* absorption in the λ 3968 [*Ne* III] emission. The large discrepancy in this case between the observed and expected equivalent widths of the minimum is probably due to the great intrinsic width of the *H* line. The small systematic difference of approximately one angstrom between the observed and expected wave lengths may or may not be significant.

VI. DISCUSSION

Ten of the twelve extragalactic nebulae known to exhibit high-excitation nuclear emission are spirals of either early or intermediate type (i.e., Sa or Sb). The remaining two, NGC 1275 and NGC 3077, are objects which could be classified as either peculiar elliptical or irregular nebulae. The average absolute magnitude of the twelve emission spirals (−15.8) is somewhat brighter than the average nonemission spiral. All emission spirals have nuclei of high luminosity, which on direct photographs are scarcely distinguishable from stars—a fact first noted by Humason in his paper on NGC 1275.

The widths of the emission bands are probably correlated with the physical properties of the nucleus. The data in Table 7 suggest that the maximum width of the hydrogen

TABLE 7*

RELATION BETWEEN MAXIMUM WIDTHS OF BALMER LINES AND THE PHYSICAL PROPERTIES OF NUCLEI

NGC	Max. Width of H Lines (in Km/Sec)	Abs. Mag. of Nucleus	Percentage of Total Light in Nucleus
4051	3600	−12.0	12
1068	3600	−13.0	6
1275	>4500	−15.0	10
4151	7500	−14.0	48
3516	8500	−14.8	25
7469	8500	−15.5	30:

* The maximum widths of the hydrogen lines are from Table 5. The absolute magnitude and the percentage of the total light in the nucleus are derived from the data in Table 1. The absolute magnitude of NGC 1275 is calculated on the assumption of $0^m.5$ photographic interstellar absorption, a value suggested by the low galactic latitude and counts of faint nebulae in the vicinity of NGC 1275.

emission lines increases with absolute magnitude and with the ratio of light in the nucleus to the total light of the nebula. No definite correlation seems to exist between the line widths and color temperatures or spectral type of the nucleus, and the number of nebulae investigated is too small to indicate any certain correlations of widths of the emission lines with emission-line intensity ratios.

Since some of the brightest emission knots in the periphery of other extragalactic nebulae have total absolute magnitudes comparable with those of the emission nuclei, the question arises whether such emission knots show spectra with wide lines. Spectra of NGC 5471 (abs. mag. −9) and NGC 604 (abs. mag. −10), the brightest emission nebulae in the spirals M 101 and M 33, revealed no evidence of widening of the lines. At the writer's request, Dr. Mayall kindly examined the available Lick Observatory spectra of the giant emission nebula 30 Doradus (abs. mag. −14) in the Large Magellanic Cloud. He reports that the emission lines on the existing plates show no conspicuous evidences of broadening. Mayall also states that the very bright knot in NGC 2366 reveals no large line width. Evidently there is no close connection between the giant diffuse nebulae and the nuclei of spirals showing nebular emission lines.

Further discussion of the data will be presented in a contribution being prepared jointly by Dr. R. L. Minkowski and the present author.

It is a pleasure to express my sincere gratitude to the National Research Council for the Fellowship which made this investigation possible and to Dr. W. S. Adams, director of the Mount Wilson Observatory, for allowing me full use of the facilities of the observatory. I am greatly indebted to Dr. E. P. Hubble for his continued guidance in this investigation, and I want to thank both Dr. Hubble and Mr. M. L. Humason for generously placing their observational material at my disposal. The helpful advice of Dr. R. L. Minkowski and all the other members of the Mount Wilson Observatory staff is heartily acknowledged.

CARNEGIE INSTITUTION OF WASHINGTON
MOUNT WILSON OBSERVATORY
October 1942

ON THE EXISTENCE OF A THIRD COMPONENT IN THE SYSTEM 70 OPHIUCHI

DIRK REUYL AND ERIK HOLMBERG

ABSTRACT

Photographic observations of 70 Ophiuchi at the Leander McCormick Observatory give some anomalies that may be explained by the assumption of a third body. The photographic material consists of 33 grating plates (1932–1942) and 64 parallax plates (1914–1917, 1928–1932, 1939). The perturbations have a period of about 17 years and an amplitude, in X and Y, of about 0".015. The mass of the invisible companion amounts to 0.01 solar units.

The system 70 Ophiuchi, A and B ($\alpha = 18^h0^m.4$, $\delta = +2°31'$, 1900), with magnitudes 4.3 and 6.0, is one of the most interesting and one of the most frequently observed double stars. The latest determination of the orbit by K. A. Strand[1] resulted in a period of 87.85 years and a semi-major axis of 4".558. Certain apparently periodic deviations in the older visual observations have at various times given rise to the suspicion that the system contains a third, invisible body, the period of the perturbation ranging from 6 to 36 years. However, these observations have a comparatively low accuracy, and it is probable that the observed deviations from Keplerian motion must be attributed to the effect of systematic errors in the visual observations rather than to the influence of a third component. In the investigation by Strand, photographic observational material of high accuracy is used for the first time. According to the author, these observations do not support the theory of a third body. However, the photographic observations discussed by him extend over comparatively short intervals of time, 1915–1922 and 1931–1935. A discussion of all the material up to and including the 1941 McCormick observations was presented at the sixty-eighth meeting of the American Astronomical Society at the Yale Observatory in June, 1942. In the present paper a new discussion will be made, based on Strand's material together with the photographic observations made at the McCormick Observatory during the period from 1914 to 1942. The former consists of 29 grating plates taken at the Potsdam and Johannesburg observatories, the latter comprises a total of 1150 measured exposures on 97 grating and parallax plates.

On account of their relatively low accuracy, the older visual observations will not be taken into account.

The McCormick observations of 70 Ophiuchi are listed in Table 1. Most of the material consists of objective grating plates taken by one of us during the period 1932–1942. A minor part is represented by 64 parallax plates secured in the course of the systematic parallax work at the McCormick Observatory. For the grating plates three different kinds of gratings have been used, giving reductions of $2^m.9$, $2^m.5$, and $1^m.8$, respectively. In the last case the secondary image of the bright component is practically identical in magnitude with the primary image of the faint component. Thus, possible guiding errors are effectively neutralized. The grating plates have been taken only under the best possible conditions of seeing, with the result that the quality of nearly all the images is good. The exposures, ranging in number from 15 to 60 per plate, are placed in a regular pattern, close to and symmetrically located with respect to the center of the plate. Only the best images were selected for measurement. The number of measured images, which averages about 30 per plate, is given in the second column of the table. The measurements have been made by the present writers, each of them accounting for about half the number of plates. In order to check possible systematic differences, we have measured a number of

[1] *Leiden Ann.*, **18**, Part II, 1937.

TABLE 1

THE McCORMICK MATERIAL

Epoch	No.	X_{B-A} (2000.0)	Y_{B-A} (2000.0)	Remarks
1914.80	21	*+2".778 ± 0".006*	*−3".469 ± 0".005*	11 paral. pl.
1917.47	18	*+3.436 .006*	*−3.677 .005*	9 paral. pl.
1929.54	25	*+5.454 .007*	*−3.592 .005*	13 paral. pl.
1931.70	25	*+5.674 .007*	*−3.482 .005*	13 paral. pl.
1932.42	24	5.721 .007	3.367 .006	No grat.
32.42	30	5.714 .006	3.447 .004	Grat. 2.9
32.49	33	5.739 .004	3.431 .006	No grat.
32.54	46	5.683 .006	3.429 .004	Grat. 2.9
1932.47		*+5.711 .003*	*−3.424 .002*	
1934.44	26	5.887 .006	3.301 .004	Grat. 2.5
34.46	25	5.963 .010	3.318 .009	Grat. 2.5
34.47	33	5.894 .008	3.292 .004	Grat. 2.5
1934.46		*+5.906 .004*	*−3.302 .003*	
1935.58	32	5.931 .005	3.222 .005	Grat. 2.5
35.58	32	5.938 .005	3.205 .005	Grat. 2.5
35.58	43	5.949 .005	3.207 .005	Grat. 2.5
35.64	59	5.939 .005	3.218 .004	Grat. 2.5
1935.59		*+5.939 .003*	*−3.213 .002*	
1936.52	22	5.997 .007	3.122 .004	Grat. 2.5
36.52	26	5.980 .004	3.124 .004	Grat. 2.5
36.63	10	6.026 .012	3.130 .013	Grat. 2.5
36.67	42	5.976 .005	3.135 .005	Grat. 2.5
36.69	12	6.005 .015	3.146 .009	Grat. 2.5
1936.59		*+5.990 .003*	*−3.129 .002*	
1937.54	23	6.051 .005	3.057 .005	Grat. 1.8
37.59	15	6.024 .010	3.060 .008	Grat. 1.8
37.63	40	6.038 .006	3.042 .005	Grat. 1.8
1937.58		*+6.040 .004*	*−3.052 .004*	
1938.50	25	6.068 .006	2.963 .007	Grat. 1.8
38.50	22	6.053 .009	2.969 .011	Grat. 1.8
38.62	19	6.067 .011	2.941 .007	Grat. 1.8
38.62	33	6.055 .007	2.951 .006	Grat. 1.8
1938.56		*+6.061 .004*	*−2.956 .004*	
1939.60	27	6.080 .005	2.842 .004	Grat. 1.8
39.60	27	6.082 .005	2.824 .005	Grat. 1.8
1939.60		*+6.081 .004*	*−2.833 .003*	
1939.76	36	*+6.077 .005*	*−2.816 .004*	18 paral. pl.
1941.47	37	6.078 .004	2.650 .004	Grat. 1.8
41.64	36	6.054 .006	2.636 .005	Grat. 1.8
41.64	36	6.066 .005	2.635 .006	Grat. 1.8
41.66	36	6.066 .006	2.630 .006	Grat. 1.8
1941.59		*+6.067 .003*	*−2.639 .003*	
1942.47	53	6.070 .003	2.538 .004	Grat. 1.8
42.65	20	6.056 .006	2.504 .007	Grat. 1.8
42.65	40	6.073 .005	2.491 .005	Grat. 1.8
42.68	41	6.073 .005	2.508 .004	Grat. 1.8
1942.59		*+6.069 0.002*	*−2.512 0.004*	

plates in common. However, no differences of a systematic nature could be found. The plates have been measured in the usual way on the two Gaertner measuring machines of the McCormick Observatory. Each plate has been oriented by means of a trail of a near-by bright star and measured in direct and reversed positions.

In Table 2 the deviations of the observed values from those corresponding to the latest orbit, as derived by Strand, are listed. The positions corresponding to the orbit have been derived graphically, which gives an accuracy sufficient for the present purpose. In order to have a complete picture, the seven normal places corresponding to Strand's observations have been included in the table. A superficial inspection of the table shows that the deviations are of a systematic nature. This is especially the case in declination

TABLE 2

DEVIATIONS OF OBSERVED VALUES FROM STRAND'S ORBIT

Epoch	Wt.	Right Ascension		Declination		Material
		Obs.	Dev.	Obs.	Dev.	
1914.80	1	+2″.778	−0″.029	−3″.469	+0″.028	McCormick paral. pl.
15.25	3	2.915	− .005	3.521	+ .011	Strand
16.80	3	3.298	+ .005	3.637	− .004	Strand
17.47	1	3.436	− .010	3.677	− .010	McCormick paral. pl.
19.25	4	3.837	+ .002	3.744	− .008	Strand
22.43	2	4.438	− .011	3.802	− .017	Strand
29.54	1	5.454	− .007	3.592	+ .012	McCormick paral. pl.
31.27	7	5.637	.000	3.497	+ .011	Strand
31.70	1	5.674	− .002	3.482	− .001	McCormick paral. pl.
32.45	6	5.734	− .007	3.428	+ .005	Strand
32.47	2	5.711	− .031	3.424	+ .009	Reuyl
34.46	2	5.906	+ .019	3.302	− .016	Reuyl
35.56	5	5.960	+ .010	3.202	− .003	Strand
35.59	3	5.939	− .013	3.213	− .016	Reuyl
36.59	3	5.990	− .009	3.129	− .018	Reuyl
37.58	3	6.040	+ .003	3.052	− .032	Reuyl
38.56	3	6.061	− .006	2.956	− .028	Reuyl
39.60	3	6.081	− .007	2.833	− .010	Reuyl
39.76	1	6.077	− .015	2.816	− .010	McCormick paral. pl.
41.59	3	6.067	− .036	2.639	− .027	Reuyl
1942.59	3	+6.069	−0.025	−2.512	−0.013	Reuyl

where the last ten deviations all have a negative sign, their average value amounting to about −0″.017. For the subsequent least-squares solutions the weights given in column 2 of the table have been adopted. In order to take into account the different gratings used and, furthermore, to avoid an excessively large range in weights, a simple system of weighting, equal to w/P.E., has been adopted. In the case of plates taken without grating the quantity w is taken as 0″.005, whereas for grating plates w is put equal to 0″.007, 0″.008, and 0″.010, corresponding to gratings of $2^m.9$, $2^m.5$, and $1^m.8$ reduction, respectively. In this way the normal places obtained from parallax plates are given a weight of 1, whereas most of the normal places corresponding to the McCormick grating plates receive a weight of 3.

Since the present material is still not large enough to justify a new determination of the orbit of components A and B, the deviations listed in Table 2 will be used as a starting-point for the study of possible perturbations. For a least-squares solution, the following relation will be used:

$$\Delta = a \sin b(t - t_0) + c + (t - t_0)\mu .$$

The expression $a \sin b\,(t - t_0)$ corresponds to a motion in a circular orbit by the third body. The present material obviously is not large enough to reveal a possible eccentricity. The amplitude of the perturbation equals a, whereas b is inversely proportional to the period ($b = 2\pi/P$). The term $c + (t - t_0)\,\mu$ gives a correction to Strand's orbit. To make possible a least-squares solution the above expression is differentiated:

$$d\Delta = A\,da + B\,db + C\,dt_0 + d\,c' + t\,d\mu\,,$$

where

$$A = \sin b\,(t - t_0)\,, \qquad B = a\,(t - t_0)\cos b\,(t - t_0)\,, \qquad C = -a\,b\cos b\,(t - t_0)\,.$$

Preliminary values of a, b, and t_0 are derived graphically in order to determine the factors A, B, and C. A least-squares solution then gives the corrections da, db, dt_0, dc, and $d\mu$.

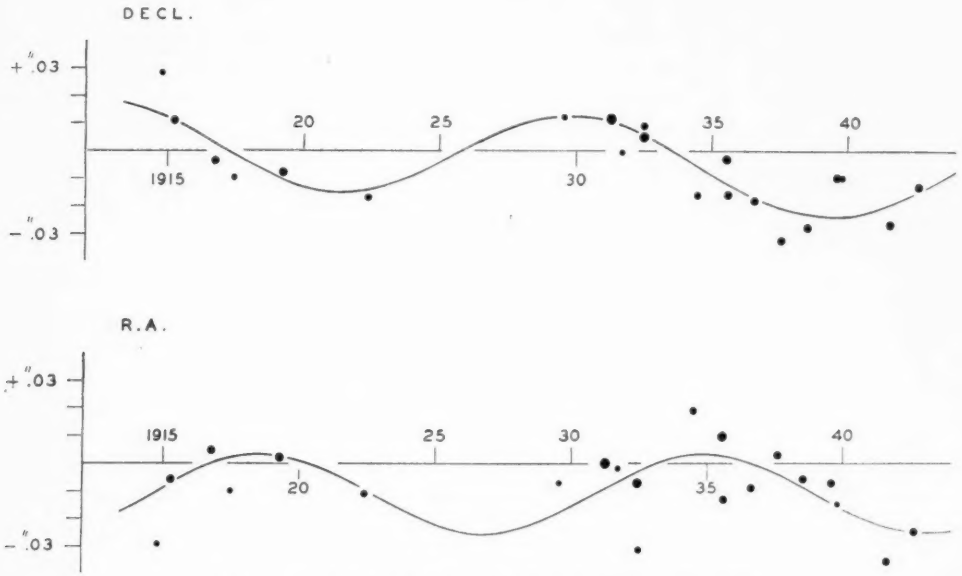

FIG. 1.—Deviations of observed values from Strand's orbit

By using the above procedure we obtain the following results:

	RIGHT ASCENSION			DECLINATION	
a =	0".014	± 0".003	a =	0".015	± 0".002
P =	16^{y}3	0^{y}9	P =	17^{y}9	0^{y}7
t_0 =	1930.8	0^{y}4	t_0 =	1925.6	0^{y}6
C =	−0".011	0".002	C =	−0".001	0".003
μ =	0".0000	0".0002	μ =	−0".0005	0".0002

Thus, a perturbation is obtained with a period of about 17 years and an amplitude, in X and Y, of about 0".015. The residuals obtained in the least-squares solutions correspond to probable errors of 0".0075 in right ascension and 0".0051 in declination, the average weight being 2.86. It may be remarked that the average observed probable errors of the positions of Table 2 amount to 0".0031 and 0".0028, respectively.

Figure 1 gives an illustration of the anomalies found above. By reference to Table 2 it will be seen that the normal points of greatest weight are represented in Figure 1 by

the filled circles of largest diameter. The perturbation seems to be rather well established in declination, whereas in right ascension additional observations are desirable. In the latter case the form of the curve depends to a large extent on the observations made during 1941 and 1942. Additional observations during the next few years will decide whether or not the right-ascension curve has to be changed.

Adopting a parallax of 0".20, the above amplitude of 0".015 corresponds to 0.075 astronomical units. The number of parallax plates available at the present time is insufficient to determine whether the third body belongs to component *A* or to component *B*. In the first case, if the mass of component *A* is assumed to be equal to 1.1 solar units,[2] a period of 17 years would correspond to a total orbital radius of 6.8 astronomical units. Thus, the resulting mass of the third component would be 0.012 solar units. In the second case, if the mass of component *B* is taken as 0.7 solar units, the total orbital radius would be 5.9 astronomical units, resulting in a value of 0.008 solar units for the mass of the third body.

As to the possibility of the blending of a fairly bright third component with *A* or *B*, this has been dismissed in view of the value of the orbital radius of 1".4 or 1".2. It may be remarked that a spectroscopic study of a perturbation of this kind would be extremely difficult, since the orbital velocity of the star (component *A* or *B*) would amount to only about 0.15 km/sec. The orbital radius of 6 or 7 astronomical units is rather large, as compared with the semi-major axis of the orbit of components *A* and *B* of about 23 astronomical units. It is to be expected that the orbit of the third body will not be very stable. The period, as well as the amplitude, of the observed perturbation may change considerably in the course of time. When more extensive photographic observational data are collected in the future, the system 70 Ophiuchi may furnish an illustration of a very interesting three-body problem.[3]

LEANDER MCCORMICK OBSERVATORY
UNIVERSITY OF VIRGINIA
October 1942

[2] Holmberg, *Determination of the Mass Ratio of 70 Ophiuchi* (in press).

[3] The following photographic observations of high quality, listed in *Pub. A.A.S.*, **10**, 70, 1940, have been inadvertently omitted from the discussion and should be entered in Table 2:

Epoch	Right Ascension		Declination		Material
	Obs.	Dev.	Obs.	Dev.	
1937.62	+6".026	−0".012	−3".020	−0".004	Lick
39.48	+6.084	− .001	−2.851	− .017	Sproul
40.56	+6.078	−0.023	−2.732	−0.010	Sproul

The average deviation of these values from the curves is 0".000 in right ascension and +0".012 in declination. Their inclusion will result in a small change in the curve in declination but will leave the curve in right ascension unchanged. It is noted that there will be no effect upon the discussion of the masses in the system.

A SPECTROGRAPHIC STUDY OF METEORITES

W. W. A. JOHNSON AND DANIEL P. NORMAN

ABSTRACT

Eighteen meteorites were investigated spectrographically for the presence of sixty-nine elements. Forty elements were found, twelve of which had not previously been reported by King. The spectrograms were taken by a jumping-plate technique that permitted estimates to be made of the relative volatility of the elements found, all of which, with the exception of aluminum and titanium, vaporized in the order expected from considerations of their boiling-points and abundances. No obvious grouping of these meteorites could be made on the basis of their atomic constituents. The two iron meteorites investigated contained less titanium than the stones, in agreement with previous chemical and spectroscopic data.

Dr. A. S. King's[1] interesting spectroscopic examination of thirteen meteorites suggested a further spectrographic study stressing the differences rather than the similarities in the minor atomic constituents of meteorites. Mr. H. H. Nininger, of the American Meteorite Laboratory, very kindly furnished us with samples of eighteen meteorites, which he described as follows (they have been arbitrarily numbered by us):

1. Holbrook, Arizona; fell July 19, 1912 (described by Foote and Merrill, *Smithsonian Misc. Coll.*, **69**, No. 9, Pub. 2149)
2. Miami, Texas; date of fall unknown
3. Washougal, Washington; July 2, 1939 (sawings produced by sawing very friable material)
4. Whittman, Nebraska; date of fall unknown
5. Johnstown, Colorado (crystalline inclusion separated from matrix)
6. Springwater, Saskatchewan; date of fall unknown (pallasite)
7. Loomis, Nebraska; date of fall unknown
8. Texline, Texas; date of fall unknown
9. Arcadia, Nebraska; date of fall unknown
10. Smith Center, Kansas; date of fall unknown
11. Oxidized crust of Monahans, Texas, iron meteorite
12. Richardton, North Dakota; fell June 30, 1918 (*Jour. Geol.*, **27**, 431)
13. Sandia Mountains, New Mexico; date of fall unknown
14. Pasamonte, New Mexico; fell March 24, 1933
15. Leeds, Quebec (nodule)
16. Johnstown, Colorado; fell July 6, 1924 (described by Hovey and Merrill)
17. Sofer, Oklahoma; sawings from an iron meteorite
18. Graphite nodule from Xiquipilco, Mexico, iron meteorite

(Meteorites Nos. 12, 14, and 18 appear to be common to King's list and ours)

The spectrographic technique used has been developed by the authors on the basis of qualitative analyses of a wide variety of ferrous samples of known composition. A pair of special spectrographic electrodes of quarter-inch diameter (Dow Chemical Co., Midland, Michigan) were introduced in the arc stand. In the lower (cathode) electrode a crater 5 mm wide and 6 mm deep was drilled by a special fixture. The upper electrode was pointed in a pencil sharpener reserved exclusively for this purpose. The arc was operated at 15 amperes (d.c.) for 1 minute to volatilize any traces of metal that might have been introduced in preparing the electrodes; then a 40-second spectrogram was taken to identify any impurities intrinsically present in the electrodes (boron was usually the only impurity; occasionally there were traces of magnesium and silicon), and the electrodes were allowed to cool in the arc stand. The sample (weighing approximately 100 mg.) was introduced in the crater of the lower electrode, the spectrograph shutter opened,

[1] *Ap. J.*, **84**, 507, 1936.

the arc started, and the spectrograph plateholder racked down every 40 seconds until the sample was burned to completion. (This procedure is essentially the jumping-plate system used in eclipse spectrography.) The exposure time used was the optimum exposure dictated for our instruments by the twin opposing factors of maximum exposure for faint lines and minimum exposure for the background to permit maximum visibility for faint lines.

The direct-current arc was operated at 15 amperes (230-volt input), while the inter-electrode gap was held at 3 mm as the carbons burned away. The gap length and amperage were maintained rigidly. The voltage across the gap fluctuated roughly from 40 volts at the start of a run to 50 volts when the sample had been completely consumed. Even the most refractory samples were completely volatilized at the end of 10 minutes' arcing. We cannot stress too strongly the importance of thus burning samples to completion, since small traces of refractory elements (particularly the noble metals) and of elements which form high-boiling carbides in the reducing atmosphere present in the arc, notably zirconium,[2] will be markedly concentrated in the last few minutes of exposure time.

An enlarged image of the arc was formed on the slit of the spectrograph with a quartz lens and was so adjusted that the image of the cathode fell just off the edge of the Hartmann slide delimiting the slit length, thus making use of the enhanced sensitivity of many elements in the cathode layer.[3] Two grating spectrographs were used in making the spectrograms. The wave-length range from λ 2175 to λ 3525 was photographed on Eastman 33 plates in the first order of a 3-meter grating spectrograph having a dispersion of 5.6 A/mm. The wave-length region from λ 3200 to λ 6800 was photographed on Agfa Superpan Press film in the first order of a 1-meter grating spectrograph having a dispersion of 15A/mm (the second-order ultraviolet was absorbed by a Wratten 2A filter).

The following sixty-nine elements (which are usually detected in qualitative spectrochemical analyses) were sought: *Ag, Al, As, Au, B, Ba, Be, Bi, Ca, Cb, Cd, Ce, Co, Cr, Cs, Cu, Dy, Er, Eu, Fe, Ga, Gd, Ge, Hf, Hg, Ho, In, Ir, K, La, Li, Lu, Mg, Mn, Mo, Na, Nd, Ni, Os, P, Pb, Pd, Pr, Pt, Ra, Rb, Re, Rh, Ru, Sb, Sc, Si, Sm, Sn, Sr, Ta, Tb, Te, Th, Ti, Tl, Tm, U, V, W, Yb, Yt, Zn, Zr.* The elements found are listed in Table 1. The first column of the table contains the elements in the alphabetical order of their symbols. The succeeding eighteen columns list the approximate abundance of the elements found, on the following logarithmic scale:

1 = 100–1 per cent	5 = Less than 0.01 per cent
2 = 10–0.1 per cent	? = Abundance estimate uncertain
3 = 1–0.01 per cent	*m* = Partially masked by lines of other constituents.
4 = 0.1–0.001 per cent	

The last two columns list the elements found by King,[4] in irons and in stones, respectively. His numerical intensity scale has, however, been inverted to agree with our magnitude scale.

The limit of identification[5] for the spectrographic analysis of the elements varies markedly with the element concerned and with the matrix in which it is present.[6] Since iron is a major constituent of all meteorites, stones as well as irons (the fact that carbon is the major constituent of graphitic meteorites is counterbalanced by the fact that all the samples are burned in graphite electrodes), the matrix may be considered, to a first

[2] D. Richardson, *Proc. Fifth Summer Conference on Spectroscopy*, p. 68, New York: John Wiley & Sons, 1938.

[3] L. W. Strock, *Spectrum Analysis with the Carbon Cathode Layer*, London: Adam Hilger, 1936.

[4] *Op. cit.*, p. 510.

[5] F. Feigl, *Mikrochem.*, **1**, 4, 1923.

[6] Pierce, Torres, and Marshall, *Ind. Eng. Chem. Anal. Ed.*, **12**, 44, 1940.

TABLE 1

ABUNDANCES OF ELEMENTS IN METEORITES

ELEMENT	METEORITE NO.																		KING	
																			Irons	Stone
	1	2	3	4	5	6	7	8	9	10	11	12	13	14	15	16	17	18	19	20
Ag	3	...	3	5	5	5	3	5	...	...	...	4	...	4	...	...	...	5	5	5
Al	3	3	2	2	2	3	3	3	2	3	...	2	...	1	5	3	5	5	3	2
As	5	...	...	4	5	4	...	...	...	...	5	5	...	...	...	...	...	...	...	...
Au	...	...	...	...	...	...	...	5?	...	...	...	...	...	...	...	...	...	2?	5	...
Ba	...	...	4	...	5	...	5	...	3	...	5	5	5	5	5	...	5	...	5	5
Be	...	...	...	...	...	...	...	...	...	...	4?	4?	4?	...	4?	...	4?	3	...	...
Ca	3	4	4	4	4	5	4	4	4	4	5	4	4	4	4	4	4	4	4	2
Cd	...	...	...	...	...	...	...	...	...	...	...	5	5	...	...	5	5	...	...	...
Ce	...	...	5?	5?	...	...	4	...	5	...	5	5?	4	...	...	...	5	...	...	...
Co	1	2	2	2	2	2?	2	2	2	2	2	2	2	...	2	4	2	2	3	4
Cr	2	1	1	2	1	5	2	2	1	2	3	1	5	2	3	1	5	2	5	2
Cs	...	4	3	...	5	...	5	...	5	5	4	4	3	5	4	5	4	5	...	5
Cu	3	3	3	3	5	3	3	3	3	3	2	2	3	3	3	3	4	3	3	4
Fe	1	1	1	1	1	1	1	1	1	1	1	1	1	1	1	1	1	1	1	2
Hg	...	...	...	...	...	...	...	5?	...	...	5?	...	5?	...	5?	5?	...	...	...	...
In	4	4	3	4	4	4	4	4	3	4	...	3	...	3	...	2	...	5	...	...
Ir	...	...	...	...	...	...	...	...	...	...	3?	...	...	...	...	...	...	3?	...	...
K	5	5	5	5	5	4	5	5	5	...	5	5	5	5	5	5	...	5	5	3
Li	...	...	...	...	5	5	...	...	5	5	5	4	5	4	5	4	...	...	5	4
Mg	1	1	1	1	1	1	1	1	1	1	3	1	3	1	2	1	3	3	4	1
Mn	1	1	1	1	1	1	2	2	2	2	4	2	...	1	4	1	3	1	5	2
Mo	5	5	2	5	5	5	5	5	...	4	4	5	5	5	4	5	4	5	5	...
Na	2	2	2	2	5	...	2	2	2	2	...	2	5	2	3	2	...	...	5	1
Ni	1	1	1	1	2	1	1	1	1	1	1	1	2	3	1	1	1	1	1	3
P	2	3	3?	3	3	*m*	3	2	3	3	2	3	2	...	2	...	2	1	5	?
Pb	...	...	5	5	...	...	4	...	...	...	...	...	...	...	...	...	...	5	5	5
Pd	...	...	...	...	...	...	...	...	...	...	...	5	...	...	...	5	5	5	...	...
Pt	5?	...	5?	5?	5?	...	...	5?	5?	5?	5?	5?	5?	5	...	5	5	...	...	...
Ru	...	...	...	...	...	...	...	...	...	5?	...	5?	5?	...	5?	5?	...	...	5	...
Sb	3	3	2	3	2	...	3	4	4	4	...	4	...	3	...	3	...	5	5	...
Sc	...	...	...	...	...	...	...	...	...	...	...	...	3?*m*	...	...	...	...	...	...	5
Si	1	1	1	1	1	1	1	1	1	1	3	1	4	1	1	1	5	3	3	2
Sn	...	...	...	...	...	...	5	...	...	...	...	...	...	5?	...	...	5?	...	5	...
Sr	4	...	...	4	5	...	...	4	4	5	3	...	4	5	5	...	5	...	5	5
Te	...	...	5	...	...	...	...	...	4	5	...	5	...	4	...	4	...	...	...	...
Ti	2	2	1	1	1	4	2	4	2	3	5	3	...	1	...	2	...	...	5	3
Tm	3	5	4	4	4	...	4	...	...	5	...	...	...	...	...	4	...	...	...	...
V	2	2	2	2	2	2*m*	2	4	3	3	4	3	5	3?	5	2	5	5	5	5
Zn	...	...	...	5	3	...	...	...	5	5	5?	5	...	4	...	...	...	5	5	5
Zr	...	4?	...	...	...	5	...	5?	...	...	...	...	...	...	...	...	...	...	...	...

approximation, as reasonably similar in all the meteorites and as comparable to terrestrial ferrous samples. However, even in the case of samples having identical major constituents, minor constituents, such as sodium, can be detected in concentrations of 1×10^{-5} per cent, whereas an element such as tungsten might not be detected in concentrations of 1×10^{-2} per cent.

Our estimates of the abundances of the various elements found have been corrected for these differences in sensitivity on the basis of our experience with samples of known composition. However, such a correction cannot be applied to the twenty-nine elements (out of the sixty-nine sought) which were not detected. These elements can be divided roughly into two groups: elements whose limit of detection is of the order of 10^{-4} per cent or greater and elements whose limit of detection is 10^{-3} per cent or less. These two groups are listed respectively in the first and second columns of Table 2. The third column lists the elements not found whose ultimate lines may have been masked by subordinate lines of other elements.

TABLE 2

SENSITIVITY OF ELEMENTS NOT FOUND IN METEORITES

Sensitivity Greater than 10^{-4} Per Cent	Sensitivity Less than 10^{-4} Per Cent			Masked
Bi	*Dy*	*Nd*	*Tb*	*B*
Cb	*Er*	*Os*	*Th*	*Ga*
Ge	*Eu*	*Pr*	*Tl*	*Gd*
Ra	*Hf*	*Re*	*U*	*Rb*
Rh	*Ho*	*Sm*	*W*	
Yb	*La*	*Ta*	*Yt*	
	Lu			

The following twelve elements not reported by King[4] were present in the meteorites we analyzed: *As, Be, Cd, Hg, In, Ir, Pd, Pt, Te, Tm, Zr.* We note that they are all present in amounts of four or less. King found three elements in the meteorites he studied that we did not find: *Rb, Ga, Ge.* The ultimate lines of rubidium (λ 7800 and λ 7947), used by King, were not on our plates, and the lines we used (λ 4202 and λ 4215) are masked when iron is a major constituent. The ultimate lines of gallium were masked by subordinate lines of other elements. The ultimate lines of germanium were favorably placed in the wave-length range covered by our plates and would not have been masked by lines of other elements. Repeated search failed to disclose any trace of germanium, and we must conclude, therefore, that it simply was not present in the samples we analyzed.

The various elements observed should appear and disappear, in successive spectra taken by the jumping-plate technique, in the order of their boiling-points and abundances. Measurements show that the elements found fall into four groups: (1) elements which appear only in the first two spectra: *Ag, Ba, Ca, Cd, Cs, Cu, Hg, In, K, Li, Na, Pb, Sn, Sr, Zn;* (2) elements persisting about halfway down the plates: *Be, Mg, Mn, Mo, P, Si;* (3) elements appearing in the last few spectra only: *As, Au, Ir, Pd, Pt, Ru, Sb, Te, Tm, Zr;* and (4) elements persisting throughout all spectra: *Al, Ce, Co, Cr, Fe, Ni, Ti, V.* We note that aluminum and titanium in terrestrial samples usually occur in group 2; and an explanation of their anomalous behavior would probably have to be sought in the nature of the negative radicals attached to them, since the latter are known to affect their volatility.[7] Elemental phosphorous boils at about 270° C.; but anions containing

[7] Brode and Hodge, *J.O.S.A.*, **31**, 58, 1941.

phosphorous dissociate at very much higher temperatures, even in a reducing atmosphere, and hence the appearance of phosphorous in group 2 is not unexpected. In general the time sequence of the elements is in good agreement with expectations based on their volatilities and abundances.

An attempt was made to group these meteorites on a rational system based on the observed abundances of various elements. We note that iron was always high and could not be used for classification, in agreement with King's observation that iron was high in stones, irons, and graphite nodules.

Titanium, however, appeared to offer a satisfactory peg on which to hang a classification. Accordingly, the meteorites were divided into two groups depending on (1) whether titanium was abundant or of intermediate abundance or (2) whether titanium was poor or lacking. An attempt to divide (1) further on the basis of aluminum content, yielded two subdivisions: (A) high in *Al* and *Ti:* Nos. 3, 4, 5, 9, 14; (B) low *Al*, intermediate *Ti:* Nos. 1, 2, 7, 10, 12, 16. A different regrouping of these meteorites rich in titanium was attempted on the basis of the presence or absence of certain volatile elements (*As, Li, Sr, Zn*), which yielded (A′) volatiles present: Nos. 4, 5, 10, 12, 14; and (B′) volatiles absent: Nos. 1, 2, 3, 7, 9, 16. We do not feel that great significance should be attached to these correlations, and no further correlation is apparent in the data for this group.

The meteorites low or lacking in titanium (2) could in turn be subdivided into two groups depending on their silicon content: (C) high silicon: Nos. 6, 8, 15, and (D) low silicon: Nos. 11, 13, 17, 18. We note further that in these groups high silicon goes hand in hand with high magnesium, while low silicon is accompanied by intermediate magnesium content. There is a virtual absence of aluminum and sodium in group D, while phosphorous is higher in group D than in group C.

Considering the diversity of origin and of physical structure of the samples we have studied, it is not surprising that they fail to fall into simplified groupings.

An important question remains unanswered at present: What are the variations in the distribution of the minor elements throughout a single meteorite, and is there any evidence of a radial inhomogeneity in the distribution of the more volatile elements as we go from the center of a meteorite outward? We know that the inclusions in meteorites differ markedly from the matrix (cf. Nos. 5 and 16), and we know that, mineralogically speaking, meteorites are not uniform (pallasite, e.g., consists of a magnesium-iron silicate in a network of metal[8]); but we know of no studies of the variation of representative samples taken along radial borings of a single meteorite. We hope, in the future, to be able to carry out such studies.

NEW ENGLAND SPECTROCHEMICAL LABORATORIES
WEST MEDWAY, MASSACHUSETTS
November 1942

[8] G. P. Merrill, *U.S. Nat. Mus.*, Bull. 94, 1916.

THE CONTINUOUS SPECTRUM OF MODEL STELLAR ATMOSPHERES

RALPH E. WILLIAMSON

ABSTRACT

On the assumption that atomic hydrogen and the negative hydrogen ion are the only sources of continuous opacity in stellar atmospheres, the properties of the continuous spectra of twelve model atmospheres characterized by various values of the effective temperature T_e and the average electron pressure p_e, are investigated. An improved value of the atomic continuous absorption coefficient for H^- is used in the computations. Approximate values for the Rosseland mean absorption coefficients $\bar{\kappa}$ are derived for a wide range of the parameters p_e and T_e and for the twelve model atmospheres (with $10 \leqslant p_e \leqslant 10^4$; $5600° \leqslant T_e \leqslant 10{,}080°$); the monochromatic mass-absorption coefficients κ_ν are calculated for a number of selected frequencies covering a wave-length range of 2500–10,000 A. The ratio $\bar{\kappa}/\kappa_\nu$ is used to determine the logarithm of the ratio of the monochromatic flux F_ν through each model atmosphere to the black-body flux $F_\nu^{(e)}$ corresponding to T_e for the atmosphere. Color temperatures for regions 3300–3650 A, 3850–4550 A, and 5550–7150 A, as well as the magnitudes of the Balmer and the Paschen discontinuities in the continuous spectrum, are computed for each of the model atmospheres. Comparison of the calculated values of the Balmer discontinuity with observations of this quantity indicate a value of $p_e = 10^3$ for stars of spectral types A and a somewhat smaller value for stars of type F. Plots of the reciprocal color temperature $\Theta_c = 5040/T_c$ in three spectral regions, as a function of $\Theta_e = 5040/T_e$ for observations on stars, for the models here considered, and for those of Wildt, who used older values of the absorption coefficient of H^- (both the latter for $p_e = 10^3$), show that the agreement of theory and observation has been improved by the present calculations. In general, the agreement with the observations is less satisfactory in the longer wave lengths. It is shown that the present models predict some *increase* of T_c with frequency for the visual and near infrared, while the observations of Williams and of Hall show a slight *decrease* of T_c with frequency. The magnitude of the Paschen discontinuity for Vega as observed by Hall and Williams is satisfactorily predicted by an appropriate model ($\Theta_e = 0.5$, $p_e = 10^3$).

I. INTRODUCTION

An important problem of theoretical astrophysics is the prediction from purely physical principles of the radiant flux F_ν emerging from the surface of a star. While an ideal treatment of the problem would involve an accurate computation of F_ν (including the rapid variations in it which will constitute the absorption lines) for a number of model atmospheres defined by certain values of the parameters T_e, g, and the chemical abundances, it appears that in practice we can formally distinguish between a problem of the continuous spectrum of a star and a problem of the absorption lines.

On this understanding we suppose that we can consider the *continuous* spectrum of a star as arising from sources of opacity which change only slowly with frequency and can treat absorption lines as superposed on this background in such a way that the original large-scale distribution of energy is unaffected by them.

The calculation of the energy distribution in the continuous spectrum of a model stellar atmosphere of specified constitution was first undertaken by McCrea.[1] He investigated atmospheres composed of a mixture in different proportions of hydrogen and a hydrogen-like element with an ionization potential of 5 volts and compared the calculated continuous spectra with the observations of Yü. Since then similar calculations have been made, assuming various chemical compositions of the model atmospheres, by Unsöld[2] and by Pannekoek.[3] However, Wildt's discovery[4] of the importance of the negative hydrogen ion as a source of opacity in stellar atmospheres has necessitated a revision

[1] *M.N.*, **91**, 836,1931.

[2] *Physik der Sternatmosphären*, Berlin: Julius Springer, 1938.

[3] *Pub. Astronomical Institute of U. of Amsterdam*, No. 4.

[4] *Ap.J.*, **89**, 295, 1939.

of these calculations. For the continuous spectrum this has been done by Wildt,[5] while Strömgren[6] has incorporated it into his treatment of the line spectrum of the sun. Wildt's work was based on values of the continuous absorption coefficient for H^- as computed by Massey and Bates,[7] who used an approximate wave-function for the ion derived by Bethe[8] and by Hylleraas.[9] It has been recently found by the writer[10] that a more accurate wave-function for H^- yields an absorption coefficient substantially different from that obtained by Massey and Bates. It is therefore of some interest to see in what way the change in the absorption coefficient will affect the calculations of Wildt on the continuous spectra of model stellar atmospheres. This is the principal object of this paper. More particularly, we shall investigate the emergent flux F_ν of the radiation in the continuous spectra of model stellar atmospheres, whose continuous opacity is supplied entirely by atomic hydrogen and negative hydrogen ions.[11] In the calculations the customary assumptions of local thermodynamic equilibrium and of the constancy of the ratio $\kappa_\nu/\bar{\kappa}$ throughout the atmosphere have been made. Because of the latter assumption it is convenient to use as the independent parameters the effective temperature T_e and the electron pressure p_e[12] (instead of g).

II. THE ROSSELAND MEAN ABSORPTION COEFFICIENT

It is well known from the classical investigations on radiative equilibrium of stellar atmospheres by Milne and others[13] that the emergent flux F_ν is given by

$$F_\nu = \frac{2h\nu^3}{c^2}\int_0^\infty \frac{K_2\left(\tau\cdot\frac{\kappa_\nu}{\bar{\kappa}}\right)}{e^{h\nu/kT_e[3/4[\tau+q(\tau)]]^{-1/4}}-1}\,\frac{\kappa_\nu}{\bar{\kappa}}\,d\tau\,, \tag{1}$$

where κ_ν and $\bar{\kappa}$ denote the monochromatic and the Rosseland mean mass-absorption coefficients, respectively. Further, in equation (1) τ denotes the optical depth derived from κ and $q(\tau)$ is a slowly varying function of τ and approximately equal to $\frac{2}{3}$. Finally,

$$K_2(x) = \int_1^\infty e^{-tx}\frac{dt}{t^2}\,. \tag{2}$$

Burkhardt[14] has evaluated equation (1) numerically and gives a table of the quantity $\log_{10} F_\nu/F_\nu^{(e)}$ as a function of the two parameters $h\nu/\kappa T_e$ and $\bar{\kappa}/\kappa_\nu$, where

$$F_\nu^{(e)} = \frac{2h\nu^3}{c^2}\,\frac{1}{e^{h\nu/kT_e}-1}\,. \tag{3}$$

[5] *Ap.J.*, **90**, 611, 1939; **93**, 47, 1941.

[6] *Festschrift für Elis Strömgren*, p. 218, Copenhagen, 1940.

[7] *Ap.J.*, **91**, 202, 1940.

[8] *Zs. f. Phys.*, **57**, 815, 1929.

[9] *Zs. f. Phys.*, **60**, 624, 1930.

[10] *Ap.J.*, **96**, 438, 1942.

[11] For a discussion of the validity of this assumption cf. Wildt, *Ap.J.*, **90**, 611, 1939.

[12] Thus the presence of free electrons from other sources than hydrogen is assumed, but no calculations based on abundances and ionizations of the "metals" are considered. Such calculations more properly belong in the theory of the formation of absorption lines (see Strömgren).

[13] Cf. *Handbuch der Astrophysik*, **3**, Part III, 130, 147–55, Berlin: Julius Springer, 1930.

[14] *Zs. f. Ap.*, **13**, 56, 1936.

It is therefore necessary to have a knowledge of both κ_ν and $\bar{\kappa}$ for each pair of values of T_e and p_e for which we desire the emergent flux F_ν. Since the run of F_ν with frequency is insensitive to small errors in κ and since a direct evaluation of $\bar{\kappa}$ would be quite tedious, the following approximate method may provide sufficient accuracy for our present purposes.

Let the Rosseland mean of the mass-absorption coefficient of atomic hydrogen alone be $\kappa(H)$ and that due to the negative hydrogen ion alone, $\bar{\kappa}(H^-)$. For most values of T_e and p_e one of the two mean absorption coefficients is much larger than the other. We can then take account of the presence of the less important source of opacity as a small correction to the more predominant one. Such a table of corrections has been provided by Strömgren[15] in his work on the solar atmosphere. He tabulates the quantity $\log_{10} \bar{\kappa}/\kappa(H)$ as a function of $\log_{10} \bar{\kappa}(H^-)/\bar{\kappa}(H)$ and of T. It is further seen that the dependence on T of this correction term is practically negligible. The problem of obtaining the Rosseland mean $\bar{\kappa}$ is now greatly simplified, involving only the calculation of $\bar{\kappa}(H^-)$ and applying the appropriate correction term to the already well-known quantity $\bar{\kappa}(H)$.[16]

The contribution to the monochromatic absorption coefficient of H^- is made by bound-free and free-free transitions of the optical electron. The latter is comparatively unimportant except for wave lengths greater than 12,000 A.

Let $a_\nu(H^-)$ denote the absorption coefficient per negative hydrogen ion due to the bound-free transitions; further, let $a_\nu^{(f)}(H^-)$ denote the absorption coefficient per neutral hydrogen atom and per unit electron pressure due to the free-free transitions. Then

$$\kappa_\nu(H^-) = \frac{1}{m_H}\left\{\frac{N_{H-}}{N_{H-}+N_H+N_{H+}}\, a_\nu(H^-) + \frac{N_H}{N_{H-}+N_H+N_{H+}}\, p_e a_\nu^{(f)}(H^-)\right\} . \quad (4)$$

N_x denotes the number of X-atoms (or X-ions) per unit volume, and m_H is the mass in grams of the hydrogen atom. Now

$$\left.\begin{aligned} \frac{N_H p_e}{N_{H-}} &= 4\,\frac{(2\pi m)^{3/2}(kT)^{5/2}}{h^3}\, e^{-h\nu_{H^-}/kT} = \phi(T) , \\ \frac{N_{H+} p_e}{N_H} &= \frac{(2\pi m)^{3/2}(kT)^{5/2}}{h^3}\, e^{-h\nu_H/kT} = \phi_0(T) , \end{aligned}\right\} \quad (5)$$

where $h\nu_X$ is the first ionization energy of the X-atom or X-ion. Since $N_{H^-} << N_H$ for all cases of interest in stellar atmospheres, we may write equation (4) as

$$\kappa_\nu(H^-) = \frac{1}{m_H}\,\frac{p_e^2}{\phi_0 + p_e}\left\{\frac{1}{\phi}\, a_\nu(H^-) + a_\nu^{(f)}(H^-)\right\} . \quad (6)$$

The effect of stimulated emissions (as negative absorptions) is readily taken into account. Denoting the "effective" absorption coefficient by κ'_ν, we have

$$\kappa'_\nu = \kappa_\nu(1 - e^{-h\nu/kT}) . \quad (7)$$

[15] *Op. cit.*, Table 4.

[16] See, e.g., Wildt, *Ap.J.*, **90**, 611, Table 1, 1939.

Now

$$\overline{\kappa'}(H^-) = \frac{1}{m_H} \frac{p_e^2}{\phi_0 + p_e} \bar{a}(H^-) , \tag{8}$$

where

$$[\bar{a}(H^-)]^{-1} = \frac{15}{4\pi^4} \int_0^\infty \frac{dB_\nu}{dT} \left\{ (1 - e^{-h\nu/kT}) \left[\frac{1}{\phi} a_\nu(H^-) + a_\nu^{(f)}(H^-) \right] \right\}^{-1} d\nu . \tag{9}$$

In future by "absorption coefficient" we shall always mean the "effective" absorption coefficient including the stimulated emissions as in equation (7); we shall accordingly suppress the primes. Since the integrand in equation (9) is independent of p_e, it is clear that one set of integrations for different values of T is all that is needed to obtain $\bar{\kappa}(H^-)$. Table 1 gives $\bar{a}(H^-)$ as computed by graphical integration, using the revised

TABLE 1

ROSSELAND MEAN OF H^- ABSORPTION COEFFICIENT/GRAM NEUTRAL H/DYNE p_e

$\theta = \frac{5040}{T}$	$\bar{a}_{H^-} \times 10^{27}$ Present	$\bar{a}_{H^-} \times 10^{27}$ Wheeler and Wildt	$\theta = \frac{5040}{T}$	$\bar{a}_{H^-} \times 10^{27}$ Present	$\bar{a}_{H^-} \times 10^{27}$ Wheeler and Wildt
0.5	2.72	.....	1.4	26.8	27.7
0.6	5.80	.....	1.6	26.2	27.7
0.8	14.5	12.4	1.8	24.8	25.5
1.0	21.8	19.4	2.0	23.1	23.9
1.2	25.7	25.7			

values of Williamson[17] for $a_\nu(H^-)$ and the results of Wheeler and Wildt for $a_\nu^{(f)}(H^-)$.[18] The last column of Table 1 gives for comparison the results of a similar computation by Wheeler and Wildt, who used the earlier values of the bound-free absorption coefficient according to Massey and Bates. It is seen that no large changes in $\bar{a}(H^-)$ have been introduced by the new calculations. By interpolating among the values given there and substituting into equation (8), we can readily obtain $\bar{\kappa}(H^-)$. In Table 2 the common logarithm of this quantity has been entered in the top line of each square; further in this table the second line contains $\log_{10} \bar{\kappa}(H)$ from Wildt's paper,[16] while the third gives $\log_{10} \bar{\kappa}$, derived after applying Strömgren's corrections.

III. THE CONTINUOUS SPECTRUM OF THE MODEL ATMOSPHERES

As we have already stated in the introductory section, to determine the emergent flux F_ν for a given model stellar atmosphere, we need the value of the absorption coefficient at the particular frequency ν in which we are interested, as well as the Rosseland mean absorption coefficient κ. We have already provided the necessary table of κ in the pre-

[17] *Loc. cit.*

[18] *Ap.J.*, **95**, 281, 1942.

ceding section. It now remains to evaluate κ_ν, which is the sum of the absorption coefficient $\kappa_\nu(H^-)$ due to H^- and the absorption coefficient $\kappa_\nu(H)$ due to hydrogen. The function $\kappa_\nu(H^-)$ can be readily found from equation (4) and the table of monochromatic atomic continuous absorption coefficients provided by the author.[19] For $\kappa_\nu(H)$ the customary Kramers' approximation was used as outlined, for example, in Unsöld's book. Once $\kappa_\nu = \kappa_\nu(H^-) + \kappa_\nu(H)$ and $\bar{\kappa}$ are both known, the ratio of the emergent flux F_ν to

TABLE 2*

ROSSELAND MEAN ABSORPTION COEFFICIENT/GRAM STELLAR MATERIAL

θ_e	p_e							
	10^{-3}	10^{-2}	10^{-1}	1	10	10^2	10^3	10^4
0.5	.....	.....	.....	.....	.....	.....	.....	1.19
	−3.97	−2.97	−1.97	−0.97	0.02	0.96	1.59	1.77
	−3.97	−2.97	−1.97	−0.97	0.02	0.96	1.59	1.89
0.6	.....	.....	.....	.....	.....	−0.52	0.53	1.54
	−3.58	−2.58	−1.58	−0.61	0.21	0.57	0.62	0.63
	−3.58	−2.58	−1.58	−0.61	0.21	0.62	0.95	1.62
0.7	.....	.....	.....	.....	−1.23	−0.21	0.79	1.79
	−3.29	−2.30	−1.37	−0.78	−0.63	−0.61	−0.61	.....
	−3.29	−2.30	−1.37	−0.78	−0.49	0.00	0.81	1.79
0.8	.....	.....	−3.12	−2.07	−1.06	−0.06	0.94	1.94
	−3.06	−2.25	−1.90	−1.85	−1.84	.....	.....	.....
	−3.06	−2.25	−1.86	−1.58	−0.95	−0.06	0.94	1.94
0.9	.....	−3.98	−2.96	−1.96	−0.96	0.04	1.04	2.04
	−3.27	−3.11	−3.09	−3.09	.....	.....	.....	.....
	−3.27	−3.02	−2.65	−1.91	−0.96	0.04	1.04	2.04
1.0	−4.89	−3.89	−2.89	−1.89	−0.89	0.11	1.11	2.11
	−4.33	−4.33	−4.33	.....	.....	.....	.....	.....
	−4.18	−3.69	−2.88	−1.89	−0.89	0.11	1.11	2.11
1.1	−4.84	−3.84	−2.84	−1.84	−0.84	0.16	1.16	2.16
	.....	.....	.....	.....	.....	.....	.....	.....
	−4.84	−3.84	−2.84	−1.84	−0.84	0.16	1.16	2.16
1.2	−4.81	−3.81	−2.81	−1.81	−0.81	0.19	1.19	2.19
	.....	.....	.....	.....	.....	.....	.....	.....
	−4.81	−3.81	−2.81	−1.81	−0.81	0.19	1.19	2.19

* Each square contains: first line, $\log_{10} \bar{\kappa}\,(H^-)$; second line, $\log_{10} \bar{\kappa}\,(H)$; third line, $\log_{10} \bar{\kappa}$.

the flux $F_\nu^{(e)}$ (which is the black-body flux corresponding to the effective temperature T_e) can at once be obtained by interpolating in Burkhardt's table. Tables 3, 4, and 5 and Figures 1, 2, and 3 summarize the results of such computations.

In Table 3 the quantities $\kappa_\nu(H^-)$ per gram of neutral hydrogen and per bar of electron pressure and $\kappa_\nu(H)$ per gram of neutral hydrogen are tabulated for different values of the reciprocal effective temperature $\theta_e = 5040/T_e$ and for a number of selected frequencies.

[19] *Op. cit.*, Table 2.

In Table 4 the final monochromatic absorption coefficients per gram of stellar material are given for twelve different model atmospheres; Table 4 also contains the quantities $\log_{10} F_\nu/F_\nu^{(e)}$ for these models at the selected frequencies. At the Paschen and the

TABLE 3*

MONOCHROMATIC ABSORPTION COEFFICIENTS

$\nu\times10^{-15}$	θ				
	0.5	0.6	0.7	0.8	0.9
0.30	1.62 100.6	2.73 4.646	4.48 0.2207	7.14 1.070×10^{-2}	11.09 5.279×10^{-4}
0.365	2.15 {55.70 171.6}	3.85 {2.573 9.752}	6.52 {0.1222 0.5665}	10.60 {5.927×10^{-3} 3.340×10^{-2}}	16.66 {2.923×10^{-4} 1.993×10^{-3}}
0.400	2.44 130.8	4.40 7.430	7.51 0.4315	12.26 2.544×10^{-2}	19.32 1.518×10^{-3}
0.420	2.57 113.2	4.64 6.432	7.96 0.3736	13.00 2.203×10^{-2}	20.48 1.314×10^{-3}
0.540	3.04 53.26	5.60 3.026	9.66 0.1758	15.86 1.036×10^{-2}	25.07 6.185×10^{-4}
0.600	3.12 38.74	5.76 2.201	9.93 0.1278	16.32 7.540×10^{-3}	25.82 4.499×10^{-4}
0.660	3.10 29.18	5.72 1.658	9.88 9.628×10^{-2}	16.25 5.678×10^{-3}	25.71 3.388×10^{-4}
0.779	2.89 17.68	5.35 1.004	9.28 5.833×10^{-2}	15.26 3.440×10^{-3}	24.16 2.052×10^{-4}
0.800	2.84 16.34	5.27 0.9287	9.12 0.05394	15.00 3.181×10^{-3}	23.74 1.898×10^{-4}
0.822	2.79 {15.07 317.1}	5.17 {0.8562 29.74}	8.95 {0.04973 2.811}	14.73 {2.932×10^{-3} 0.2667}	23.31 {1.750×10^{-4} 2.539×10^{-2}}
0.899	2.55 242.1	4.74 22.71	8.22 2.146	13.55 0.2037	21.48 1.939×10^{-2}
1.00	2.30 176.1	4.27 16.52	7.40 1.561	12.18 0.1481	19.29 1.410×10^{-2}
1.40	1.36 64.18	2.53 6.020	4.39 0.5689	7.23 5.399×10^{-2}	11.46 5.139×10^{-3}

* Each square contains: first line, κ_ν (H^-) per gram of neutral H and for an electron pressure of 10^3 bars; second line, $\kappa_\nu(H)$/gm neutral H. The values in braces are those at either side of a discontinuity.

Balmer discontinuities the relevant quantities are given for both sides of the discontinuity.

Figure 1 shows a plot of the absorption coefficient for the model atmosphere for $\theta_e = 0.5$, $p_e = 10^3$ bar.

TABLE 4*

Absorption Coefficient and Flux in Model Atmospheres

$\nu\times10^{-15}$	p_e = 10, θ_e = 0.8	p_e = 10, θ_e = 0.9	p_e = 10^2, θ_e = 0.6	p_e = 10^2, θ_e = 0.7	p_e = 10^2, θ_e = 0.8	p_e = 10^2, θ_e = 0.9	p_e = 10^3, θ_e = 0.5	p_e = 10^3, θ_e = 0.6	p_e = 10^3, θ_e = 0.7	p_e = 10^3, θ_e = 0.8	p_e = 10^4, θ_e = 0.6	p_e = 10^4, θ_e = 0.7
0.300	0.0736 + .036	0.103 − .007	3.51 +0.002	0.575 +0.047	0.651 +0.019	1.02 −0.008	50.4 − 0.043	5.96 + 0.026	4.06 + 0.038	6.42 + 0.021	26.2 + 0.035	38.9 + 0.038
0.365	.105 .131 − .008 − .042	.160 .161 − .078 − .081	2.25 7.72 + 0.058 − 0.086	0.703 1.11 +0.029 −0.033	1.00 1.03 −0.037 −0.044	1.59 1.60 −0.078 −0.078	30.9 92.9 + 0.009 − 0.095	5.54 11.7 + 0.041 − 0.053	6.06 6.46 − 0.007 − 0.016	9.95 9.97 − 0.037 − 0.037	35.9 42.2 0.000 − 0.016	59.6 60.0 − 0.013 − 0.013
0.400	.141 − .055	.188 − .110	6.15 − 0.067	1.10 −0.031	1.19 −0.069	1.87 −0.107	73.5 − 0.084	10.5 − 0.040	7.39 − 0.038	11.7 − 0.066	46.1 − 0.032	70.3 − 0.037
0.420	.146 − .061	.200 − .121	5.45 − 0.054	1.09 −0.033	1.27 −0.079	1.99 −0.120	64.9 − 0.074	9.92 − 0.033	7.82 − 0.048	12.5 − 0.077	48.0 − 0.038	75.1 − 0.049
0.540	.166 − .093	.249 − .183	2.97 + 0.041	1.11 −0.034	1.57 −0.127	2.48 −0.182	33.7 + 0.002	8.11 0.000	9.56 − 0.086	15.6 − 0.127	56.2 − 0.067	94.1 − 0.092
0.600	.169 − .101	.257 − .204	2.34 + 0.097	1.10 −0.032	1.62 −0.144	2.57 −0.203	25.6 + 0.051	7.58 + 0.015	9.87 − 0.097	16.2 − 0.143	57.7 − 0.074	97.6 − 0.104
0.660	.167 − .103	.257 − .217	1.89	1.07 −0.024	1.62 −0.154	2.56 −0.217	20.0 + 0.103	7.10 + 0.034	9.85 − 0.103	16.2 − 0.153	57.4 − 0.076	97.7 − 0.110
0.779	.155 − .084	.242 − .229	1.32	0.976 +0.007	1.53 −0.153	2.41 −0.230	13.01 + 0.260::	6.19 + 0.084	9.28 − 0.095	15.2 − 0.153	53.8 − 0.066	92.3 − 0.104
0.800	.153 − .078	.237 − .227	1.25	0.957 +0.016	1.50 −0.149	2.37 −0.227	12.2	6.04 + 0.093	9.12 − 0.089	15.0 − 0.149	53.0 − 0.062	90.8 − 0.101
0.822	.150 .413 − .072 − .336	.233 .258 − .226 − .256	1.18 26.1 + 0.42:: − 0.326	0.937 3.67 +0.027 −0.302	1.47 1.74 −0.146 −0.193	2.33 2.35 −0.224 −0.229	11.4 203. + 0.320:: − 0.259	5.89 34.1 + 0.104 − 0.267	8.96 11.7 − 0.085 − 0.155	14.7 15.0 − 0.144 − 0.151	52.0 80.6 − 0.059 − 0.156	89.2 91.9 − 0.097 − 0.105
0.899	.338 − .320	.234 − .238	20.0 − 0.323	2.95 −0.281	1.56 −0.168	2.17 −0.209	156. − 0.254	26.9 − 0.250	10.3 − 0.128	13.7 − 0.125	69.6 − 0.131	84.2 − 0.080
1.00	.269 − .274	.207 − .195	14.7 − 0.304	2.29 −0.239	1.37 −0.123	1.94 −0.167	115. − 0.234	20.4 − 0.215	8.95 − 0.084	12.3 − 0.083	59.0 − 0.091	75.5 − 0.039
1.40	.126 +0.126	.120 +0.210	5.45 − 0.045	1.00 +0.128	0.777 +0.273	1.15 +0.240	42.4 + 0.003	8.42 + 0.105	4.96 + 0.284	7.29 + 0.316	31.3 + 0.215	44.5 + 0.318

* Each square contains: first line, κ_ν in cm²/gm; second line, $\log_{10} F_\nu/F_\nu^{(\omega)}$. The values in braces are those at either side of a discontinuity.

Values of the quantity $\log_{10} F_\nu/F_\nu^{(\omega)}$, which have been omitted from the above table, correspond to values of $\bar{\kappa}/\kappa_\nu$, which lie outside the range of Burkhardt's table. In a few instances approximate values for $\log_{10} F_\nu/F_\nu^{(\omega)}$ have been arrived at by extrapolation of Burkhardt's data, and these have been marked by the symbol :: .

In Figure 2 we have plotted the values of $\log_{10} F_\nu/F_\nu^{(e)}$ as a function of frequency for the various models. For practical purposes it is convenient to have values of $\log_{10} F_\nu/F_\nu^{(e)}$ because it is directly comparable with the observations for the gradients made on the continuous spectra of stars and also because it is closely related to color temperatures. On such a plot as Figure 2, energy distributions corresponding to any color temperature are approximately straight lines. Thus index marks made in this figure show the slopes corresponding to various reciprocal color temperatures.

Figure 3 gives the distribution of the emergent flux in absolute units as a function of frequency for two of the model atmospheres considered: $\Theta_e = 0.5$, $p_e = 10^3$; and $\Theta_e = 0.8$, $p_e = 10^3$.

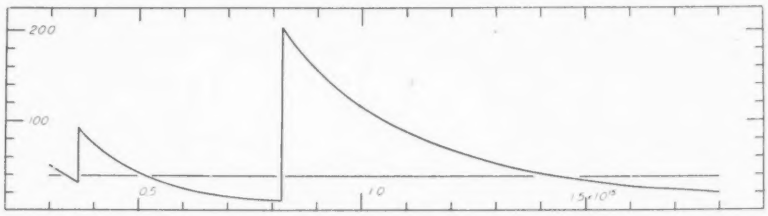

FIG. 1.—The monochromatic absorption coefficient κ_ν for a model stellar atmosphere with $\Theta_e = 5040/T_e = 0.5$, $p_e = 10^3$ bar. The ordinates denote κ_ν in units of cm² per gram, while the abscissae denote frequencies in cycles per second, one small division representing 0.1×10^{15} cycles. The ordinate of the horizontal line corresponds to the value of $\bar{\kappa}$.

Table 5 gives computed color temperatures for the models at various frequency ranges of astrophysical interest, as well as the logarithm of the ratio of the fluxes on either side of the Balmer and the Paschen discontinuities.

IV. COMPARISON OF THE RESULTS FOR MODEL STELLAR ATMOSPHERES WITH THE DATA OF OBSERVATIONS

An important feature of the emergent flux of the radiation of stellar atmospheres is the sudden discontinuity at the head of the Balmer series. Since the model atmospheres show large variations in the amount of this discontinuity with the electron pressure, it is natural to suppose that for a given effective temperature the average electron pressure in a stellar atmosphere will be indicated by the observed magnitude of the Balmer discontinuity. Now Barbier and Chalonge[20] give as the final averages of their measures of the quantity $D = \Delta \log_{10} F_\nu$ at the Balmer discontinuity, for more than 200 main-sequence stars, the following values: A0, 0.47; A2, 0.44; A3, 0.42; A5, 0.39; F0, 0.28; F2, 0.22; F5, 0.17; F8, 0.11. Using Kuiper's temperature scale,[21] we can refer these values for the different spectral types to appropriate effective temperatures; and in this manner we can compare the observed values of D with those given in Table 5, calculated for the model atmospheres. It is found that with $p_e = 10^3$ we obtain values of D agreeing with those observed in the earlier spectral types, while a slight decrease of p_e is indicated for the later ones.

Barbier and Chalonge[22] have also measured stellar color temperatures on either side of the Balmer discontinuity. The spectral ranges of their measures correspond closely with those of the computed color temperatures B and C of Table 5. Figure 4 contains a

[20] *C.R.*, **210**, 99, 1940.

[21] *Ap.J.*, **88**, 429, 1938.

[22] *Op. cit.*

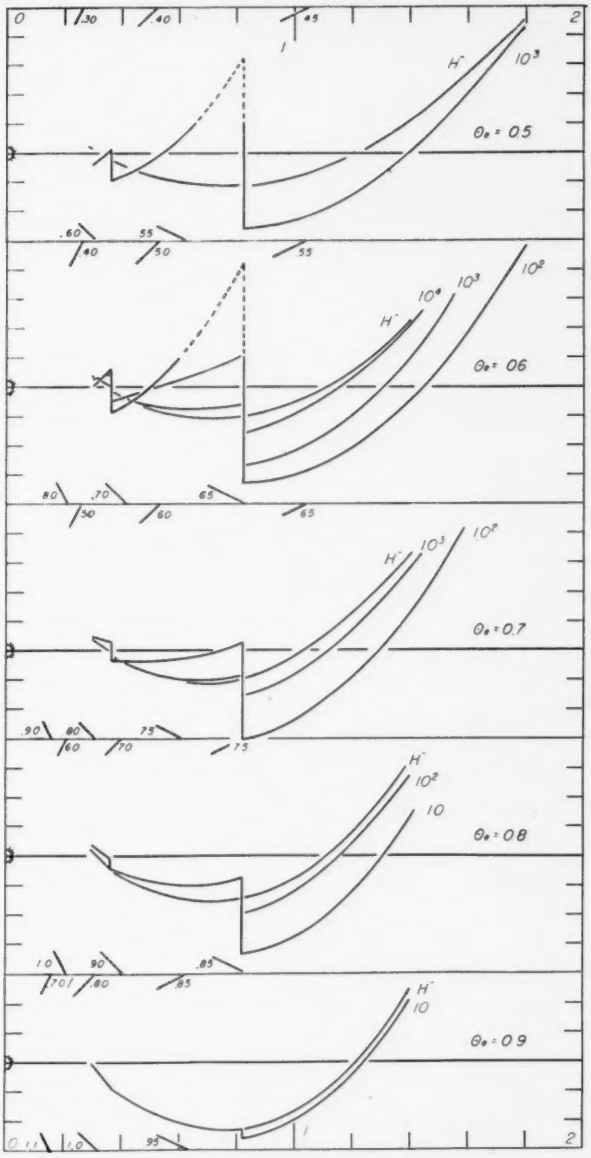

FIG. 2.—The deviations of the emergent flux F_ν of model stellar atmospheres from the radiation $F_\nu^{(e)}$ from a black surface at the effective temperature. The ordinates represent $\log_{10} F_\nu/F_\nu^{(e)}$ (one small division corresponding to 0.1 in the logarithm), while the abscissae represent frequencies (one small division corresponding to a frequency difference of 0.2×10^{15} cycles per second). The numbers labeling the curves correspond to the electron pressures of the model atmospheres which they represent. The curves marked "H^-" correspond to the results for atmospheres of pure H^-. Index marks give the approximate slopes corresponding to the various values of Θ_e.

plot of the reciprocal color temperatures as a function of the reciprocal effective temperatures: (1) of Barbier and Chalonge's observations; (2) of Wildt's[23] earlier calculations for $p_e = 10^3$; and (3) for the model atmospheres computed in this paper, also for $p_e = 10^3$. In both cases the present models give a slope nearer that of the observed stars. It

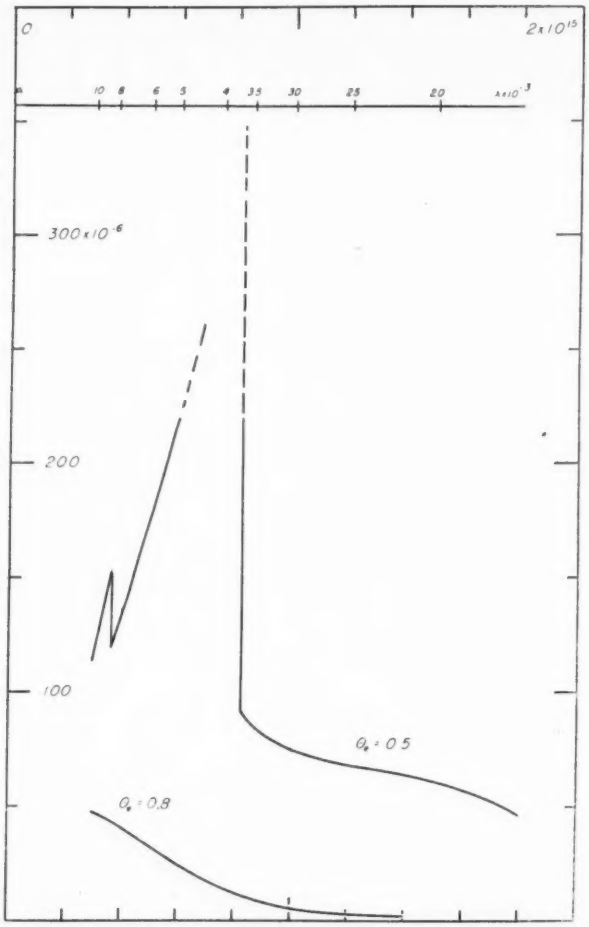

FIG. 3.—The frequency dependence of the emergent flux for two model stellar atmospheres ($\Theta_e = 0.5$, $p_e = 10^3$; $\Theta_e = 0.8$, $p_e = 10^3$). The quantity F_ν (in cgs units) is plotted along the ordinate, while one small division of the abscissa corresponds to a frequency difference of 0.2×10^{15} cycles per second. An auxiliary scale represents the wave length in thousands of angstroms.

should be noted that the point with the largest value of Θ_e is for the sun, measured by Arnulf, Chalonge, and Jardin,[24] and is doubtless not directly comparable with the other observations. This is because of the fact that they may be based on slightly different zero points and also because the dispersions were different, thus introducing a variable influence of absorption lines on the gradients. Since the zero point of the Barbier and

[23] *Ap.J.*, **93**, 47, 1941.

[24] *C.R.*, **210**, 325, 1940.

Chalonge color observations may be uncertain, the vertical placing of the observed points in Figure 4 may be subject to uncertainties. However, it appears that the differences between the reciprocal color temperatures for the two regions should be less subject to errors of the zero point than are the quantities themselves. Accordingly, in Figure 5 we have compared observed values of the differences in the color temperatures at λλ 4600–3700 and λλ 3700–3150 with the results for the model atmospheres. It is seen that the

TABLE 5*

THEORETICAL RECIPROCAL COLOR TEMPERATURES

	θ_e	0.5	0.6	0.7	0.8	0.9
$p_e=10$	*A*				0.86	1.02
	B				.76	0.92
	C				.75	0.84
	D				.264	0.030
	E				0.034	0.003
$p_e=10^2$	*A*		0.42	0.70	0.89	1.02
	B			.64	.80	0.93
	C		.59	.63	.72	0.84
	D		.75::	.329	.047	0.005
	E		0.144	0.062	0.007	0.000
$p_e=10^3$	*A*	0.36	0.54	0.77	0.90	
	B	.31::	.50	.68	.80	
	C	.48	.55	.61	.72	
	D	.58::	.371	.070	.007	
	E	0.104	0.094	0.009	0.000	
$p_e=10^4$	*A*		0.65	0.78		
	B		.58	.69		
	C		.52	.62		
	D		.097	.008		
	E		0.016	0.000		
Limit	*A*	0.57	0.67	0.79	0.90	1.02
	B	.51	.61	.68	.80	0.93
	C	0.48	0.54	0.63	0.73	0.83
	p_e*	10^7	10^6	10^4	10^3	10^2

The bottom row gives limiting values of the color temperatures for stellar atmospheres, where only the opacity due to H^- is effective. The electron pressure, p_e*, at which this occurs, is also shown for each temperature.

* $\theta_e = 5040/T_e =$ *A*, *B*, *C*,
$10^4/\lambda = 1.40$–1.80, 2.20–2.60, 2.74–3.00,
D = Δ log$_{10}$ F_ν at Balmer limit, *E* = Δ log$_{10}$ F_ν at Paschen limit.

computed relations are not in exact agreement with the observed ones, but it is also seen that our present calculations represent a slight improvement over Wildt's calculation.[25]

Now the Greenwich observers have determined the color temperatures of a total of more than 300 stars,[26] in a wave-length region between 4100 A and 6500 A. This is a range which is nearly equal to the extremes of the ranges of the computed reciprocal color

[25] The fact that the point for the sun is in such marked disagreement with the run of the other observed values seems to indicate that the solar observation is not directly comparable with the others.

[26] Sir Frank Dyson, *Observations of Color-Temperatures of Stars, 1926–1932*, London, 1932; also *M.N.*, **100**, 189, 1940.

temperatures A and B (see Table 5). Thus an approximate value of the reciprocal color temperature of the model atmospheres throughout the whole region may be taken to be the average of A and B. Figure 6 shows the relation between the reciprocal effective temperatures and the reciprocal color temperatures for this spectral region for (1) averages of stars of various spectral types as observed at Greenwich; (2) Wildt's model atmospheres; and (3) the model atmospheres computed here (both [2] and [3] corresponding to $p_e = 10^3$). A value of $\phi_0 = 1.00$ was taken for the Greenwich gradients; and so the whole set of observed points in Figure 6 may be subject to a slight displacement in the vertical direction. However, the general disagreement of slopes could not be re-

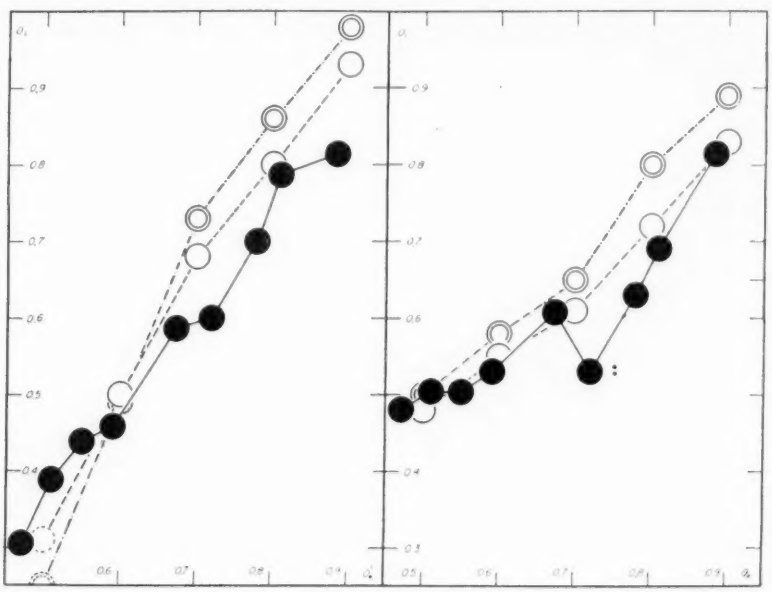

FIG. 4.—($\Theta_c - \Theta_e$) relations as observed and computed, for the intervals λλ 4600–3700 (the diagram to the left) and λλ 3700–3150 (the diagram to the right). The solid dots represent observations of Barbier and Chalonge. The single circles represent theoretical values for model atmospheres, with $p_e = 10^3$; and the double circles correspond to the earlier calculations of Wildt (*Ap.J.*, **93**, 47, 1941). The observed point at $\Theta_e = 0.72$ is quite uncertain (cf. Barbier and Chalonge, *Ann. d'ap.*, Vol. **3**, No. 2, 1940). The point at $\Theta_e = 0.89$ is for the sun; and, since it was obtained in a different manner from the others, is not strictly comparable with them.

moved by any such translation. It is obvious that the agreement of the model atmospheres with the visual (Greenwich) gradients is less satisfactory than with either the photographic or the ultraviolet gradients (Barbier and Chalonge). However, the disagreements, such as they are, are all in the same sense: the $\Theta_c - \Theta_e$ relation is steeper for the model atmospheres than that which the observations indicate. Altogether, the more accurate H^- absorption coefficient which has been used in the present calculations seems to have decreased—definitely, if not sufficiently—the disagreement between the model atmospheres and the true stellar atmospheres. Wildt has pointed out[27] already that this discrepancy cannot be traced to the effect of absorption lines, since it operates in the opposite direction.

The model atmospheres show a discontinuity in F_ν at the head of the Paschen series similar to that at the head of the Balmer series, although considerably smaller. Hall and Williams[28] have measured the quantity $D_P = \Delta \log_{10} F_\nu$ at the Paschen discontinuity for

[27] *Ap.J.*, **93**, 47, 1941.

[28] *Ap.J.*, **95**, 225, 1942.

the A0 star Vega and find it to be approximately 0.092. Reference to Table 5 shows that for a model atmosphere with $\Theta_e = 0.5$ and $p_e = 10^3$ the quantity $D_P = 0.104$, which is in satisfactory agreement with the estimate of Hall and Williams. However, it should be remarked that Hall and Williams give their value as a minimum and state that further observations will be necessary to establish the exact magnitude of the discontinuity.

Accurate investigations of the linearity of stellar gradients in the visual and the near infrared regions have been made recently by Williams[29] and by Hall,[30] respectively. Williams finds only slight systematic deviations from linearity in the region λλ 4000–6700, for stars of types A and F. The small differences in gradient which he does find

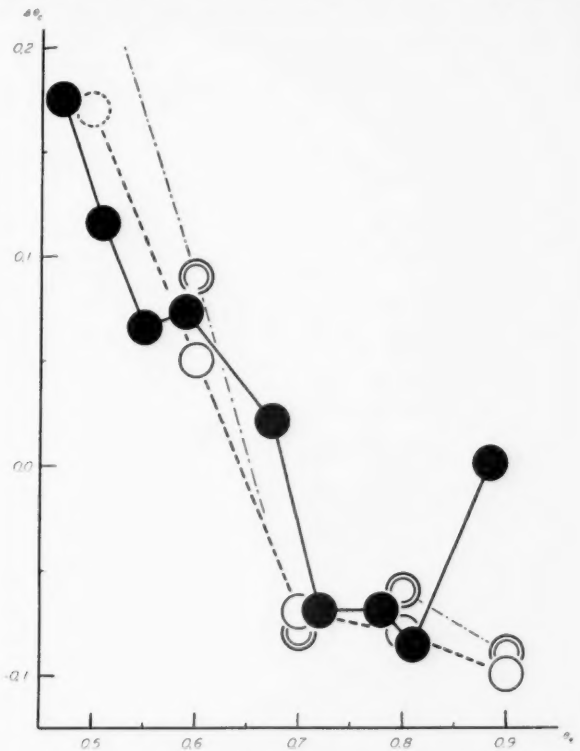

FIG. 5.—$\Delta\Theta_e = \Theta_e(\lambda\lambda\ 3700\text{–}3150) - \Theta_e(\lambda\lambda\ 4600\text{–}3700)$ as observed and as calculated. The ordinates denote $\Delta\Theta_e$, and the abscissae denote Θ_e. The other symbols have the same meaning as in Fig. 4.

make the color temperatures higher in the red than in the blue. Reference to Figure 2 shows that this curvature is opposite in sign to that exhibited by the model atmospheres. Hall's results for the near infrared (λλ 4600–10,000) support the assumption that the main-sequence stars of types A and F radiate essentially as black bodies in this region of the spectrum, except for the Paschen discontinuity. On the scale of Figure 2 the curvature found by either Hall or Williams would not be noticeable over the ranges of their respective observations.

To summarize: The model atmospheres studied in this paper, with the help of the continuous absorption coefficient of H^- as recently recomputed, predict an effective temperature to color temperature relation which fits observed curves fairly satisfactorily in the ultraviolet, less so in the photographic region, and still less so in the visual region.

[29] *Pub. Obs. U. Michigan*, **7**, 93, 147, 159, 1939. [30] *Ap.J.*, **95**, 231, 1942.

In all three cases, however, the theoretical relations derived here lie somewhat closer to the observational ones than those obtained earlier by Wildt, who used a less accurate absorption coefficient for H^-.

The models treated in the present paper show a definite trend of the color temperature to increase with increasing frequency, while actual stars seem to show a fairly constant color temperature, which, if anything, decreases slightly with frequency.

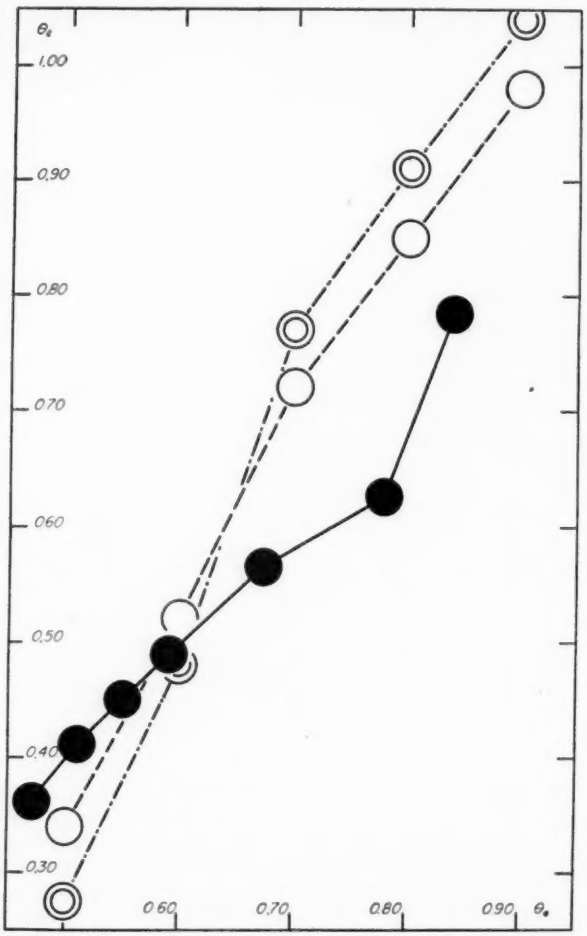

FIG. 6.—The (Θ_c–Θ_e) relation in the spectral region λλ 6500–4100, as observed and as calculated. The filled circles represent the Greenwich observations. The single circles correspond to the values calculated in the present paper with $p_e = 10^3$, while the double circles represent the values according to Wildt's earlier calculation.

The writer is deeply indebted to Dr. S. Chandrasekhar for his constant guidance and friendly encouragement, without which this paper would have been impossible. Dr. Jesse L. Greenstein is to be thanked for helpful discussions of observational data on stellar spectrophotometry. The writer's wife, Dorothy C. Williamson, was of great assistance in much of the computing and in typing the manuscript.

YERKES OBSERVATORY
November 13, 1942

OBSERVATIONS OF THE LIGHT OF THE NIGHT SKY WITH A PHOTOELECTRIC PHOTOMETER*

C. T. Elvey

ABSTRACT

A preliminary report is given of the observations of the brightness of the night sky with a photoelectric photometer sensitive to the infrared region of the spectrum. A brief description of the apparatus is given. Curves of the nocturnal variation of intensity of the light of the night sky have been obtained on 45 nights, and it is found that they may be classed in two groups: one with a minimum near midnight and the other in which the intensity decreases through the night.

The irregular variations of intensity during the night, which are greater and more numerous when there is considerable magnetic activity, are not the same in different directions in the sky, thus showing the nonuniform character of the light of the night sky at such times.

Tests to determine the height in the atmosphere and the motions of the irregular patches of light have given no positive results. Also no correlations were found between the fluctuations in the light of the night sky and the variations of the ionosphere as indicated by the signal strength of reflected radio waves, the night sky being observed around the downcoming radio wave.

Many interesting results have been obtained from spectrophotometric observations of the light of the night sky; and, although this method has certain distinct advantages, there are also some disadvantages: the accuracy is limited and the length of time that it takes to obtain a single observation is long. The latter is a particularly important disadvantage in connection with studies of the rapid changes in brightness which occur in the light of the night sky. The photoelectric photometer is valuable for this work, since it combines accuracy with a rapid indication of the intensity, a single observation taking only a few seconds or perhaps two or three minutes when the greatest sensitivity of the instrument is required.

This paper is intended as a preliminary report on the photometry of the light of the night sky with a photoelectric photometer. It is a brief presentation of the observations which have been made during the past year. Several problems have arisen, but their solutions will have to wait until much more observational material can be collected. For instance, additional observations will be needed to redetermine the variation with zenith distance of intensity of the light of the night sky in the infrared region, so that the height of the auroral layer may be checked. The preliminary observations with the photoelectric photometer indicated a height of 125 km for this layer,[1] whereas the spectrophotometric observations of Elvey and Farnsworth[2] for the stronger lines in the red-green regions of the spectrum indicate a height of 500 km.

Three photometers have been constructed for this work, all of them having the same general design. Slight variations, however, were made both in the optical systems and in the amplifiers. In one photometer the entire unit excepting a storage battery is housed in a box. In the others the optical system, the photoelectric cell, and the amplifier tubes were separated from the control cabinet by a shielded cable, thus making it possible to operate the instrument from a lighted room.

The optical system consists of a condensing lens whose aperture is 109.5 mm and whose focal length is 139.7 mm. The lens focuses the sky on an aperture of a metallic box which shields the electrical system. The photoelectric cell is placed immediately

* *Contributions from the McDonald Observatory, University of Texas*, No. 62.

[1] A paper presented at the dedication of the National Astrophysical Observatory at Tonanzintla, Puebla, Mexico.

[2] *Ap. J.*, **96**, 451, 1942.

behind the aperture; and, in order that it may be effectively shielded, a copper screen is soldered over the aperture. This reduces the intensity of the light slightly, but it greatly increases the stability of the electrical circuit. A sharp-cutting red filter, Corning No. 241, removes most of the visual part of the spectrum and only that part of the spectrum which is greater than λ 6400 is effective. A shutter operated by a bulb and a long rubber tube serve to expose the photoelectric cell to the night sky.

The receiver is a caesium oxide photoelectric cell, No. 71-TA, made by the G-M Laboratories. Its maximum sensitivity is λ 7000. At ordinary temperatures these photoelectric cells have a dark current—mostly thermal emission from the cathode—which is five to ten times the size of the photoelectric current when the cell is exposed to the night sky. Slight temperature changes will thus vitiate the observations. A gust of wind causes fluctuations of the indicating meter which are sometimes larger than that produced by the photoelectric current. It was found by experiment that the temperature variations could be sufficiently dampened by surrounding the photoelectric cell with a layer of cork an inch or more in thickness and by using a double window to admit light to the cell. This produces a steady drift in the electrical circuit for several hours at the beginning of the night when the temperature has dropped several degrees, but it is slow enough that the zero may be adjusted and read only once prior to each observation. The observations are made at 5-minute intervals throughout the night; but during twilight and dawn, when the intensity is changing rapidly, the rate of making readings is doubled.

The photoelectric current is measured by means of a direct-current amplifier of the negative feedback type described by Roberts.[3] However, some slight changes and adjustments were made, since the amplifier is always used at its highest gain. The current is read on a microammeter with a scale of 0–50. The power supply is from batteries. Two of the instruments use storage batteries for the filament current, and the other uses low-drain tubes and employs dry cells for the filament current. The other potentials are from small B batteries.

Each photometer is equipped with a standard lamp built into the lid which covers the lens, thus making it possible to test the instrument in a lighted room. The intensity of the light is adjusted so that it produces a deflection of the same order or magnitude as that from the night sky. The lamps are similar and can be readily removed so that intercomparisons can be made. One lamp has been set aside and designated as a primary standard and all the other lamps are compared with it. The standard lamp has given a check on the stability of the instruments through the night and from night to night. If the problem can be continued, it is expected that the lamps will give a means of intercomparing the brightness of the night sky as observed on different nights and at different localities.

It is possible to observe the sky with some moonlight, since this photometer is sensitive to the infrared portion of the spectrum. Tests have been made on nights of photometric quality with the full moon in the sky. The brightness of the region around the pole was increased by only 1 mag. over a night without a moon. Whenever the sky is free from haze and thin clouds, it is possible to observe until the moon reaches quarter-phase, with hardly any noticeable influence on the brightness of the sky. With moonlight there is no trouble in distinguishing whether haze is present, for then the sky is abnormally bright. Also a very thin cloud passing across the field of the photometer will cause a large, sudden change in brightness. On the other hand, the haze and thin clouds without a moon in the sky have very little effect upon the brightness of the sky. There is merely a smoothing of the irregular variations, since the haze integrates the light from the entire sky.

During the 14 months ending in June, 1942, the curves of the nocturnal variation of intensity of the night sky have been obtained on 45 nights with only a few of them

[3] *Rev. Sci. Inst.*, **10**, 181, 1939.

having 1 or 2 hours missing. In addition, many parts of nights have been observed. For all these observations the instrument was pointed toward the north pole.

An inspection of the general shape of the curves indicates that they may be grouped into two classes, one which has a tendency to produce a minimum of light around local midnight or shortly after and the other which shows a tendency for a steady decrease in the light through the night. In both cases there are irregular variations, but in the latter they seem to be more pronounced. There are a few cases when it is rather uncertain to which class the curve might be assigned. It is further noticed that there is a tendency for a grouping of the curves of a given class. For two or three nights the curves would be similar. During this period of observation there was found no evidence that the classes of curves are related to the seasons; however, the examples cited below happen to have one group all of which are winter observations and the other all spring or summer observations.

Examples of the class of curves for which there is a minimum of intensity in the vicinity of local midnight are shown in Figure 1. The dates and abscissae are expressed in Universal Time. Some of the curves are quite free of the irregular fluctuations in intensity, while others have moderately large ones. The last curve in the diagram is one of the few which could not be assigned to either of the two classes.

In Figure 2 are presented a series of curves in which there is a general decrease in the intensity of the light of the night sky through the night. Different degrees of the irregular fluctuations are shown. It has been known for some time that the irregular fluctuations are associated with times when the terrestrial magnetic activity is great; and recently D. N. Barber[4] has shown an excellent correlation between the irregularities of the light of the night sky as observed at the Lick Observatory and the terrestrial magnetic activity as observed at the Mount Wilson Observatory.

The observations have been extended into the evening and the morning twilights; and, since the region observed is that of the pole, it is symmetrically placed with respect to the setting and the rising sun. Since the photometer integrates both the continuous and the emission spectra over a large range of wave lengths, we cannot be certain whether the twilight effect is a result of scattered sunlight or an emission spectrum. By comparing the morning and evening observations at the pole we find that the change of intensity is symmetrical with respect to the position of the sun. If it were caused by an emission spectrum, we should expect differences between the morning and the evening intensities. For the evening twilight the sky will have been in the sunlight for the preceding hours, while for the morning twilight it will have been in the shadow for a similar length of time. We can conclude that the observed enhancement at twilight is a result of scattered light from the twilight portions of the atmosphere.

Observations have been made with two photometers pointed to different parts of the sky, and these have shown that the irregular fluctuations of intensity are not the same. Hence it must be concluded that the light of the night sky is not uniform as observed from one point and that the irregularities are probably due to patches of light. Since it was thought that the light from the night sky comes from the region of the *E*-layer,[1] a series of observations have been planned to determine the character of the irregular fluctuations. These have not been completed, but the observations of the following paragraphs indicate that the luminous areas are probably not in the *E*-layer; the series of observations will have to be greatly extended.

Observations have been made with one photometer at the McDonald Observatory pointing toward the pole, while another instrument was taken to various positions in the near vicinity. The purpose was to determine the height and the motions of the patches of light which produced the irregular variations during the night. One of the first sets of observations indicated a lag of several minutes between the fluctuations of intensity as observed at Mount Locke and at a point near Fort Davis, a distance of

[4] *Lick Obs. Bull.*, **19**, 105, 1941.

12 miles approximately in the east-west direction. However, repeated trials have not verified this result. The longest distance that has separated the two stations to date is approximately 25 miles. If the problem is to be carried on, the stations should be set up at least 100 miles apart.

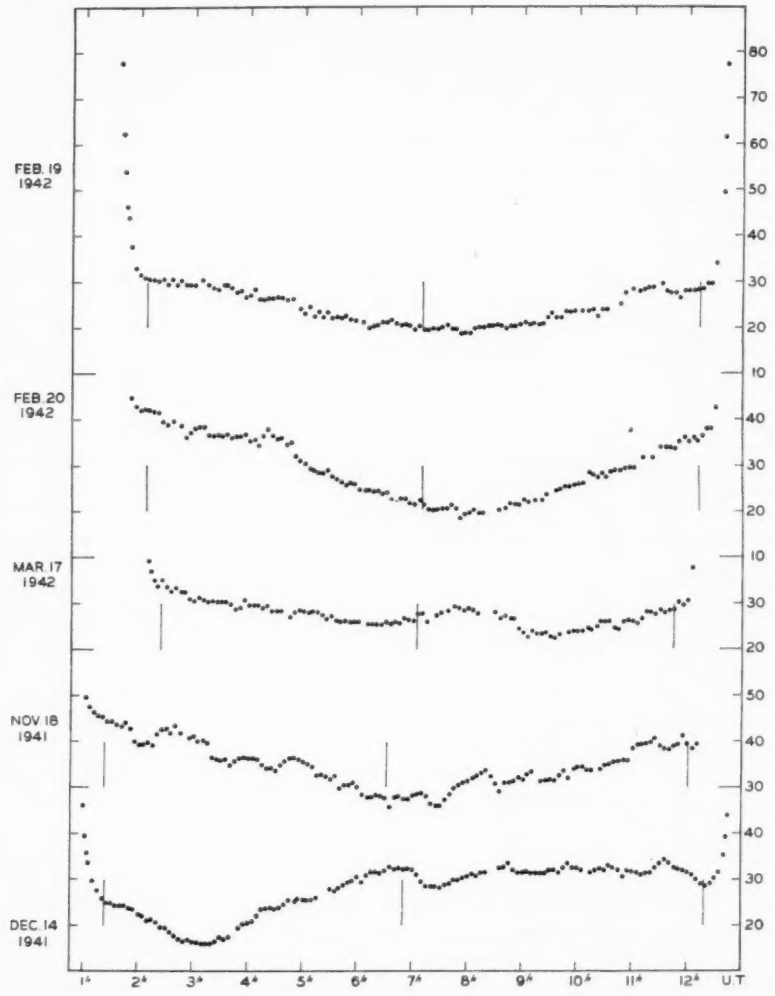

FIG. 1.—Curves of nocturnal variation in the intensity of the light of the night sky, showing minima. The dates of the curves are February 18 and 20 and March 17, 1942; November 18 and December 14, 1941.

An attempt was made to obtain observations over a base line of 425 miles, between McDonald Observatory and Forth Worth, Texas, but poor observing conditions have made it impossible to obtain simultaneous observations. The observations at Fort Worth were being made through the kind co-operation of Mr. Dan C. Taulman, an amateur astronomer, but have had to be discontinued because his work in defense projects now consumes most of his time.

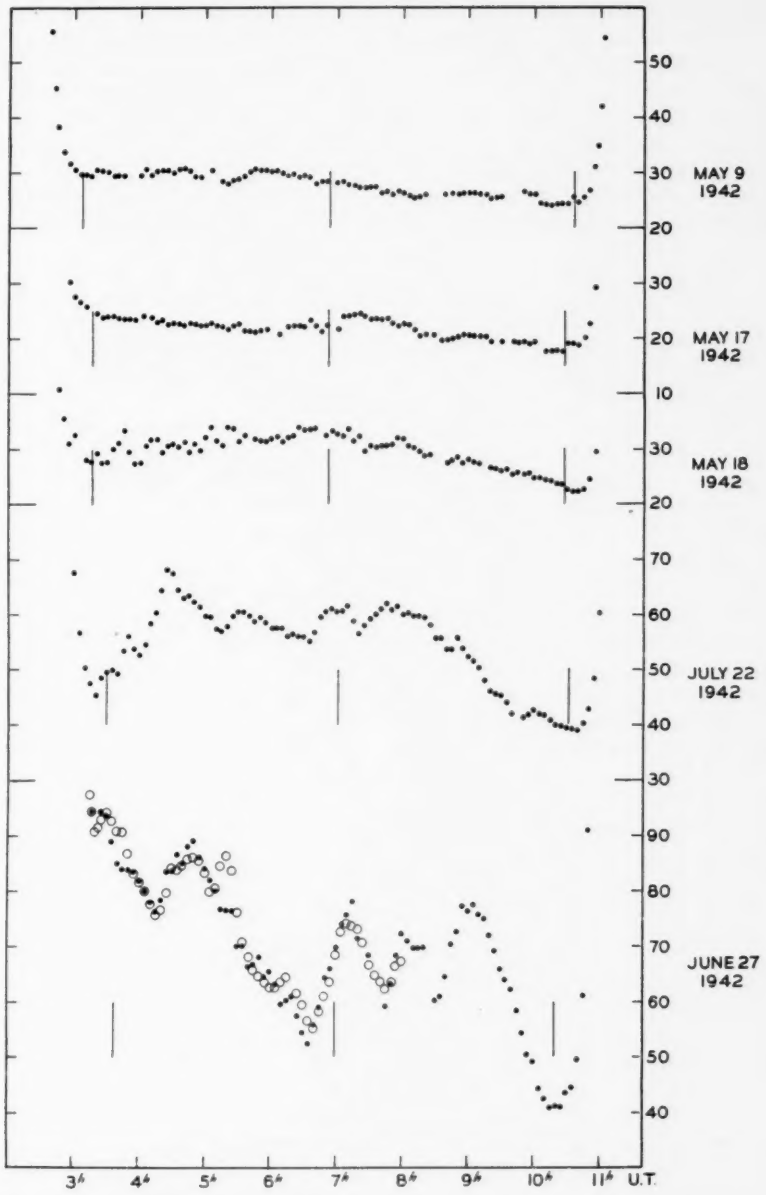

FIG. 2.—Curves of nocturnal variation in the intensity of the light of the night sky, showing a decrease of intensity through the night. The dates of the curves are as follows: May 9, 17, and 18, 1942; June 27 and July 22, 1941.

The agreement between observations taken with two photometers has been checked a number of times. The bottom diagram of Figure 2 shows the agreement between observations taken at McDonald Observatory (Mount Locke) and a point near Fort Davis, a distance of 12 miles approximately east-southeast. These observations were made on a night in which there was some large variation in the intensity of the light of the night sky; it will be noticed that most of the features are quite accurately reproduced by the two instruments. There are a few discrepancies which are well above the accuracy of the instruments, showing that for short durations the light was of different intensities as observed from the two locations. Notice particularly the difference at $5^h\ 20^m$.

On this night I was operating the instrument at Fort Davis and had excellent opportunities of watching the sky. The readings of the meter were made with a faint flashlight and my eyes were dark adapted. The brightness of the sky changed greatly in the infrared region, but the eye had difficulty in noticing that the sky was brighter at one time than at another. In my notes I have recorded that at $7^h\ 00^m$ the northern horizon appeared brighter than the southern horizon.

The irregularities in the light of the night sky probably represent areas of increased brightness over that of the background, and it is reasonable to suppose that these areas are regions of greater excitation. If the height to the layers in which the radiation is produced is that indicated by the preliminary observations, i.e., the *E*-layer, then we might expect to find correlations between the irregular fluctuations in the light of the night sky and the characteristics of the ionosphere. Bradbury and Sumerlin,[5] observing at the Lick Observatory with a photoelectric photometer and making observations of the ionosphere at Stanford University, in California, did not find any correlation between the brightness of the sky and the ionospheric conditions; however, it is possible that the disturbed areas of the upper atmosphere are too localized to give a correlation between these two localities. We do not have sufficient equipment available to conduct investigations of the ionosphere with pulse transmitters simultaneously with our observations of the brightness of the night sky. However, it might be expected that the radio signals reflected from the ionosphere would give some idea of the variations in the ionized layers; and we have tried observing simultaneously the signal strength of a radio station and the brightness of the night sky in the region surrounding the computed position of the downcoming radio wave. The field of view of the photometer is 8°, and it is very probable that this is sufficiently large to include the difference between the computed and the actual positions of the downcoming wave for signals in the broadcast band, but this may not be the case for the shorter waves which are reflected from the *F*-layer. For the latter case the position of the photometer has been shifted from night to night.

The preliminary trials were conducted by using the broadcast station KRLD, in Fort Worth, Texas, whose frequency is 1080 kilocycles. There was a suggestion of a correlation of the frequency of the fading of the signal with the intensity of the light of the night sky, but there were no correlations with signal strength.

Further tests were tried by using the signals from radio station KRCA in San Francisco, California, which is broadcasting on a frequency of 9.48 megacycles. Some excellent records were obtained of both the radio-signal strength and the brightness of the night sky; but no correlations were evident, although both showed well-defined variations.

The negative results given above and also those of Bradbury and Sumerlin[5] point toward the origin of the radiation as being in the high atmosphere, in contradiction to the preliminary observations of height as given by the photoelectric photometer, perhaps from the same region as the green auroral line, about 500 km above the surface of the earth.

[5] *Terr. Mag. and Elec.*, **45**, 19, 1940.

The time constant of the electrical circuit of the photometer is an appreciable fraction of a minute, and consequently variations of intensity of the light of the night sky which might be of the order of a second or so would hardly be detectable. During the times when the instrument was exposed to the sky at or near the maxima of the irregular variations, it was noticed frequently that the needle of the indicating meter was unsteady. Tests have shown that this unsteady condition is not of instrumental origin. With no light on the cell the needle of the meter is steady, and this is also the case if the cell is exposed to the standard lamp. This would indicate that there are very rapid fluctuations of intensity of the light of the night sky, but this should be verified with a photometer which is constructed to detect rapid changes of intensity.

This work has been greatly assisted through grants of financial aid given both by the American Academy of Arts and Science and by the American Philosophical Society, for which I am very grateful. It is a pleasure to acknowledge also the assistance of Mrs. C. T. Elvey and of Mr. Joseph Ross Brown, each of whom helped to obtain long series of observations.

McDonald Observatory
September 1942

TENTATIVE IDENTIFICATION OF THE HERZBERG BANDS OF O_2 IN THE ULTRAVIOLET SPECTRUM OF THE NIGHT SKY*

P. SWINGS

As is well known, the identifications of the night-sky bands are still very unsatisfactory; even the strongest ultraviolet feature at λ 3556, which appears always in long spectroscopic exposures on faint nebulae, is still unidentified. Some time ago, I had the privilege of receiving from Dr. J. Dufay, of Lyons (France), a manuscript copy of an interesting paper in which a rather convincing identification is suggested for the strong ultraviolet bands, including λ 3556.[1] Dufay believes that these may be due to the "forbidden" transition $^3\Sigma_u^+ \rightarrow {}^3\Sigma_g^-$ (Herzberg system) of O_2. This band system has been observed only in absorption in the region λ 2400–λ 2900. The absorption consists of a progression $v'' = 0$, each $(v', 0)$ band having only a Q branch ($\Delta K = 0$) degraded to the red; the lower electronic level is the ground state of O_2. Dufay suggests that several night-sky emission bands are the $(v' \rightarrow v'' > 0)$ transitions of the Herzberg system.

The $v'' = 0$ progression, which was found in laboratory absorption by G. Herzberg,[2] has been measured by several authors[3] either in the laboratory or in atmospheric absorption. The measured wave lengths of the origins agree within about one angstrom unit for the bands of $\lambda \leqslant 2637$. Herman has measured three additional weak bands to the red of λ 2637, at λλ 2685.0, 2737.6, and 2795.2; and there may still be two more at approximately λ 2843 and λ 2912. Hence the actual v' designations are still in doubt, but the energies E' (v') are fairly well known.

To obtain the $v' =$ constant progressions, Dufay determines the $\nu(v', v'')$ formula of the system by least-squares solutions, accepting for the v'' term a simplified expression obtained from the Schumann-Runge and the atmospheric O_2 bands, which have the same lower electronic level $^3\Sigma_g^-$. Then Dufay compares the calculated values of $\lambda(v', v'')$ with his wave lengths of the night-sky features and finds several cases in satisfactory agreement.

I have undertaken a similar discussion on the basis of the results on the night-sky spectrum obtained at the McDonald Observatory.[4] Instead of using least-squares solutions, I have simply taken for the upper state the "best" $\nu(v')$ corresponding to the observed Herzberg absorption bands.[5] For the ground electronic state I have used the formula, including the v''^3 and v''^4 terms, obtained by J. Curry and G. Herzberg,[6] which is better for large values of v'' than the simplified quadratic formula used by Dufay. More refined calculations are useless. The wave lengths of the night-sky spectrum are not accurately known, and we do not have accurate information on the widths or profiles of the bands. Moreover, we do not know what the rotational-intensity distribution should be in the night-sky bands of a specific molecule. From the observations we gather that the rotational-intensity distribution is of a low-temperature type. Yet we

* *Contributions of the McDonald Observatory, University of Texas*, No. 63.

[1] Dufay's note has probably been published in the *Comptes rendus*, Paris. See Bull. 3 of the Committee for the Continued Distribution of Astronomical Literature, October, 1941.

[2] *Naturwissenschaften*, **20**, 577, 1932.

[3] Chalonge and Vassy, *C.R.*, **198**, 1318, 1934; Herman, *Ann. de Phys.* (11th ser.), **11**, 548, 1939; Miss N. Morguleff and Mrs. A. Vassy, *Ann. d. Ap.*, **1**, 427, 1939.

[4] Elvey, Swings, and Linke, *Ap. J.*, **93**, 337, 1941.

[5] The uncertain bands λ 2843 and λ 2912 are not retained; hence $v' = 0$ is adopted for λ 2795.2.

[6] *Ann. der Phys.*, **19**, 800, 1934.

cannot, a priori, determine the amount by which the observed rotational centers of gravity of specific bands should be shifted to the red, relative to the band origins. Such a temperature shift may even be different for different values of v'![7]

Taking into account the various sources of uncertainty, a number of coincidences are found, the majority of which are probably real. They are listed in Table 1: column 1

TABLE 1

HERZBERG BANDS OF O_2 IN THE NIGHT-SKY SPECTRUM

λ AND INT. IN NIGHT SKY	O_2 IDENTIFICATION		λ AND INT. IN NIGHT SKY	O_2 IDENTIFICATION	
	Transition	λ (Calc.)		Transition	λ (Calc.)
3110 (0)	(6,5)	3111	3598 (0)	((6,8)	3585)
3145 (1)	(1,3)	3141	3636 (2)	(1,6)	3631
	(3,4)	3143		(3,7)	3637
3157 (0)	((5,5)	3164)	3664 (1)	(5,8)	3656
3211 (3)	(7,6)	3205	3707 (3)	(7,9)	3702
	(0,3)	3208			
	(2,4)	3209	3742 (4)	((0,6)	3733)
				(4,8)	3737
3233 (0)	(4,5)	3224			
			3834 (4)	(1,7)	3828
3263 (1)	(6,6)	3257		(3,8)	3831
3298 (3)	(3,5)	3294	3948 (3)	(4,9)	3939
				(0,7)	3942
3321 (2)	(5,6)	3315			
			3984 (2)	((6,10)	3973)
3378 (5)	(2,5)	3367			
	(0,4)	3368	4048 (2)	(1,8)	4044
	(4,6)	3381		(3,9)	4044
3425 (1)	((6,7)	3414)	4072 (5)	((5,10)	4060)
3460 (2)	(1,5)	3451	4174 (5)	((4,10)	4160)
	(3,6)	3459		(0,8)	4172
3488 (3)	(5,7)	3478			
3556 (10nn)	((2,6)	3539)			
	(0,5)	3542			
	(4,7)	3552			

contains the night-sky wave lengths and intensities, as found at the McDonald Observatory;[4] columns 2 and 3 contain the identifications which should be added to the ones previously given.[4] The v' values are uncertain, and they may possibly have to be increased by one or two units. The wave lengths in column 3 refer to the band origins, which should lie slightly to the violet of the observed maxima of the night-sky lines.

The O_2 bands provide probably the major contributions for all the lines of wave length $\lambda < 3598$, excepting possibly λ 3378 and λ 3425 but including the strong, unidentified lines. For $\lambda > 3598$ the influence of the Vegard-Kaplan system becomes important.

[7] This shows again the importance of renewed attempts to obtain the ultraviolet spectrum of the night sky with a better resolving power than has hitherto been available.

Assuming that the identification is correct, the average red shift of the observed bands, relative to the calculated band origins, corresponds to a temperature of the order of 150° K.

In a number of details the identifications given in Table 1 differ from the ones suggested by Dufay, but they favor his general hypothesis. As mentioned by Dufay, the excitation potential of the Herzberg bands is of the order of 4.5 volts; hence, it is not very different from the energy of the upper level of the green [*O* I] line (4.2 volts). The emission of the O_2 bands may be expected if the luminescence is excited according to Chapman's mechanism (recombination of two oxygen atoms). According to Herzberg,[8] the $^3\Sigma_u^+ \rightarrow {}^3\Sigma_g^-$ system is more likely to appear than the Schumann-Runge bands of O_2.

McDonald Observatory
August 1942

[8] Private communication.

PLATE II

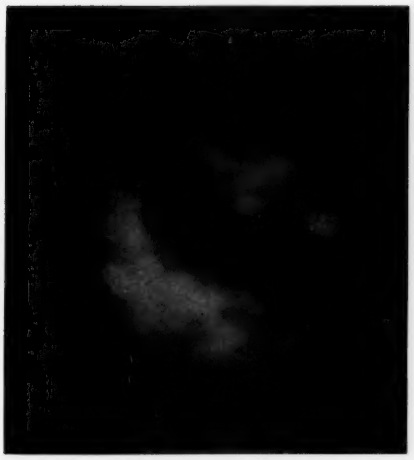

MARS ON OCTOBER 8, 1941, AT 0^h20^m U.T.

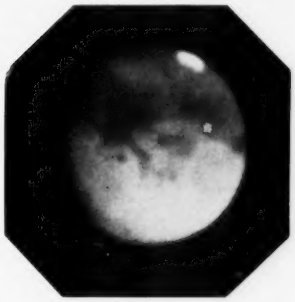

MARS ON SEPTEMBER 20, 1941, AT 1^h59^m U.T.

PLATE III

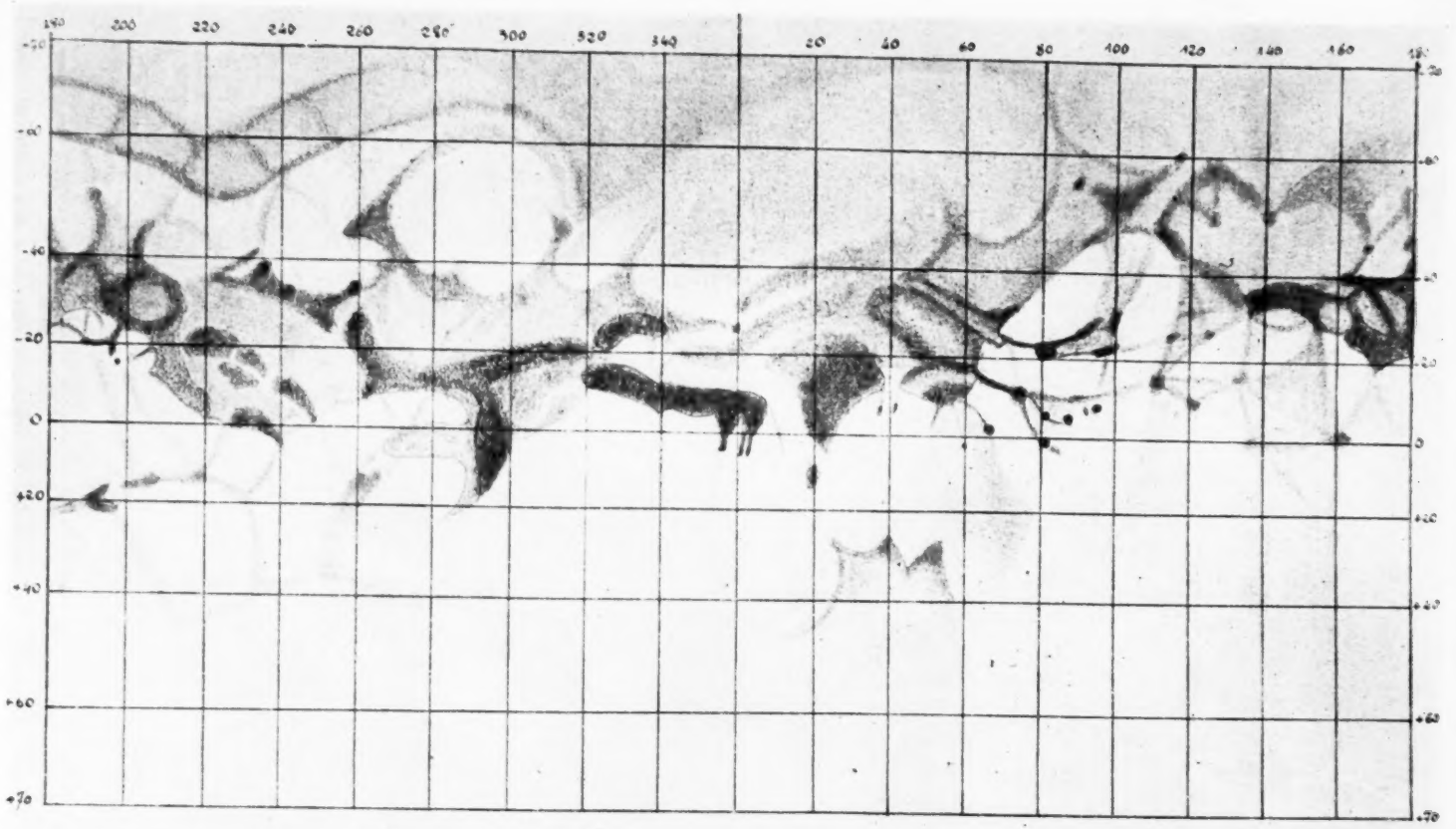

PLANÈTE MARS - OPPOSITION DE 1941

OBSERVATOIRE DU PIC DU MIDI.

RECENT PROGRESS IN ASTROPHYSICS[1]

OBSERVATIONS OF THE PLANETS BY LYOT, GENTILI, AND CAMICHEL FROM THE PIC DU MIDI IN 1941 AND 1942

Letters and photographs have been received in this country from MM. Bernard Lyot and Marcel Gentili describing numerous excellent observations of the planets made by them and M. Camichel at the Pic du Midi in 1941 and 1942. Prior to 1941 the largest telescope at the Pic had been a 23-cm. refractor. For the 1941 opposition of Mars a 38-cm. objective was borrowed from the Observatory of Toulouse and installed at the mountain station. The observing conditions were evidently very superior, and the lens proved to have excellent definition. According to Lyot, "it showed finer detail on the planet (Mars) than had been observed with the 83-centimeter refractor at Meudon under the best seeing conditions."

The 1941 opposition of Mars was studied visually and photographically at the Pic du Midi. The visual observations are combined and presented in the accompanying map of Mars. At first the observers felt that some of the details were too geometric to be real, but the canals and other fine details of the map have been fully confirmed by photographs made with the same instrument.

The several hundred photographs of Mars which were secured during the 1941 opposition were examined and studied at Meudon the following winter. In particular, Lyot prepared a series of 18 composite photographs of the planet. For each of these positives, several negatives were superimposed, thereby eliminating the chance grain or dust effects of a single photograph but enhancing the contrast for the faint details common to all of them. These composite pictures are on glass and were shown at a meeting of the Société Astronomique de France early in May, 1942. No copies have as yet been received in this country. The photographs of Mars (Pls. II and III) are reproductions of individual pictures made at the Pic du Midi in September and October, 1941.

In addition to these observations of Mars, studies have been made of Mercury, Saturn, Jupiter, and Jupiter's satellites. During the summer of 1942, Mercury was studied photographically and visually. Numerous details were seen on the little disk, and the work was continued until the planet was within a degree and a half of the solar limb. Photographs of Saturn show a faint band and a small bright spot on the surface of the planet, and the disk is clearly visible through the outer ring. Surface markings on the four bright satellites of Jupiter were carefully examined. Each observer made an independent series of drawings over many nights, and the mutually confirmed details proved to be sufficient for the preparation of maps for each of the satellites.

HELEN W. DODSON

WHITIN OBSERVATORY
WELLESLEY, MASSACHUSETTS
November 1942

[1] [This new section of the *Journal* will be devoted to critical summaries of research carried out abroad, which, because of war conditions, is not generally available to American astronomers. In some cases proofs or single copies of important foreign publications have reached this country; in others the information will be based upon private communications from the authors or from astronomers in neutral countries. In some instances the original authors have expressed the wish that their work be recorded in an American journal. Since in most cases it is not possible to send manuscripts or proofs to the original authors, the responsibility for these articles will rest with the American reviewers, and their names will appear at the end of each article.—EDITOR.]

NOTES

NOTE ON DR. STERNE'S REVIEW OF VOLUME VI OF THE *ANNALS OF THE ASTROPHYSICAL OBSERVATORY OF THE SMITHSONIAN INSTITUTION*

The Editor has kindly sent me advance proof of Dr. Sterne's review of Volume VI of the *Annals* of the Smithsonian Astrophysical Observatory. It seems unfair to my colleagues and to the readers of the *Journal* to leave them with the prevailing impression that our campaign of measurement of the solar constant of radiation amounts only to this: it is acknowledged to be a worthy example of perseverance and accurate measurement and may be compared to a large pearl—costly, beautiful, worthy to be preserved, to be admired, but useless.

I therefore quote from Dr. Sterne as follows in regard to the variation of the sun: "The crucial test . . . . is to see whether independently obtained measures, at different stations show significant correlation." Since receiving the advance proof of his review, I have made such a crucial test by comparing cases of well-marked day-to-day rise and fall of solar radiation, as given in the *Annals* and observed at Montezuma, Chile, with corresponding cases of rise and fall of solar activity of another kind, universally believed in, reported from an observatory of the Old World. The cases selected came from occurrences in two autumn months scattered throughout the years 1923–1937. The comparisons were 75 in number, and the average change of the solar constant in them, as measured at Montezuma, was 0.7 per cent. The correlation coefficient between these wholly independent variables is 43.1 ± 6.3 per cent.

As one of the independent variables is undoubtedly a solar phenomenon, ordinarily observed on the sun's surface by photography, and as the coefficient of correlation is seven times its probable error, I feel that only prejudice will deny that this comparison indicates the reality of day-to-day solar-constant variation, as measured by Smithsonian observers.

I cannot agree with Dr. Sterne as to the absence of correlation between the variation of the solar constant and the variation of Greenwich faculae areas, as plotted in Figure 17 of the *Annals*. For first having removed the average solar constant and the average facula number for each solar rotation separately from the individual values plotted in Figure 17, so as to leave the variations unaffected by the march of sunspot activity and of solar radiation periodicities, I computed the correlation coefficient between the remaining departures of the two variables. From 173 pairs the result is:

$$r = 39.3 \pm 4.3 \text{ per cent.}$$

The correlation coefficient is thus nine times its probable error. If I had computed the correlation with regard to the fact that the solar-constant changes anticipate the changes of facula numbers, as suggested at page 196 of the *Annals*, the correlation would have resulted still higher.

I will not prolong this note to prove that Dr. Sterne is also in error in stating that the solar rotation period is not shown by our observations of the solar constant.

As to the reality of the long-period solar changes, whose unorthodox derivation Dr. Sterne condemns, I may recall that he himself verified some of them from our preliminary publication of the observations.[1] Using his own approved mathematical method of analysis, he found probabilities of the reality of seven of them, ranging from 10^5 to 10^{19}. It may be a fatuous satisfaction; but I like to see, from Figure 14 of Volume VI of the *Annals*, that the summation of these unorthodox periodicities represents the

[1] *Proc. Nat. Acad.*, **25**, 562, 1939.

curve of original monthly means from 1920 to 1938 with great fidelity. I look forward hopefully to the year 1945 for a crucial test of their excellence, arising from our prediction through them of a large decrease then in the intensity of solar radiation.

Again applying Dr. Sterne's criterion, quoted above, to verify the long solar periodicities, I will refer to my paper "An Important Weather Element Hitherto Generally Disregarded."[2] Here, in Tables 1, 2, and 3 and Figure 7, it is shown by 37 repetitions that our solar period of $8\frac{1}{8}$ months has continued in the temperature records of Vienna, Copenhagen, and New Haven for 140 years unchanged in phase except as affected by yearly seasonal influences. The temperature range is 1.15° C. I have in manuscript the proofs that others of these solar periods have also affected the weather to a controlling degree during that long interval. This evidence is based upon the records maintained by the official weather bureaus of these several countries, which are surely sources independent of the Smithsonian Institution.

Thus I feel encouraged in the belief that the Smithsonian campaign of solar-constant measurement is not merely a useless, costly jewel of exact measurement, to be looked upon as a classic gallery specimen, as critics would imply. I can see that it is destined to furnish to meteorology an important and, indeed, controlling weather element, hitherto unused. I regret that I am at a disadvantage in making this rejoinder, because at this time it would be improper to publish my evidence in full. Should Dr. Sterne be in Washington, I will be glad to show it to him confidentially.

C. G. ABBOT

WASHINGTON, D.C.
November 1942

CORRECTED POSITION AND SPECTRAL CLASS OF FURUHJELM 31

A curious error has come to light as a result of the accidental discovery of a dM2 star of the eleventh photographic magnitude on the McCormick spectroscopic survey plates. The star is AC+44°472.15 ($\alpha = 11^h5^m50^s.19$, $\delta = +43°58'24''.0$)[1] with a proper motion of $0''.753$ found by Furuhjelm and published as No. 681 in his "Recherches sur les mouvements propres . . . . , I"[2] and again as No. 31 in a reprint[3] in which large proper motions only were listed. However, both publications contain a clerical error of 2° in the declination of the star. That the declination should be +43° and not +45° is easily ascertained by consulting the references in column 8 of Furuhjelm's catalogue.[2]

Unfortunately, the error has been carried to several other publications. It is repeated in Luyten's "List of Stars . . . ."[4] (star No. 293), in the Cincinnati Catalogue[5] (star No. 615), and in Kuiper's "Notes on Proper Motion Stars."[6] As far as could be found from the literature, the only attempt to observe the star was made by Kuiper. He observed a star of 12.5 visual magnitude at the erroneous position and determined its spectral class as K1, from which he concluded that it must be regarded as a subdwarf. As might be expected, under the circumstances no trigonometric parallax has been determined as yet.

A. N. VYSSOTSKY

LEANDER MCCORMICK OBSERVATORY
December 1942

[2] *Smithsonian Misc. Coll.*, **101**, 1941.

[1] *Helsingfors Astr. Catalogue*, **4**, 1903.

[2] *Acta Soc. Sc. Fennicae*, Tome **48**, No. 1, 1916.

[3] *Finska Vetens.-Soc. Förh.*, **59**, 1916–17; *Afd. A N:o*, **22**, 1917.

[4] *Lick Obs. Bull.*, **11**, 1, 1923.

[5] *Pub. Cincinnati Obs.*, **20**, 1930.

[6] *Ap. J.*, **92**, 126, 1940.

REVIEWS

Magnitudes and Colors of Stars North of +80°. By F. H. SEARES, F. E. ROSS, and M.C. JOYNER. ("Papers of the Mount Wilson Observatory," Vol. VI; Carnegie Institution of Washington Publication 532.) Baltimore: William Byrd Press, 1941. Pp. 89+iii. Paper bound, $1.50; cloth bound, $2.00.

The Mount Wilson Catalogue of magnitudes and colors for 2271 stars surrounding the North Pole is the fruit of nine years' photometric work and has taken its place as one of the few collections of fundamental photometric standards.

The requirements of photometric standards, though simple to state, are difficult to meet. Only those who have had practical experience in photographic photometry are aware of the severe requirements by which the three essentials (accuracy of scale, determination of zero point, and knowledge of color coefficient) are circumscribed and may be attained. The difficulty of the problem may be measured by the rarity with which these requirements are met.

The difficulty of the problem is equaled by its importance. Few branches of modern astronomy are independent of the magnitude scale, though the relationship is not always immediately apparent. In determinations of the distances of stars or stellar systems the apparent magnitude is as important a factor as the period of a Cepheid; discussions of absolute magnitudes of groups of stars on the basis of their motions depends no less on the apparent magnitudes: to give a concrete example, the apparent magnitudes of most red variable stars that have been based on the B.D. scale (and their great number is apparent only to the student of the subject) will be revised downward by about a magnitude when accurate magnitudes for these stars are determined—and their absolute magnitudes will likewise be diminished.

Standard photometry, then, is not a subject to be studied only for its own sake. It is an urgent necessity for all other branches of the science. Dr. Seares and his co-workers have established the backbone of a reliable and consistent system, first in his work on the North Polar Sequence and, now, in the extension of the standards that is contained in the volume under review. The importance, and the ungratefulness, of the task may both be measured by the remark in the Introduction: "Ten years after their adoption [by the I.A.U.] the relation of the various photometric catalogues to the NPS system was still mostly unknown *and some of the current investigations gave little evidence that any such system existed.*" (Italics the reviewer's.)

At its last meeting the International Astronomical Union appointed a subcommittee to deal with problems of standard sequences, and it is greatly to be regretted that the labors of such a committee should be in abeyance. Four principal needs in the domain of standard sequences should be focused by such a committee: (1) the need for standard magnitudes between the thirteenth and twentieth magnitude, south of the equator; (2) standards of photovisual magnitudes are needed for faint stars, especially south of the equator; (3) several groups of carefully standardized magnitudes are desirable in intermediate declinations, for use in investigations where the North Polar Sequence cannot be used; (4) a *catalogue raisonné* of existing published sequences.

The Mount Wilson studies of standard magnitudes are essential bases for the first three of these four requirements: (1) will rely on the Mount Wilson photographic magnitudes in Selected Areas, (2) would be greatly indebted to the catalogue now under review, and (3) must be based entirely upon that catalogue. There has been some question in recent years concerning the desirability of keeping to the International System of Magnitudes as originally defined, partly because the aluminization of mirrors has changed the color system, partly because the stars at the North Pole itself, used to establish the zero point, are found to be obscured and therefore not of normal color for their spectral classes. But the system has established its usefulness by the most important of all tests—accuracy and consistency—and these have made it the accepted system for pragmatic reasons. The Mount Wilson Catalogue of stars north of +80°, like the North Polar Sequence and the Mount Wilson Catalogue of Selected Areas, is a cornerstone of present-day astronomy. As was said of the work of an eminent physicist, "When other people publish

results, we say that they should be checked and confirmed; but when he publishes something, we say it is so." It is doubtful whether the photographic standards surrounding the North Pole will be redetermined in the near future.

CECILIA H. PAYNE GAPOSCHKIN

Harvard Observatory

Essentials of Astronomy. By JOHN CHARLES DUNCAN. New York: Harper & Bros., 1942. Pp. 181. $1.85.

This new text on astronomy impresses the reader as being different in several ways from the usual college text. The author has used a novel arrangement of the material, presenting first "a description of the sky as it appears to the most casual observer," then "the changes in that appearance that take place with changes in the observer's position and with the lapse of time," and the interpretation of "these appearances as to the simple and majestic motions of the heavenly bodies." The author goes on to present Kepler's laws, the law of gravitation, and the physical laws underlying modern astronomical work, together with the results of these investigations. The facts are presented clearly and concisely, so that, in only 161 pages of textual material, the essential facts of astronomy are treated in a surprisingly comprehensive manner. The book has been prepared with care, so that the accuracy is high, even for a college text, and fourteen appendixes increase the value of the book for reference purposes.

For a class in descriptive astronomy, composed primarily of nonscience majors, the reviewer would favor a fuller text, such as Duncan's earlier text, *Astronomy*, even if certain sections of the book must be omitted. This type of student does better with a relatively full treatment of whatever points are studied. The fact that the arrangement of the new text requires treatment of a subject, such as precession, in two or more places, may increase the difficulty for these students.

For a class composed primarily of majors in mathematics and science, especially a small class, the new text appears well suited. The arrangement is in agreement with scientific procedure, helping the students to distinguish the facts of science, strictly speaking, on the one hand, from hypotheses and speculation, on the other. The brief treatment should cause these students no real difficulty, and the comprehensive coverage in a short space will be an advantage, especially in wartime. Professor Duncan has made a real contribution in writing a text for this type of course.

C. C. WYLIE

University of Iowa

National Geographic Society–National Bureau of Standards Solar Eclipse Expedition of 1940 to Brazil: Contributed Technical Papers of the National Geographic Society. ("Solar Eclipse Series," No. 2.) Washington, 1942. Pp. 97.

The *Contributed Technical Papers of the National Geographic Society* contain an account of the results secured in the joint expedition of the National Geographic Society and the National Bureau of Standards to observe the total eclipse of the sun on October 1, 1940. The station was Patos, Brazil. Although clouds partially obscured the total eclipse, much valuable information was obtained in spite of the meteorological handicaps. The publication consists of a foreword by Lyman J. Briggs, director of the National Bureau of Standards, followed by eight papers by various members of the expedition.

In the first of these papers, Dr. Irvine C. Gardner discusses the design and construction of eclipse apparatus. The astronomical equipment consisted of two cameras for the corona, one fitted with polarizing apparatus for coronal studies, and two spectrographs, which together were ready to record the complete spectrum from 3000 to 10,000 A. The lenses of the corona cameras were coated with nonreflecting layers of calcium fluoride for the purpose of diminishing secondary reflections.

The operation of the equipment was automatic, or at least semiautomatic, a feature that is, in the reviewer's opinion, extremely desirable for eclipse equipment. Electric motors, fortu-

nately, have no tendency to get "buck fever" at the moment of totality. The corona cameras embody a number of excellent features. One wonders, however, whether the polaroid might not have been more advantageously placed just in front of the sensitive film rather than in front of the primary lens.

In 1932 the reviewer designed a spectrograph in which the film was moved, semiautomatically, parallel to the dispersion between exposures. In 1936 he used a fully automatic camera, with wide film moved perpendicularly to the dispersion. The second method seemed definitely preferable, although the limitations produced by the finite width of the film and the consequently short spectrum were serious. Gardner has circumvented the difficulties very neatly with a camera in which the film moves diagonally, relative to the dispersion. As a result, he is able to record 40 inches of spectrum upon a film only $9\frac{1}{2}$ inches wide, with an advance of approximately 12 inches between exposures.

Dr. C. C. Kiess, of the National Bureau of Standards, in the next paper reports on the flash spectrum secured with the eclipse instruments. A fortunate break in the clouds near the end of totality enabled the scientists to obtain a record from about 3000 A to about 5000 A with a dispersion of 2.4 A/mm in the first order. The spectra were taken a few seconds after the end of totality. Hence the flash lines appeared as crescent-shaped projections extending beyond the belt of continuous spectrum. Kiess has measured the wave lengths, estimated the flash intensities, and recorded the character of the various lines. To designate the appearance, Kiess uses the letters *a*, *b*, or *c*, according to the degree of line reversal in the strip of Fraunhofer continuum. The classification is of undoubted astrophysical significance, but it seems unfortunate that Kiess has used a classification that resembles the one introduced by Menzel, without adopting the earlier classification. As a matter of fact, Kiess's system is very similar to that of Menzel for types *a* and *b*. But Kiess's term *c* is generally denoted by *d* in the earlier classification. Kiess has failed entirely to note the distinctive behavior of the rare-earth lines which led Menzel to introduce an intermediate class *c*, which has no counterpart in Kiess's system. Considerable confusion may result from the double classification.

The next paper, by Stair and Coblentz, of the Bureau of Standards, describes the methods of calibration of the standard lens which was employed as a comparison for the flash spectrum. Kiess and Humphreys then discuss the determination of flash-spectrum intensities, microphotometrically, in what is unquestionably the most important paper of the series. They have investigated only a few lines, H and K of *Ca* II, the *b* lines of *Mg* I, and the lines of the Balmer series of hydrogen from $H\beta$ to $H\phi$. The authors find that for the metallic lines the well-known square-root law holds for the intensities. In view of the fact that their measures refer to very low-level flash, the result is not surprising.

The authors have tabulated the hydrogen intensities in the customary manner, with $H\beta$ fixed at unity, and have compared their measures with those of Cillié and Menzel on a similar scale. The intensities of the earlier members of the Balmer series, as given by Menzel and Cillié, are admittedly very uncertain, the values having been derived for the most part by extrapolation.

The emission,[1] per frequency interval $d\nu$ from a unit volume of gas in thermodynamic equilibrium, containing N_i hydrogen ions and N_ϵ electrons per cm^3, is

$$E_{\kappa n'}\,d\nu = N_i N_\epsilon \frac{h^3}{(2\pi mk)^{3/2}} \frac{8\pi^2\epsilon^2R^2}{mc^3} \frac{2^4}{3\sqrt{3}\pi} \frac{g_{II}h\,d\nu}{T_\epsilon^{3/2}n'^3}\, e^{-h(\nu-\nu_{n'})/kT_\epsilon},$$

where g_{II} is the Kramers-Gaunt factor, T_ϵ the electron temperature, and n' the quantum member of the lower level. Similarly, the total emission for a line involving the transition n to n' is

$$E_{nn'} = N_i N_\epsilon \frac{h^3}{(2\pi mk)^{3/2}} \frac{8\pi^2\epsilon^2R^2}{mc^3} \frac{2^4}{3\sqrt{3}\pi} \frac{g_I}{T_\epsilon^{3/2}n'^3} \frac{2hR}{n^3}\, e^{hR/n^2kT_\epsilon}.$$

Near the series limits $g_I \sim g_{II}$, $\nu \sim \nu_{n'}$ and $n \to \infty$. Hence the ratio of the intensity of a high-series line to the emission per unit frequency of the continuum at the limit is

$$\frac{E_{nn'}}{E_{\kappa n'}} = \frac{2R}{n^3}.$$

[1] Menzel, *Ap. J.*, **85**, 330, 1937.

If, then, in any spectrum we arbitrarily set $E_{nn'} = 1$, for convenience, the high-series members that flow without break into the continuum will follow the law

$$E_{nn'} = \frac{2R}{n^3} .$$

The intensities of the remaining members should be referred to the continuum as a standard.

TABLE 1

n	Line	Observed Intensities					Theoretical Intensities			
		Menzel and Cillié, 1932			1940 K and H	1936 Thackeray	Thermodynamic Equilibrium		Baker and Menzel	
									B	A
		P_1	G_1	P_2			$T=\infty°$	$T=10{,}000°$	10,000°	10,000°
3	$H\alpha$	.....	12.88*	.....	.....	12.35	12.37	13.12	12.07	11.70
4	β	12.07*	11.90*	.....	11.45	11.87	12.03	12.45	11.67	11.43
5	γ	11.48*	11.33*	.....	11.19	11.34	11.75	12.01	11.38	11.19
6	δ	11.14*	11.08	.....	10.84	10.98	11.52	11.70	11.17	11.01
7	ϵ	10.92*	10.93	.....	10.75	.....	11.34	11.47	11.00	10.85
8	ζ	10.73*	10.89	.....	10.75	.....	11.14	11.24	10.82	10.68
9	η	10.66*	10.67	10.69	10.50	10.70	10.99	11.07	10.69	10.56
10	θ	10.42*	10.45	10.45	10.46	10.66	10.86	10.92	10.57	10.45
11	ι	10.36*	.....	10.39	10.38	10.38	10.73	10.78	10.45	10.33
12	κ	10.33*	.....	10.36	10.34	10.29	10.62	10.66	10.37	10.23
13	λ	10.29*	.....	10.31	10.29	10.26	10.52	10.55	10.27	10.14
14	μ	10.19*	.....	10.21	10.24	10.17	10.43	10.46	10.17	10.07
15	ν	10.11*	.....	10.11	10.13	10.15	10.33	10.35	10.07	9.97
16	ξ	10.05	.....	10.03	10.07	9.99	10.25	10.27	10.00	9.90
17	o	10.00	.....	10.01	9.98	9.95	10.18	10.20	9.94	9.84
18	π	9.91	.....	9.95	9.91	9.86	10.09	10.10	9.85	9.75
19	ρ	9.89	.....	9.89	9.88	.....	10.02	10.03	9.79	9.69
20	σ	9.82	.....	9.79	9.83	9.85	9.96	9.97	9.73	9.64
21	τ	9.81	.....	9.77	9.79	9.79	9.89	9.90	9.66	9.57
22	υ	9.71	.....	9.70	9.75	9.72	9.83	9.84	9.61	9.52
23	ϕ	9.71	.....	9.65	9.65	9.70	9.75	9.76	9.54	9.45
24	χ	9.62	.....	9.50	.....	9.65	9.67	9.67	9.45	9.38
25	ψ	9.59	.....	9.49	.....	9.59	9.61	9.61	9.39	9.32
26	ω	9.57	.....	9.45	.....	9.55	9.57	9.57	9.35	9.27
27	.....	9.51	.....	9.40	.....	.....	9.52	9.52	9.30	9.22
28	.....	9.48	.....	9.41	.....	.....	9.47	9.47	9.26	9.18
29	.....	9.41	.....	9.33	.....	.....	9.43	9.43	9.22	9.14
30	.....	9.39	.....	9.45	.....	.....	9.39	9.39	9.18	9.10

The observational data for the 1932 eclipse clearly show that the chromosphere lines at n = 25–30 do grade properly into the continuum. Hence, setting $R = 3.29 \times 10^{15}$, we may take

$$\log E_{30,\,2} = 9.39 .$$

This procedure is infinitely more satisfactory than the usual one of setting the intensityof $H\beta$ equal to unity, although we can use it only if the measures include the continuum at the series limit. The reviewer presents in Table 1 a summary of the observational material with a comparison of theoretical values adjusted to the above scheme. Columns 1 and 2 designate the Balmer lines by upper quantum number and customary notation. Columns 3, 4, and 5 sum-

marize the observations of Cillié and Menzel[2] from the 1932 eclipse. The designations P_1 and G_1 refer to two spectrograms taken simultaneously with prism and grating; P_2 refers to a prism film of a higher chromospheric level wherein the lines are weaker than in the other spectra. The intensities marked with an asterisk represent extrapolated values. Column 6 gives the values of Kiess and Humphreys, from the work under review. Column 7 lists intensities measured by Thackeray[3] at the 1936 eclipse.

Except for the first four or five lines of the series, the agreement is excellent. Over the range from $H\theta$ to $H\phi$ the mean discrepancy, taken without regard to sign, is only 0.03 in the logarithm. Also, since self-reversal may be present in varying amounts at the different eclipses and at different levels at the same eclipse and since its action would be greatest in the lower members, one has no right to question the relative accuracy of the different determinations. Changes of excitation conditions also have their greatest effect at $H\alpha$ and $H\beta$.

The remaining columns give values calculated from theory. The theoretical intensities for $T = \infty$, from the Schroedinger-Sommerfeld formula, come next. Column 9 gives the intensities from an assembly in thermodynamic equilibrium at 10,000°. Columns 10 and 11 list the theoretical intensities for two cases discussed by Baker and Menzel,[4] respectively, for complete absorption of higher Lyman members (B) and for no absorption of Lyman members, i.e., for a pure capture spectrum (A).

The authors state that the Schroedinger-Sommerfeld formula for the line intensities of the hydrogen spectrum "applies to atoms undisturbed except for exposure to radiation of the Lyman series." A more accurate statement would be that this formula applies to the emission of radiation by atoms whose population in the various levels is proportional to the weight of those levels; in other words, it applies strictly to the case of an infinite exciting temperature. A correction for the external condition must be introduced either by a Boltzmann factor or by the evaluation of the capture coefficients and mean lifetimes, as has been done by various theorists working on problems of planetary nebulae. The formula intensities, if uncorrected, have no physical significance in conjunction with the observations, except possibly near the series limit, where small differences in excitation potential have no marked effect on the partition of atoms in the various levels over small ranges of energy and wave lengths.

The reviewer is not in entire agreement with the astrophysical discussion of Kiess and Humphreys. It is true that the chromosphere presents some problems similar to those of the gaseous nebulae and emission-line stars. But the authors' statement that "the hydrogen spectrum in all these astronomical sources is regarded as essentially a recombination spectrum, little influenced by absorption of Lyman radiation from the central star or reabsorption of this radiation from the gas itself," is not confirmed by the observations. Also, it is by no means certain that the gas is too tenuous for collisions to play a significant part. The Balmer decrement, as measured by the ratio of the intensities of low- or intermediate-series members to the intensities of high-series members, is far too small to be explained on the basis of any Boltzmnan distribution, even at infinite temperature. As Menzel and Cillié pointed out long ago, there is an underpopulation of intermediate atomic levels which may amount to as much as a factor of 3 or 4.

An analogous underpopulation is seen in the spectra of the planetary nebulae, where a very marked drop in the intensity of the continuum occurs where the lines overlap at the head of the series. For the chromosphere, the drop is by no means so pronounced, but the intensity measures clearly prove its existence, i.e., the entries in the observed intensity columns tend to be less than those in columns 6 or 7. A theoretical investigation, however, shows that for a pure capture spectrum (col. 9) the drop is even more marked than observed for the planetary nebulae, whose intensities conform fairly well to the values tabulated in column 8. To account for the Balmer decrement, we shall have to suppose that reabsorption of the Lyman radiation is considerable both in the chromosphere and in the nebula. Since the lower members of even the Balmer series are probably partially reversed, the optical depth of the chromosphere in both the Lyman series and the continuum must be very high. The observed intensities are intermediate between those predicted on the capture theory, either with or without Lyman absorption, and those predicted on the basis of pure thermodynamic equilibrium for infinite temperature. Lower temperatures merely increase the decrement and tend to heighten the discrepancy.

[2] *Harv. Circ.*, No. 410, 1935; *Ap. J.*, **85**, 88, 1937.

[3] *M.N.*, **97**, 672, 1937.

[4] *Ap. J.*, **88**, 52, 1938.

It seems entirely reasonable to suppose that atomic collisions, despite the low densities, may play some role in redistributing atoms among the high atomic levels. Furthermore, self-absorption of the lower members of the Balmer series, which is not taken into account in the elementary theory, is in the right direction to account for any discrepancy. The fact that prominence and even chromospheric phenomena are clearly visible on the disk in *Hα* spectroheliograms is in itself the confirmation of the suggestion. Further theoretical work along these lines is clearly indicated.

The advantage of the tabulation system here adopted is evident when we compare the theoretical intensities with the observed. The Balmer decrement is not dissimilar for the two cases. But, if we follow our first impulse to add a constant to the figures tabulated in columns 10 and 11, we must remember that we are also multiplying the predicted intensity of the continuous spectrum by a factor. For the chromosphere this multiplication would predict a continuum more intense than that observed. The reviewer reiterates the conclusion by Menzel and Cillié that the chromospheric spectrum is not predominantly one of pure capture and that considerable excitation by Lyman absorption or by electron impact must take place.

In the next succeeding paper, Paul A. McNally, S.J., director of the Georgetown College Observatory, discusses the determination of contact times of the total solar eclipse from photographs of the partial phases. In spite of the fact that the clouds interfered seriously, McNally found it possible to determine accurate contact times from the measured lengths of the occulted chords and the widths of the crescents.

E. O. Hulburt, of the United States Naval Research Laboratory, in the following paper, discusses the determination of sky brightness at Patos, Brazil, during twilight and during the total solar eclipse. In the final scientific paper of the series, T. R. Gilliland, of the National Bureau of Standards, discusses the radio observations. One of the of the primary results derived from the observations was the determination of the order of magnitude of the recombination coefficients for the ions of the E, F_1, and F_2 layers. Gilliland finds that there is some evidence of an ionizing force extending around the edge of the moon prior to reappearance of the sun after totality. The detection of this interesting phenomenon was made possible only because of the rapidity of the recording. The technique of observation well deserves close scrutiny by other prospective observers of eclipse-ionosphere phenomena. The last paper of the series is a narrative of the expedition, by Irvine C. Gardner.

The complete set of papers represents a marked contribution. The generosity of the National Geographic Society in making the expedition possible has been amply rewarded by the excellence of the results. It is unfortunate indeed that the eclipse was partially cloudy; for the general value of the results obtained, despite the handicap, merely indicates how important the observational data would have been had the full program been carried out.

DONALD H. MENZEL

Harvard Observatory

The Practical Essentials of Pre-training Navigation. By WILLIAM T. SKILLING and ROBERT S. RICHARDSON. New York: Henry Holt & Co., 1942. Pp. v+113. $0.75.

The problem of supplying large numbers of flyers for the Army and Navy is a serious one in wartime, and the length of their training period is necessarily drastically curtailed, so that the student pilot gets his instruction under considerable pressure. The preflight-training courses which have been instituted in many high schools and colleges have the dual purpose of easing this strain to some extent and of providing a background to make the methods and procedures less sets of rules to be learned and applied. Begun in Britain in 1940, when the need for pilots was great, the plan has recently had considerable support in the United States. It is now well past the experimental stage and will continue to expand until the end of the war. Although no one can predict what the post-war world will be like, it is certain that aviation will play an important part and that the high schools and colleges will be called upon to supply the physical and mathematical training for navigation, aerodynamics, and meteorology.

It is the aim of the authors of this small volume to provide a text for certain of the subjects covered in such a course. The subtitle, *Celestial Navigation—Meteorology—Map Projection*, indicates the exact subjects treated. The reader is supposed to possess an almanac and a source of the correct time (not nearly so drastic an assumption as it would have been some years ago), and he may or may not have a sextant. In presenting the material from this standpoint, the

authors are able to restrict themselves to the general fundamental ideas involved and to avoid a great part of the complicated details of the use of instruments and equipment. The first chapters treat the spheres of the earth and the sky, the co-ordinates required to locate points upon them, and the different ways of attempting to represent a section of a sphere upon a plane surface. The chapter on "Time" is presented as clearly as such a puzzling subject can be, although it is not very likely that the practical navigator of the future will have much use for apparent time, sidereal time, the equation of time, or right ascension, and the marine navigator can even dispense with sidereal hour angle.

The authors present a celestial fix as the intersection of two circles of position whose centers are the subsolar, lunar, or astral points and then show how to draw a line of position as a section of such a circle. It is to be hoped a treatment of this type should remove much of the mystery of celestial navigation. The last chapter is devoted to a short summary of the fundamentals of meteorology.

Since the subject matter is specifically limited to celestial navigation, one cannot complain at the absence of any mention of plane or great-circle sailing, wind drift, or the plotting of terrestrial lines of position, which would have to be included in a complete pretraining course in navigation.

The illustrations are very carefully and clearly drawn and should contribute to the reader's understanding, although he will be puzzled by the authors' method of constructing a mercator projection on page 12.

The instructor of a high-school course in navigation will find in this volume a manual for his students which presents the fundamentals of the subjects clearly and avoids the confusing details which make the more complete texts difficult for the beginner.

JOHN TITUS

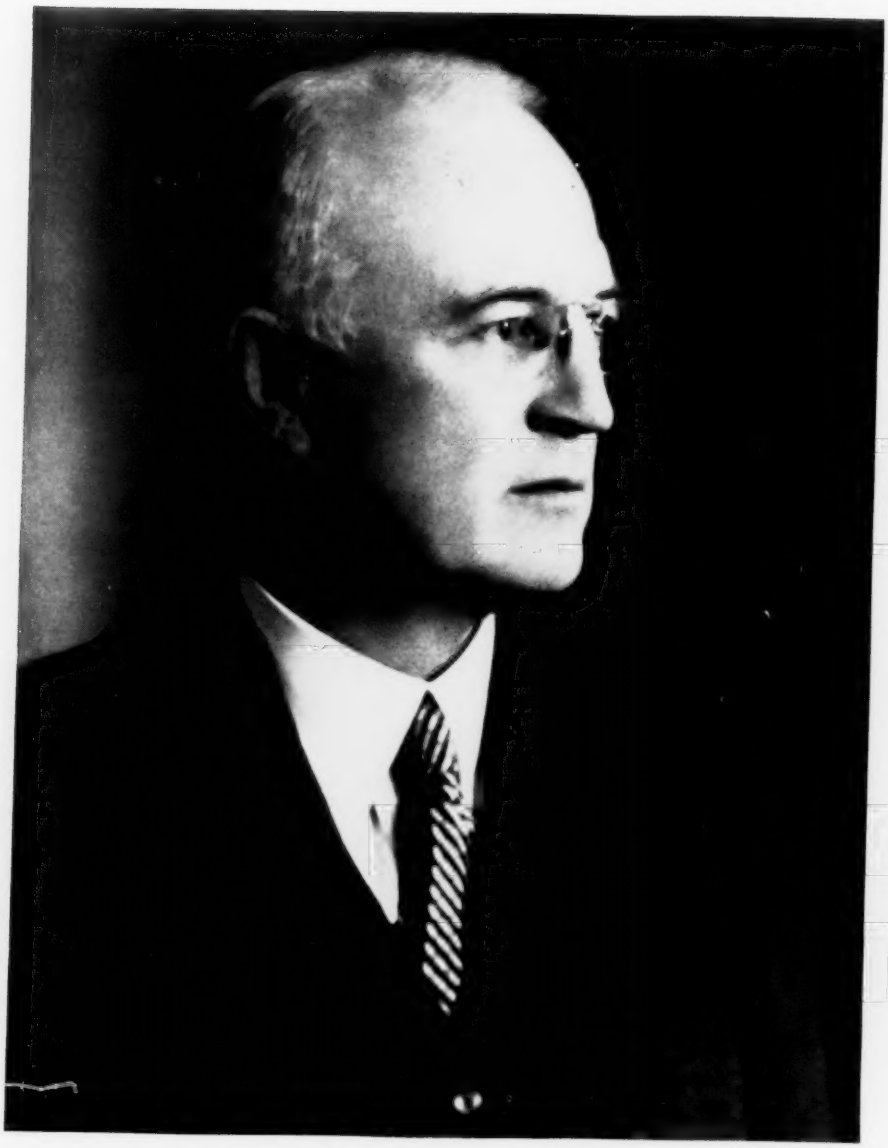

HENRY GORDON GALE
1874–1942